

DOCTORAL DISSERTATION

**SONOPHOTODEPOSITION:
COUPLING OF SONICATION
AND PHOTODEPOSITION
IN THE SYNTHESIS
OF TITANIUM DIOXIDE-BASED
PHOTOCATALYTIC MATERIALS**

AGNIESZKA MAGDZIARZ



INSTITUTE OF PHYSICAL CHEMISTRY
POLISH ACADEMY OF SCIENCES
KASPRZAKA 44/52
01-224 WARSAW, POLAND

A Doctoral Dissertation

SONOPHOTODEPOSITION: COUPLING OF SONICATION AND PHOTODEPOSITION IN THE SYNTHESIS OF TITANIUM DIOXIDE–BASED PHOTOCATALYTIC MATERIALS

Agnieszka Magdziarz

Supervisor:

**Juan Carlos Colmenares Quintero PhD DSc
Assoc Prof IPC PAS**

Institute of Physical Chemistry of the Polish Academy of Sciences

This dissertation was prepared within the International PhD
in Chemistry Studies at the Institute of Physical Chemistry
of the Polish Academy of Sciences in Warsaw

Biblioteka Instytutu Chemii Fizycznej PAN

F-B.498/17



Warsaw, September 2017

<http://rcin.org.pl>



B. 498/17

Acknowledgements

Most of all, I would like to acknowledge Professor Juan Carlos Colmenares Quintero for all the experience I got being a part of his group. I deeply appreciate his guidance, sharing of knowledge, encouragement of my research at each stage, and provision of opportunities that converted me in a scientist.

Warm thanks go to former and current colleagues in my research group and at the whole Institute of Physical Chemistry PAS. Thanks for the collaboration, friendship, support, fruitful discussions, relaxing lunch breaks, and the wonderful time we had together.

I am utterly grateful to my friends and family, whose encouragement and loving presence enabled me to accomplish my PhD studies. I am indebted to my friend Marta Nicewicz, who helped me to believe at the beginning of my doctoral journey that I could do it. Special thanks go to my mother for taking care of my little son Staś while I was writing this dissertation.

I especially want to thank my boys Zbyszek and Staś for their priceless presence and believing in me. Thank you Zbyszek for your help, your always good advice, and also your criticism, which motivated me to finish this dissertation.

I also acknowledge the National Science Centre (Poland) for its financial support through the Preludium research project No. DEC-2013/11/N/ST5/01923. I also received partial support through these other projects: the Marie Curie International Reintegration Grant within the 7th European Community Framework Programme, which was co-financed by the Ministry of Science and Higher Education of Poland by project No. 473/7.PR/2012, and Sonata Bis project No. 2015/18/E/ST5/00306 from the National Science Centre (Poland).



To my beloved Father and Mother

Abstract

This thesis presents basic experimental studies in the field of materials synthesis. The application of green energy sources, ultrasound, and light irradiation in the synthesis procedure of materials with photocatalytic properties is studied herein. In situ coupling of sonochemistry with photochemistry, in so-called sonophotodeposition, for deposition of metal species on the surface of semiconducting material (e.g., TiO_2) may result in the formation of a new powerful methodology. This synergistic action between ultrasound and light irradiation may provide many advantages for this process: no need to add harmful chemical-reducing agents, time-saving, and simplicity of the process, among others.

My dissertation is composed of introduction to the subject area and discussion of the submitted publications. In the introductory part, key information about sonochemistry, photochemistry, and the synergism between the ultrasound and photochemical processes is presented. The research part of this dissertation is submitted in the form of six publications. The first one (patent application) introduces the general idea and the possibilities of the sonophotodeposition method in the synthesis of materials. The next four publications are research articles that study in detail TiO_2 -based systems doped with different metals. The first metal deposited on commercial TiO_2 surface by simultaneous use of light and ultrasound was palladium. Next, a possibility of sonophotodeposition of two metals was studied. Combinations of noble metal and transition metal—platinum-iron and palladium-iron pairs—were sonophotodeposited on the self-prepared semiconductor material composed of TiO_2 supported on zeolite Y. Another task concerned deposition of iron oxide on TiO_2 /zeolite Y. Iron is a transition metal with a negative reduction potential, which is difficult to reduce; therefore, its photodeposition was scarcely reported in the literature. In a subsequent work, a detailed comparison of this methodology with sonodeposition and photodeposition was supposed to give an answer about the real contribution of ultrasound and light irradiation to the process of sonophotodeposition. The final article of my dissertation is a review that compares the role of ultrasound in simultaneous combination with photodeposition (sonophotodeposition) and with electrodeposition (sonoelectrodeposition) and discusses the utility of these methods in the synthesis of materials.

Streszczenie

Przedstawiona rozprawa doktorska dotyczy badań podstawowych w dziedzinie syntezy materiałów. Zastosowanie „zielonych źródeł energii”, takich jak ultradźwięki i promieniowanie świetlne, w syntezie materiałów o właściwościach fotokatalitycznych jest główną tematyką tych badań. Jednoczesne połączenie sonochemii z fotochemią można wykorzystać do osadzania związków metalu na powierzchni półprzewodnika (np. TiO_2). Ta metoda, nazwana sonofotoosadzaniem, może stać się nowym i obiecującym sposobem w preparatyce materiałów. To synergiczne połączenie ultradźwięków z promieniowaniem świetlnym może przynieść wiele korzyści w tym procesie, takich jak: brak konieczności stosowania szkodliwych związków redukujących, zredukowanie czasu reakcji oraz prostota wykonania.

Na niniejszą rozprawę składa się sześć publikacji, które poprzedzone są wstępem teoretycznym oraz merytorycznym omówieniem każdej z prac. Wstęp zawiera kluczowe informacje na temat sonochemii, fotochemii oraz synergicznego działania ultradźwięków i procesów fotochemicznych. Pierwsza praca patentowa przedstawia ogólne założenia metody sonofotoosadzania oraz jej możliwości w syntezie materiałów. Cztery kolejne publikacje są artykułami badawczymi, które szczegółowo omawiają układy oparte na TiO_2 z naniesionymi różnymi związkami metali. Pierwszym metalem naniesionym na powierzchnię komercyjnego TiO_2 przy jednoczesnym użyciu światła i ultradźwięków był pallad. Następnie, sprawdzona została możliwość sonofotoosadzenia dwóch metali na powierzchni wcześniej spreparowanego kompozytu złożonego z TiO_2 osadzonego na zeolicie typu Y. Zastosowano kombinację metalu szlachetnego z metalem przejściowym w układach: platyna-żelazo i pallad-żelazo. Kolejnym zadaniem było osadzanie tlenku żelaza na wspomnianym TiO_2 /zeolit Y. Jak wiadomo żelazo jest metalem przejściowym o ujemnym potencjale redukcyjnym, co oznacza, że trudne jest uzyskanie jego formy metalicznej w procesie fotochemicznej redukcji, stąd brak przykładów w literaturze. Celem postawionym w następnej pracy było zdefiniowanie roli ultradźwięków i promieniowania świetlnego w procesie sonofotoosadzania poprzez zestawienie tej metody z sonoosadzaniem i fotoosadzaniem. Ostatni, zamykający tę rozprawę artykuł jest pracą przeglądową, w której metoda sonofotoosadzania została porównana z pokrewnym sonoelektroosadzaniem, odnosząc się do roli ultradźwięków w tych procesach oraz do zastosowania powyższych metod w syntezie materiałów.

Preface

The research presented in this dissertation was performed at the Institute of Physical Chemistry PAS in the research group 'Catalysis for sustainable energy production and environmental protection' under the supervision of Prof Juan Carlos Colmenares Quintero between September 2012 and September 2015. It was partially financed by the National Science Centre through the Preludium research project No. DEC-2013/11/N/ST5/01923 (Principal Investigator), as well as within other projects mentioned in the Acknowledgements. All experimental work regarding synthesis of the materials and photocatalytic test reactions and the majority of characterization techniques of the materials—such as diffuse reflectance UV-vis spectroscopy, X-ray diffraction, X-ray photoelectron spectroscopy, N₂ physisorption and energy dispersive X-ray fluorescence—were performed at the laboratories and using the equipment of the Institute of Physical Chemistry PAS. Additional characterization was conducted at the Faculty of Materials Science and Engineering of Warsaw University of Technology (HRTEM-EDS measurements), the Institute of Physics PAS in Warsaw (HRTEM-EDS measurements), and the Jerzy Haber Institute of Catalysis and Surface Chemistry PAS in Krakow (Mössbauer measurements).

This dissertation is structured as follows: It starts with a list of six works contributing to this dissertation. The next six articles were also completed during my PhD studies, though they are not limited to the subject of this dissertation. A list of figures and a nomenclature section, which lists all important symbols used in the thesis, are included before the Introduction. Section 1, divided into six subsections, provides a brief introduction to the articles and background in sonochemistry and photochemistry and establishes the context of the thesis work. Note that these subsections are not intended to be a full review of any of the topics but are rather meant as an introduction to readers who are not familiar with the subjects. The main research goals of the thesis work are summarized in Section 2. The summary of the main results from all six works and the thesis development are presented in Section 3. Section 4 covers final comments and gives an outlook towards future works. After this section, all literature references cited by the author are listed in order of appearance in the text. The main research results of this thesis are presented in Section 5. The published articles are displayed in the format of their respective journals. Finally, the authors' contribution statements are added in Section 6.

This thesis is written in such a way that it should be accessible and understandable for any reader with a chemistry background at the graduate level.

List of publications

In chronological order:

- Method of depositing metal nanoparticles on the surface of semiconductor materials and surface obtained by this process*
J.C. Colmenares and **A. Magdziarz**
Polish Patent PL222050 (submitted Nov 2012, accepted Nov 2015)
- A new photocatalytic tool in VOCs abatement: Effective synergetic combination of sonication and light for the synthesis of monometallic palladium-containing TiO₂*
J.C. Colmenares, **A. Magdziarz**, D. Łomot, O. Chernyayeva, and D. Lisovytskiy
Applied Catalysis B: Environmental, 147, 624–632, 2014
- Iron-containing titania photocatalyst prepared by the sonophotodeposition method for the oxidation of benzyl alcohol*
A. Magdziarz, J.C. Colmenares, O. Chernyayeva, K. Kurzydłowski, and J. Grzonka
ChemCatChem, 8, 536–539, 2016
- Sonication and light irradiation as green energy sources simultaneously implemented in the synthesis of Pd-Fe- and Pt-Fe-doped TiO₂-based photocatalysts*
A. Magdziarz, J.C. Colmenares, O. Chernyayeva, D. Łomot, and K. Sobczak
Journal of Molecular Catalysis A: Chemical, 425, 1–9, 2016
- Insight into the synthesis procedure of Fe³⁺/TiO₂-based photocatalyst applied in the selective photo-oxidation of benzyl alcohol under sun-imitating lamp*
A. Magdziarz, J.C. Colmenares, O. Chernyayeva, D. Lisovytskiy, J. Grzonka, K. Kurzydłowski, K. Freindl, and J. Korecki
Ultrasonics Sonochemistry, 38, 189–196, 2017
- In situ coupling of ultrasound to electro- and photo-deposition methods for materials synthesis*
A. Magdziarz and J.C. Colmenares
Molecules, 22, 216, 2017

Other publications (not included in this thesis):

7. *Sonication-assisted low-temperature routes for the synthesis of supported Fe-TiO₂ econanomaterials: partial photooxidation of glucose and phenol aqueous degradation*
J.C. Colmenares, **A. Magdziarz**, O. Chernyayeva, D. Lisovytskiy, K. Kurzydłowski, and J. Grzonka
ChemCatChem, 5, 2270–2277, 2013
8. *Low-temperature ultrasound-promoted synthesis of Cr-TiO₂-supported photocatalysts for valorization of glucose and phenol degradation from liquid phase*
J.C. Colmenares, **A. Magdziarz**, K. Kurzydłowski, J. Grzonka, O. Chernyayeva, and D. Lisovytskiy
Applied Catalysis B: Environmental, 134–135, 136–144, 2013
9. *Room temperature versatile conversion of biomass-derived compounds by means of supported TiO₂ photocatalysts*
J.C. Colmenares and **A. Magdziarz**
Journal of Molecular Catalysis A: Chemical, 366, 156–162, 2013
10. *High-value chemicals obtained from selective photo-oxidation of glucose in the presence of nanostructured titanium photocatalysts*
J.C. Colmenares, **A. Magdziarz**, and A. Bielejewska
Bioresource Technology, 102, 11254–11257, 2011
11. *Influence of the strong metal support interaction effect (SMSI) of Pt/TiO₂ and Pd/TiO₂ systems in the photocatalytic biohydrogen production from glucose solution*
J.C. Colmenares, **A. Magdziarz**, M.A. Aramendia, A. Marinas, J.M. Marinas, F.J. Urbano, and J.A. Navio
Catalysis Communications, 16, 1–6, 2011
12. *Chapter: Application of microwave and ultrasound irradiation in the synthesis of perovskite-type oxides ABO₃, in a book: Perovskites and related mixed oxides: concepts and applications*
J.C. Colmenares, **A. Magdziarz**, and P. Lisowski
Editors: P. Granger, V.I. Parvulescu, S. Kaliaguine, and W. Prellier.
ISBN: 978-3-527-33763-7. Wiley-VCH, Weinheim, Chapter 5, pp. 91–112, 2016

Two of the research articles (7 and 8) are related to the main subject of this thesis regarding the preparation method of TiO₂/zeolite Y substrate. However, they are not part of this dissertation. The others (9–12) are mentioned only in the list of papers. They are not part of this dissertation, because they concerned the application of ultrasound in different synthesis methods. However, they were also completed with my contributions in the laboratory during the time of my PhD work.

Contents

| | |
|--|-----|
| Acknowledgements | 5 |
| Abstract | 9 |
| Streszczenie | 11 |
| Preface | 13 |
| List of publications | 15 |
| List of figures | 21 |
| Nomenclature and abbreviations | 23 |
| 1. Introduction | 27 |
| 1.1 Theory of sonochemistry | 27 |
| 1.2 Factors affecting cavitation | 33 |
| 1.3 Physical and chemical effects of ultrasound | 34 |
| 1.4 Ultrasound application in the synthesis of nanomaterials | 37 |
| 1.5 Principles of photochemistry (photocatalysis), with emphasis on the process of metal (oxide) photodeposition on semiconductor surfaces | 42 |
| 1.6 The synergism between sono- and photochemical irradiation | 47 |
| 2. Research goals | 49 |
| 3. Thesis development: introduction to the articles | 50 |
| 4. Final comments on this work and future outlook | 68 |
| References | 71 |
| 5. Texts of articles | 87 |
| Article 1 | 89 |
| Article 2 | 109 |
| Article 3 | 121 |
| Article 4 | 127 |
| Article 5 | 139 |
| Article 6 | 153 |
| 6. Contributions of Authors | 179 |



List of figures

| | |
|--|----|
| Figure 1.1 Schematic illustration of the process of acoustic cavitation. (a) Periodic compression and expansion cycles in the liquid exposed to ultrasound. (b) The formation, growth, and implosive collapse of bubbles in a liquid irradiated with high-intensity ultrasound. Reproduced from [23] with permission of The Royal Society of Chemistry. | 29 |
| Figure 1.2 Schematic description of the bubble's growth in an acoustic field by 'area' and 'shell' effects in the process of rectified diffusion. Reproduced from [31] with permission of John Wiley & Sons, Inc. | 31 |
| Figure 1.3 Chemical effects produced in liquid divided in three reaction zones: (a) schematic view reprinted with permission from [2] (copyright (1999) American Chemical Society); (b) visual view reprinted from [7] with permission from Elsevier; (c) detailed view reprinted with permission from [3] (copyright (2001) American Chemical Society). | 36 |
| Figure 1.4 The formation of (A) a microjet when a bubble collapses near a solid surface, adapted from [63] with permission from Elsevier, and (B) a spherical shockwave registered from a laser-induced collapsing bubble, reproduced from [61] with permission of the Royal Society. | 37 |
| Figure 1.5 The application of ultrasound in the synthesis of nanomaterials. Reproduced from [23] with permission of The Royal Society of Chemistry. | 38 |
| Figure 1.6 The chart presents the 'islands of chemistry' as a function of time, pressure and energy. Reproduced from [68] with permission of Annual Reviews. | 38 |
| Figure 1.7 A variety of nanostructured materials that can be obtained from sonication of volatile organometallics. Reproduced from [70] with permission of Annual Reviews. | 39 |
| Figure 1.8 Schematic illustration of intercalation and exfoliation process in preparation of carbon scrolls. Adapted from [85]. Reprinted with permission from AAAS. | 40 |
| Figure 1.9 A schematic illustration of mechano-chemical effects of ultrasound for the synthesis of polymer-functionalized graphene. Reprinted with permission from [118]. Copyright (2011) American Chemical Society. | 41 |
| Figure 1.10 Basic primary processes of an electronically excited molecule (wavy arrows indicate non-radiative processes). Reproduced from [121] with permission of John Wiley & Sons, Inc. | 42 |
| Figure 1.11 Potential energy diagrams of thermal and photochemical reactions of substrate R to product P: (1) stoichiometric, and (2) catalytic, where C and PC symbolize a thermal catalyst and photocatalyst, respectively. Reproduced from [121] with permission of John Wiley & Sons, Inc. | 43 |

| | |
|--|----|
| Figure 1.12 (a, b) Direct and indirect semiconductor photocatalysis. Reproduced from [121] with permission of John Wiley & Sons, Inc. | 44 |
| Figure 1.13 Schematic overview of (a) reductive photodeposition and (b) oxidative photodeposition. Reprinted with permission from [128]. Copyright (2016) American Chemical Society. | 45 |
| Figure 1.14 (a) Band positions of several semiconductors in contact with aqueous electrolyte at pH 1. The lower edge of the conduction band (red color) and upper edge of the valence band (green color) are presented along with the band gap in electron volts. The energy scale is indicated in electron volts, using either the normal hydrogen electrode (NHE) or the vacuum level as a reference. Adapted by permission from Macmillan Publishers Ltd: Nature [130], copyright (2001); (b) Schematic overview of redox potentials of several aqueous metal solutions relevant for photodeposition [131]. | 46 |
| Figure 1.15 Interaction of ultrasound effects with photochemical reactions. Reprinted from [140] with permission of Springer. | 48 |
| Scheme 3.1 The steps followed in my research (dotted lines connect articles belonging to the same case studies groups; see also Scheme 3.3). | 50 |
| Scheme 3.2 Graphic representation of test reactions setups applied in the particular works. Pictures (A) and (B) adapted from [154] copyright (2014) and [155] copyright (2011) with permissions from Elsevier, respectively. | 52 |
| Scheme 3.3 Groups of articles according to the applied setup used in the synthesis of photocatalysts. | 52 |
| Scheme 3.4 Different reductive species that can be formed in the sonophotodeposition method. | 56 |
| Scheme 3.5 Sonophotodeposition vs. photodeposition reaction procedure. | 60 |
| Scheme 4.1 The schematic summary of the sonophotodeposition method. | 70 |
| Table 3.1 Photocatalytic test reactions reported in particular articles (^{1,2} : materials described in Articles 3 and 5 have been denominated with the same symbol, Fe/TiO ₂ /Zeolite, but it is important to mention that they were prepared using different ultrasound powers—25 % and 10 % respectively—and they differ in Fe loading; SPD: sonophotodeposition method). | 51 |
| Table 3.2 Techniques applied for characterization study of the synthesized materials in each article. | 53 |

Nomenclature and abbreviations

In order of appearance in the text:

AOPs – advanced oxidation processes

R – radius of bubble

\dot{R} – first derivative of the bubble's radius with respect to time

\ddot{R} – second derivative of the bubble's radius with respect to time

μ – viscosity

σ – surface tension

ρ – density of fluid

$(p-p_0)$ – pressure difference between compression and expansion cycles

P_B – critical pressure

P_h – ambient hydrostatic pressure

R_e – radius of cavity

F – frequency

$p_\infty(t)$ – pressure of the liquid far from the bubble

$p_L(R)$ – liquid's pressure just outside the bubble wall

R_{\max} – maximum radius of the bubble obtained just before collapse

P – gas's pressure in the bubble at its maximum size

P_m – liquid's pressure at transient collapse

γ – ratio of specific heats of the gas (or gas vapor) mixture

T_0 – ambient (experimental) temperature

T_{\max} – maximum temperature developed at the moment of bubble collapse

P_{\max} – maximum pressure developed at the moment of bubble collapse

))) – ultrasound

A – absorbance

$\varepsilon(\lambda)$ – molar absorption coefficient at λ

c – molar concentration

l – absorption path length

E_a, E_a^* – activation energy and activation energy for the $R \rightarrow P$ transformation in the excited state

R, R^* – substrate and substrate in the excited state, respectively

P, P^* – product and product in the excited state, respectively

C, PC – thermal catalyst and photocatalyst, respectively

IUPAC – International Union of Pure and Applied Chemistry

IFET – interfacial electron transfer reactions

SC – semiconductor

e^- – electron

h^+ – hole
 λ – wavelength
US – ultrasound
 $h\nu$ – energy of photon
VB – valence band
CB – conduction band
M – metal
D – (sacrificial) electron donor
A – (sacrificial) electron acceptor
 n – number of electrons (holes)
XPS – X-ray photoelectron spectroscopy
XRD – X-ray diffraction
UV-vis – ultraviolet-visible spectroscopy
HRTEM-EDS – high resolution transmission microscopy with energy dispersive spectroscopy
SEM-EDS – scanning electron microscopy with energy dispersive spectroscopy
EDXRF – energy dispersive X-ray fluorescence
ICP-MS – inductively coupled plasma mass spectrometry
SPD – sonophotodeposition
PD – photodeposition
SD – sonodeposition
UI – ultrasound-assisted wet impregnation method
Ze – zeolite Y
TiO₂/ZeUI – TiO₂ supported on zeolite Y by using the ultrasound-assisted wet impregnation method
TiO₂ P90 – commercial TiO₂
Pd/P90/SPD – palladium deposited on commercial TiO₂ by the sonophotodeposition method
Fe/TiO₂/ZeSPD – iron deposited on self-prepared TiO₂/Ze by the sonophotodeposition method
 r_0 – initial reaction rate
 V_o – oxygen vacancy
Me⁰/semiconductor – metal deposited on semiconductor
Me⁰/Me_xO_y/semiconductor – metal and metal oxide deposited on semiconductor
Me_xO_y/semiconductor – metal oxide deposited on semiconductor
UV-vis-IR – spectrum of 150 W Xe Hamamatsu lamp: ultraviolet-visible-infrared
BA – benzyl alcohol
BHA – benzaldehyde
PhOH – phenol
VOCs – volatile organic compounds

ACN – acetonitrile

OxA – oxalic acid

Me(acac)_x – acetylacetonate metal salt precursor

LSPR – localized surface plasmon resonance

TOF – turnover frequency

SMSI – strong metal–support interaction effect

P_L – acoustic power

E^0 – reduction potential

C – conversion

S – selectivity

1. Introduction

Sonochemistry and photochemistry in heterogeneous solutions are two specialized disciplines that are combined under sonophotodeposition. Their crosslinking provides some specific reaction conditions and gives a chance for solving problems whose solutions are beyond the scope of a single discipline. In this sense, sonophotodeposition is a classic example of interdisciplinary research, which has become a natural aspect of doing science in the last few decades. It has proved to be a very powerful tool, facilitating and broadening research and enabling us to cross borders and obstacles.

To provide a background for the scientific papers, the introductory part of this dissertation has the following layout: First, fundamental knowledge about sonochemistry is provided in Subsection 1.1; factors affecting cavitation are briefly discussed in Subsection 1.2; physical and chemical effects generated by acoustic cavitation in liquids are described in Subsection 1.3; examples of the application of ultrasound in the synthesis of different materials are presented in Subsection 1.4; general assumptions of photochemistry, with emphasis on the photodeposition method, are presented in Subsection 1.5; and the effects of conjunction between sono- and photochemical irradiation are analyzed in Subsection 1.6.

1.1 Theory of sonochemistry

Sonochemistry describes chemical processes that are initiated by ultrasound in liquids. Ultrasound refers to sound waves in the frequency range of 20 kHz to 500 MHz, which cannot be detected by the human ear [1]. In sonochemistry, low-frequency and high-intensity (in kHz) ultrasound is applied because it alters the medium through which it passes. On the other hand, high-frequency and low-intensity (in MHz) ultrasound is typically used in medicine because it has a non-destructive nature and does not alter the body medium it goes through [2]. Ultrasonic energy has so far merited a wide application in homogeneous and heterogeneous chemistry because it enhances and promotes the reaction rate and mass transfer in a variety of reacting systems [3]. Moreover, it offers mild reaction conditions, eliminates the necessity of use additional costly solvents, reduces the number of synthesis steps, permits the use of cheaper and lower purity reagents, and can influence the activity of a catalyst [2]. All these facilities make the use of ultrasound very attractive for the synthesis of nanomaterials in environmental remediation (AOPs), green organic synthesis, and many other applications, although a large-scale remains operation out of reach so far [4-6].

It is known that the effects of ultrasound action in liquids are generated by cavitation bubbles and may have a chemical as well as a physical/mechanical nature [2]. Following this

discovery, understanding the cavitation phenomenon in liquids is necessary to fully learn sonochemistry and know its applications [7]. The phenomenon of cavitation has been known since 1895, when Thornycroft and Barnaby observed erosion of the propeller of their submarine HMS Daring [2, 8]. This observation, however detrimental, aroused curiosity and provoked further research. In a short time, in 1917, Lord Rayleigh published the first mathematical model describing cavitation in an incompressible liquid [1, 9]. However, the discoveries of Loomis et al. in 1927 [2, 10, 11] revealing the chemical and biological effects of ultrasound, and later on of Brohult in 1937 [1, 12], who reported degradation of bio- and synthetic polymers, were an impulse for intensive research in this area. The formation of radicals as a result of cavitation was discovered by Weiss in 1944; this is still one of the most basic concepts of sonochemistry [2, 13]. In the 1950s, the first computer calculations modelling of a cavitation bubble was done by Noltingk and Neppiras [14]; Schulz and Henglein [15] reported the sonolysis of organic liquid, while Elder et al. [16, 17] explained the ultrasonic cleaning effect in heterogeneous systems. In the 1960s, the sonochemical effects on biological systems were published, and the physical effects of ultrasound in liquid started to be studied [2]. The number of publications in this area increased dramatically from the 1980s, when the term 'sonochemistry' was used for the first time by Neppiras [18], and Makino et al. detected and radicals during sonolysis of water using spin trapping agents and electron spin resonance measurements [19, 20]. Since then, sonochemical research has developed rapidly, with a number of books and research articles available nowadays in the literature, and conferences and meetings being organized worldwide dedicated to this topic.

Cavitation is produced in liquids as a result of pressure changes that are formed when ultrasound travels through the liquid, creating low- and high-pressure regions due to periodic compression and expansion/rarefaction cycles [7, 21]. During the expansion period, when the pressure is sufficiently reduced (negative pressure overcoming the liquid's tensile strength), microbubbles filled with vaporized liquid or gas previously dissolved in liquid are formed. Two types of microbubbles can be formed: Some are stable at their average size during various cycles, and others are transient, growing to a certain size and then violently collapsing during the compression cycle [3]. The bubbles' implosion is shorter than $1\mu\text{s}$ and creates high local pressures above 1000 bar and temperatures above $5000\text{ }^{\circ}\text{C}$ with extraordinary heating and cooling rates inside the bubbles (so-called hot spots) [22]. The creation of such extreme conditions may induce chemical and physical effects in the liquids, which are capable of promoting many chemical reactions and physical processes [3, 7]. Cavitation, often termed as 'cold boiling', can be succinctly described as the formation, growth, and implosive collapse of bubbles in liquids, as is schematically shown in Figure 1.1.

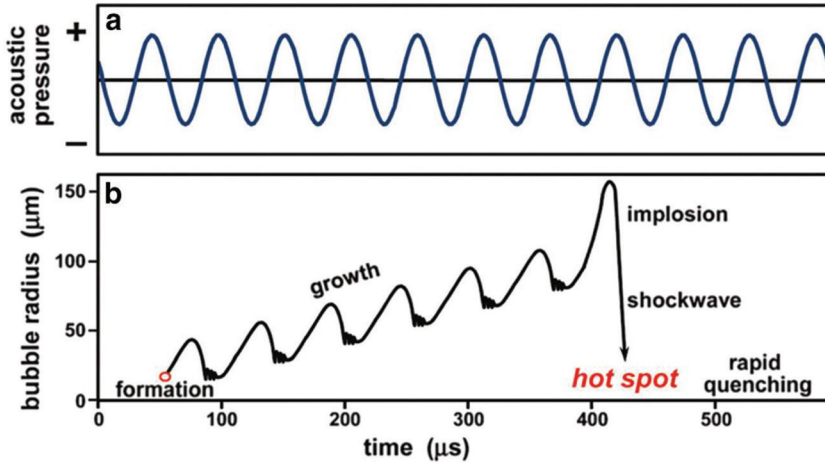


Figure 1.1 Schematic illustration of the process of acoustic cavitation. (a) Periodic compression and expansion cycles in the liquid exposed to ultrasound. (b) The formation, growth, and implosive collapse of bubbles in a liquid irradiated with high-intensity ultrasound. Reproduced from [23] with permission of The Royal Society of Chemistry.

The formation (nucleation) of bubbles in liquids is an inducing step of cavitation and can occur according to three different mechanisms [1]. First, gas molecules dissolved in liquids initiate bubble formation. They can be trapped in crevices of container walls, in motes, or on hydrophobic dust particles. They expand during the negative pressure cycle of the ultrasonic wave and are separated from the crevices when they have enlarged enough. Then a free gas bubble appears in the liquid, and the empty crevices are filled in with dissolved gas molecules, repeating the whole cycle [24]. Another mechanism assumes that bubble nuclei, which are inherently present in liquids, grow in the acoustic field by coalescence or rectified diffusion. They are protected from dissolution when they are covered with organic materials, surfactants, or hydrophobic impurities presented in the liquid [25, 26]. Nucleation can also be induced by fragmentation of the already-active bubble provoked by asymmetric collapse and shape instability. As a result, several new bubbles are formed, which again can act as nuclei hubs for cavitation [27, 28].

Bubble formation was first described by Rayleigh, but since Plesset added the effects of viscosity and surface tension, a basic model for acoustic cavitation is known as the Rayleigh-Plesset equation (1.1) [7]:

$$R\ddot{R} + \frac{3}{2}(\dot{R})^2 + \frac{4\mu\dot{R}}{R} + \frac{2\sigma}{\rho R} = \frac{(p-p_0)}{\rho} \quad (1.1)$$

where R is the radius of the bubble as a function of time, \dot{R} and \ddot{R} are respectively the first- and second-order time derivatives of the bubble's radius, μ is the viscosity, σ is the surface tension, ρ is the density, and $(p-p_0)$ is the pressure difference between compression and expansion cycles. The motion of a spherical bubble under a time-varying pressure field in an

incompressible liquid is described by this equation [1]. The acoustic pressure, generated in the liquid when an acoustic field is applied, provokes the oscillations of the molecules, varying the average distance between them [29]. During the expansion period of the acoustic pressure, the distance between molecules increases, and when it goes beyond the critical value, when intermolecular forces are not able to hold the molecules together, the liquid breaks down, creating voids or cavities. However, this requires a sufficiently large negative pressure to be applied. Equation 1.2 permits us to calculate the critical pressure P_B required to create a cavity [30]:

$$P_B \sim P_h + \frac{0.77 \sigma}{R_e} \quad (1.2)$$

where P_h is the ambient hydrostatic pressure present in the medium, σ is the surface tension of the liquid, and R_e is the radius of the cavity; the equation is valid when $2\sigma/R_e \ll P_h$. For instance, the critical pressure calculated for water was in the order of 10.000 bar, but in practice, cavitation does not need such high pressures to be applied, thanks to the presence of weak spots (e.g., gas nuclei, small particle contamination) in liquids, which lower significantly (even up to several bar) the tensile strength of the liquid [29]. Also, the generation of such extreme negative pressure would not be possible, as the most powerful ultrasound generators are currently unable to produce it [22]. Once the cavity/bubble is formed, it grows to a certain size, depending especially on the applied amplitude and frequency of the ultrasonic field [1]. When high-intensity ultrasound is applied, the bubble can grow rapidly in the course of a single cycle. In contrast, a slow bubble growth occurs over the course of several cycles when low-intensity ultrasound is applied. The bubble can expand till it reaches a critical size, when it absorbs energy from ultrasound in the most efficient way. This size depends on the ultrasound frequency—for instance, at 20 kHz the bubble can grow up to 170 μm —and can be theoretically predicted by a simple Minnaert's equation [1]: $F \times R \approx 3$, where F is the frequency [Hz] and R is the radius of the bubble [m] [22]. The growth of the bubble in the ultrasound field occurs in the process of rectified diffusion, which is schematically presented in Figure 1.2. It is composed of two effects described as 'area' and 'shell' effects. The 'area' effect describes the growth of the bubble's size during expansion and compression cycles of the sound wave. When the negative pressure goes through the liquid, the dissolved gases and vapor molecules of the solvent are taken inside the bubble. In contrast, during the compression cycle, when the positive pressure goes through the liquid, the gas and vapor molecules are expelled from the bubble into the surrounding liquid, reducing the bubble's mass. The growth of the bubble is possible over several cycles because less material is expelled than is taken in. On the other hand, the 'shell' effect describes how the thickness of the liquid shell around the bubble changes with different cycles of the ultrasound wave. The thickness of the liquid shell increases during the compression cycle. At the same time, the concentration of gases decreases in the liquid shell, producing a gradient gas concentration between the interface and the bulk. The rate of

expulsion of the gas from the bubble is proportional to the concentration of dissolved gases in the liquid shell, and when it decreases, the mass transfer of the gas expelled from the bubble also gets lower. This situation gets reversed during the expansion cycle, when the thickness of the liquid shell decreases, the gas concentration increases, and more material diffuses inside the bubble, resulting in the bubble's growth over several cycles [1]. After reaching its critical size, the bubble cannot absorb energy from the ultrasound waves and can no longer sustain itself; it therefore implodes. The compression of gases and vapors inside the cavity generates an extreme heating. The temperature of the liquid also rises, surrounding the cavity and creating a local hot spot. There have been many theoretical and experimental attempts to calculate the exact temperatures and pressures during the implosion of cavities, but the difficulty lies in measuring a very quick dissipation of heat. The experimental works performed by Suslick and his collaborators discovered two distinct temperature areas, around 5500 °C inside the cavity and 2100 °C in the surrounding liquid [22]. The pressures are even more difficult to determine; therefore, predictions with different accuracies, from hundreds to thousands of atmospheres, can be found in the literature.

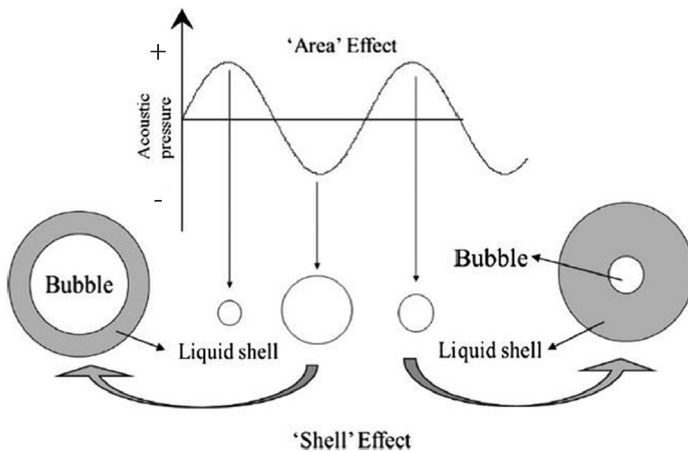


Figure 1.2 Schematic description of the bubble's growth in an acoustic field by 'area' and 'shell' effects in the process of rectified diffusion. Reproduced from [31] with permission of John Wiley & Sons, Inc.

Cavitation can occur in two different ways, transient and stable [29]. The time in which the cavities exist determines which form of cavitation takes place in the liquid medium. Stable cavities can oscillate for many acoustic cycle before collapsing or never collapse, whereas transient cavities can exist for one or at most a few acoustic cycles [2]. Stables cavities are formed at low intensities ($1-3 \text{ W cm}^{-2}$), are filled with gas or some vapor and oscillate around a mean radius. They do not grow, because the rates of mass transfer during the expansion and compression cycles are equal. Their motion in the acoustic field is described by equation (1.3) [2]:

$$R\ddot{R} + \frac{3}{2}(\dot{R})^2 = \frac{1}{\rho} [\rho_L(R) - p_\infty(t)] \quad (1.3)$$

where $p_{\infty}(t)$ is the pressure of the liquid far from the bubble, ρ is the density of the fluid, \dot{R} and \ddot{R} are respectively first- and second-order time derivatives of the bubble's radius with respect to time, and $p_L(R)$ is the liquid pressure just outside the bubble wall. In contrast, transient cavities are formed at intensities $> 10 \text{ W cm}^{-2}$; they are voids or vapor-filled, and during their short existence they grow to at least double their initial size before collapsing and disintegrating into smaller bubbles [29]. The nature of this collapse is violent, when the permanent gas cannot diffuse into a bubble and act as a cushion. Then, their motion is given by equation (1.4) [18]:

$$R\ddot{R} + \frac{3}{2}(\dot{R})^2 = \frac{1}{\rho} \left[P \left(\frac{R_{\max}}{R} \right)^{3\gamma} - P_m \right] \quad (1.4)$$

where R_{\max} is the maximum radius of the bubble obtained just before collapse, P is the gas pressure in the bubble at its maximum size, P_m is the liquid pressure at transient collapse, γ is the ratio of specific heats of the gas (or gas vapor) mixture, ρ is the density of the fluid, and \dot{R} and \ddot{R} are respectively first- and second-order time derivatives of the bubble's radius with respect to time. The growth of the bubble is an isothermal process, which changes into adiabatic during its collapse. The maximum temperature and pressure can be calculated according to equations 1.5 and 1.6, neglecting the surface tension and viscosity of the fluids as well as assuming that the bubble is filled with an ideal gas [2]:

$$T_{\max} = T_0 \left[\frac{P_m(\gamma - 1)}{P} \right] \quad (1.5)$$

$$P_{\max} = P \left[\frac{P_m(\gamma - 1)}{P} \right]^{\gamma/(\gamma - 1)} \quad (1.6)$$

where T_0 is the ambient (experimental) temperature, P is the gas pressure in the bubble at its maximum size, P_m is the liquid pressure at transient collapse, γ is the ratio of specific heats of the gas (or gas vapor) mixture. In case the bubble contains vapor as well as gas, its collapse is cushioned, and the values of T_{\max} and P_{\max} are lower. The collapse of transient cavities produces chemical effects in the sonicated liquids. However, stable cavities can be transformed into transient ones, contributing to the same chemical effects [2, 29].

Cavitation affects homogeneous and heterogeneous solutions differently [7]: homogeneous systems based on direct cavitation effects (chemical effects), which makes such systems easier to study. The physical effects are rather subsidiary without having a great impact on the solution. In contrast, in heterogeneous systems, the physical effects are dominant, which makes such systems difficult to study, as these effects are random and uncontrolled. More details about physical and chemical effects of ultrasound in liquids are provided in Section 1.3. All systems studied in this dissertation in the sonophotodeposition process are strictly heterogeneous.

1.2 Factors affecting cavitation

There are a number of parameters in irradiated systems that can significantly affect cavitation in liquids, making the whole process quite complex [29]. In this section, I briefly discuss what these parameters of local environment are and how they can influence the initiation and intensity of the cavitation process.

a) Solvent. The way the solvent affects the formation of cavities is reflected in the values of its physical parameters, such as viscosity, vapor pressure, and surface tension [29, 32]. The use of solvents characterized by low surface tensions, low viscosities, and high vapor pressures helps to reduce the cavitation threshold and to form cavities, because it is easier to overcome the natural cohesive forces in such a liquid. However, under these conditions, the intensity of cavitation is reduced. In order to increase the intensity of cavitation, the use of solvents with the opposite characteristics (high surface tension, high viscosity, and low vapor pressure) is required, which in consequence also increases the cavitation threshold [33].

b) Dissolved gases. As a general rule, the presence of dissolved gases in liquids facilitates the initiation of cavitation, because they form the nuclei for cavitation events [2, 3]. However, the exact way dissolved gases can affect cavitation depends on their physical properties: heat capacity, thermal conductivity, and solubility in liquids. Gases with a high specific heat ratio (γ) generate more intense cavitation; therefore, higher temperatures and pressures are released when monoatomic gases with large γ values are employed [29]. Thermal conductivity of the gas is taken into consideration, although the bubble's collapse is described as adiabatic, because a small amount of heat can be transferred to the bulk. Therefore, for gases with high thermal conductivity, the heat loss due to thermal dissipation is also high, resulting in the reduction of the temperature released during collapse [2, 3]. Gases with a high solubility are better able to diffuse into the bubble; to form a large number of nuclei in the liquid, reducing the cavitation threshold and the intensity of the shockwave released on the bubble collapse; and to re-dissolve into the liquid medium, affecting the intensity of the collapse [29]. The increase in gas concentration in liquid reduces the cavitation threshold and the cavitation intensity because of an increasing number of gas nuclei and an increased 'cushioning' effect in the microbubble, respectively [29].

c) Frequency. As the frequency of ultrasound increases, the expansion and compression pressure cycles are shortened [29]. As a result, the cavitation effect is reduced at high frequencies, because the negative pressure formed during the expansion cycle is often not sufficient in duration and intensity to initiate cavitation. Even though the bubble is formed, the compression cycle can also be too short for its collapse. Therefore, cavitation at higher frequencies produces small bubbles with uniform size distribution and is less violent [34]. However, it has been observed in many experiments that reaction rates are enhanced

at higher frequencies [35-37]. This observation led to the conclusion that, although the cavitation is less violent, there are more cavitation events, which means more opportunities for the production of free radicals facilitating the reactions [38]. Also, the shortened lifetimes of bubbles allowed the radicals to escape from the cavitation site to the bulk, increasing their availability for reaction [37, 39]. On the other hand, at lower frequencies, cavitation is more violent, resulting in the formation of higher localized temperatures and pressures [2, 3].

d) Power. The influence of the increasing power delivered to the system is generally reflected by increasing the reaction rate up to a critical value above which the reaction rate falls down. Such effect was explained by the formation of a dense cloud of cavitation bubbles in the tip probe area at high power, which possibly blocks the transmission of energy to the system [40, 41]. Also, the bubble dynamics may be disrupted at the moment of too drastic power increase; therefore, the optimum power level must correlate with the operating frequency in order to balance the bubble's growth [42, 43].

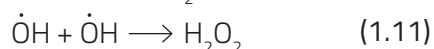
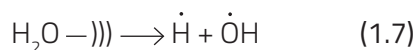
e) Ambient temperature. The ambient temperature has the opposite effect on the sonochemical reactions than on chemical reactions in general [2, 3]. This means that an increase in the reaction temperature results in decreasing the reaction rate. This is correlated with the increase in the solvent vapor pressure in the liquid, which results in easier bubble formation. However, at high vapor pressure, more vapor diffuses into the bubble, cushioning the implosion of bubbles and hence reducing the amount of ultrasonic energy produced upon cavitation. On the other hand, at lower temperatures, the bubbles contain more gas, and the bubbles' collapse is more violent. Despite the above explanation, there were cases reported in the literature in which the increase in temperature was followed by an increase in the reaction rate up to a critical amount of vapor in the bubbles, when the cushioning effect started to dominate the system [44, 45].

f) Ambient pressure. The increase in the ambient pressure in the reaction system is generally followed by the increase in the intensity of bubbles' collapse because under such condition, the vapor pressure in the liquid is reduced [2]. However, too much pressure can increase the cavitation threshold to the point that the bubbles cannot be produced or are produced in such small quantities that the overall reaction rate is significantly reduced [46, 47].

1.3 Physical and chemical effects of ultrasound

The acoustic field cannot interact directly with the molecular species because the ultrasonic radiation is not strong enough to break the chemical bonds [48]. However, the bubbles' collapse is the source of different chemical and physical effects in liquids, which can initiate different processes. According to the 'hot-spot' concept, this collapse produces three reaction zones: inside the bubbles, at the gas-liquid interface, and in the bulk liquid [49].

The schematic representation of these zones with detailed reactions occurring in each one is presented in Figure 1.3a and 1.3c. Zone 1 inside the bubbles contains a mixture of gas and vapor, and the gas-phase reactions initiated in this region (hot spot) are categorized as the primary sonochemistry (Fig. 1.3b) [7]. The harsh conditions generated in zone 1 can cause bond breakage and/or dissociation of water and other vapors and gases to produce reactive species. Next, they can either react with each other, forming new molecules and radicals, or diffuse into the bulk liquid, where they serve as oxidants [3]. Zone 2 is the liquid shell surrounding the collapsing bubble, defined as the transition region in which less volatile components are present. Herein, pyrolysis (at high solute concentrations), as well as free-radical reactions (at low solute concentrations), can take place [50]. The bulk solution at ambient temperature forms zone 3. All chemistry occurring outside the core region of the bubbles in the liquid phase is classified as the secondary sonochemistry and results from the movement of radicals produced in the cavities or at the interface [49]. These radicals can therefore undergo some secondary transformations, reacting with solutes present in the surrounding liquid [50]. Different parameters of the irradiated systems (as those discussed in Subsection 1.2) can influence the magnitude of reactions in each zone [2]. The sonolysis of water is a well-defined and complex process that involves primary and secondary reactions, as shown below by equations (1.7–1.11) [20]. First, the highly reactive hydrogen and hydroxyl radicals are formed, which diffuse to the bulk solution, initiating secondary sonochemical reactions, such as oxidation, reduction, and hydroxylation of organics, among others.



When non-aqueous liquids are sonicated, radical species are also formed, which can further initiate recombination, disproportionation, elimination, and redox reactions [50-52]. Thus, the chemical effects of ultrasound action on liquids rely primarily on the formation of free radicals or excited states, which therefore can significantly enhance the reaction rates [41, 53].

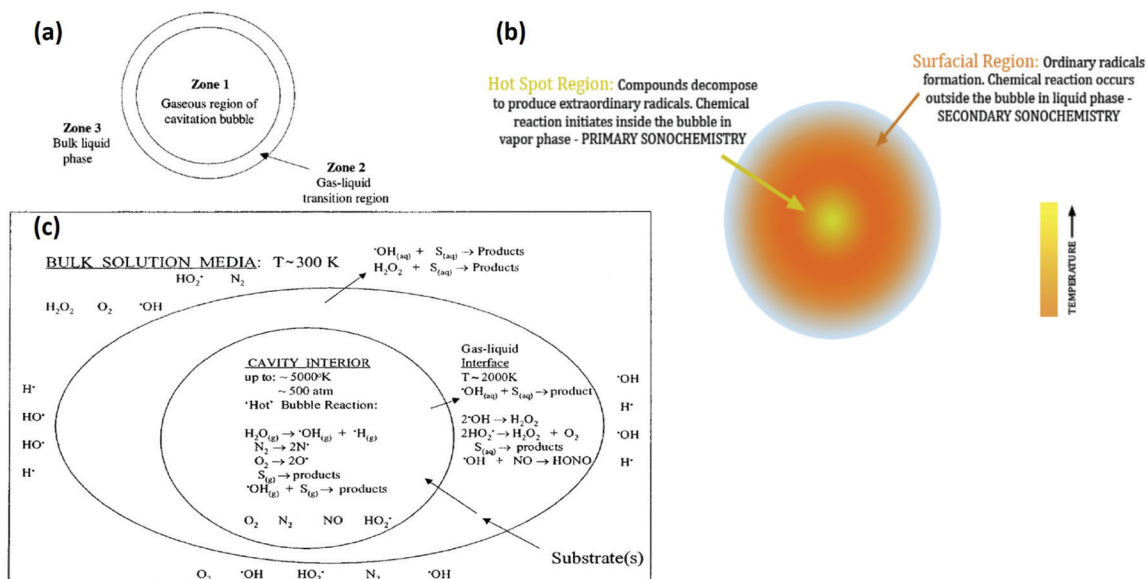


Figure 1.3 Chemical effects produced in liquid divided in three reaction zones: (a) schematic view reprinted with permission from [2] (copyright (1999) American Chemical Society); (b) visual view reprinted from [7] with permission from Elsevier; (c) detailed view reprinted with permission from [3] (copyright (2001) American Chemical Society).

Another effect generated during cavitation is the light emission from the imploding bubbles, known as sonoluminescence [54]. There are two forms of sonoluminescence: multi-bubble, when a large number of bubbles emit light, and single-bubble, when only one stably oscillating bubble is the source of light [55]. The intensity of sonoluminescence depends on various parameters of the irradiated system, primarily on the physical characteristics of liquid, dissolved gas, acoustic frequency, and pressure [1]. There are two theoretical models explaining the process of sonoluminescence. One assumes the emission of light from the center of the bubble, where plasma is generated by the shock-wave convergences [56]. Another one is the quasiadiabatic compression model, in which sonoluminescence is provoked by radiative recombination of electron-ion and electron-atom bremsstrahlung (breaking radiation) [57, 58]. The intensity of light emission can be enhanced by the addition of luminol, as a result of its reaction with $\dot{\text{O}}\text{H}$ radicals. Thus, such emission is referred to as sonochemiluminescence and is used to indicate chemically active regions in sonoreactors [59, 60]. Microstreaming, agitation, turbulence, microjetting, shockwaves, etc. are the physical effects derived from the collapsing bubbles [30]. They can enhance the reactivity of the system by promoting mixing or mass and heat transfer in the liquid and intimate contact between reagents, as well as causing velocity gradients, resulting in extensive shear stress. In heterogeneous systems, shockwaves and microjets can initiate some structural changes in the materials, such as fragmentation, deformation, exfoliation, and erosion [7]. Shockwaves are the result of symmetric collapses of bubbles, when the compression of the surrounding liquid is released into the liquid medium [23]. The step by step formation of a spherical shockwave generated from a laser-induced

collapsing bubble is shown in Figure 1.4 B [61]. Such a shockwave can, in water, reach velocities of 4 km s^{-1} and generate pressures of 60 kbar. An asymmetric collapse of bubbles may occur near a solid surface, because the bubbles' surroundings are inhomogeneous, which induces asphericity inside the bubbles and results in the formation of microjets (see the Figure 1.4 A) [62]. The velocity of such a jet is lower and can reach 0.1 km s^{-1} in water.

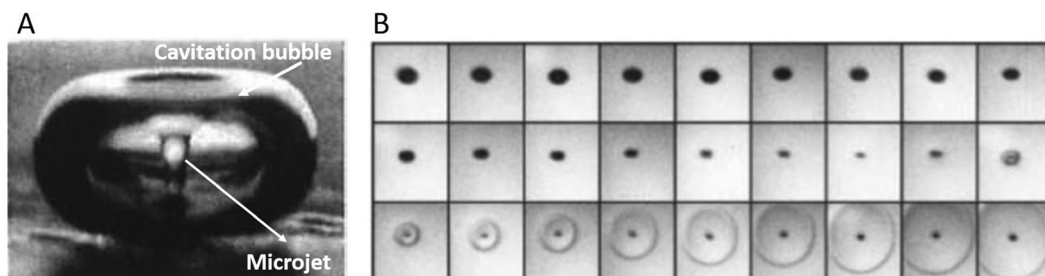


Figure 1.4 The formation of (A) a microjet when a bubble collapses near a solid surface, adapted from [63] with permission from Elsevier, and (B) a spherical shockwave registered from a laser-induced collapsing bubble, reproduced from [61] with permission of the Royal Society.

Besides the 'hot-spot' theory, three other explanations for the formation of sonochemical events have been developed: electrical theory, plasma discharge theory, and super-critical theory [3]. The electrical theory, formulated by Margulis postulates the formation of enormous electrical field gradients in the bubble, which are capable of causing bond breakage and initiating chemical activity [64, 65]. The plasma theory, proposed by Lepoint and Mullie, is also based on the formation of intense electrical fields; however, they were looking for the origin of cavitation in corona-like discharges and the formation of microplasmas inside the bubbles [66]. In the supercritical theory, by Hoffman et al., the formation of temperature and pressure conditions beyond the critical conditions of water ($374 \text{ }^\circ\text{C}$, 221 bar) in the bubble–liquid interface is suggested [67]. Nevertheless, the hot-spot theory is the most frequently adopted explanation in studies for the sonochemical reactions [3].

1.4 Ultrasound application in the synthesis of nanomaterials

The variety of possible applications of ultrasound in nanomaterials synthesis is perfectly seen in Figure 1.5. Such a wide range of possibilities is a consequence of the extreme conditions produced during acoustic cavitation [23]. The examples of sonochemically produced materials presented in this section are only a small part of those available in the literature and are meant to show the extensive possibilities of this methodology.

Materials Applications of Ultrasound

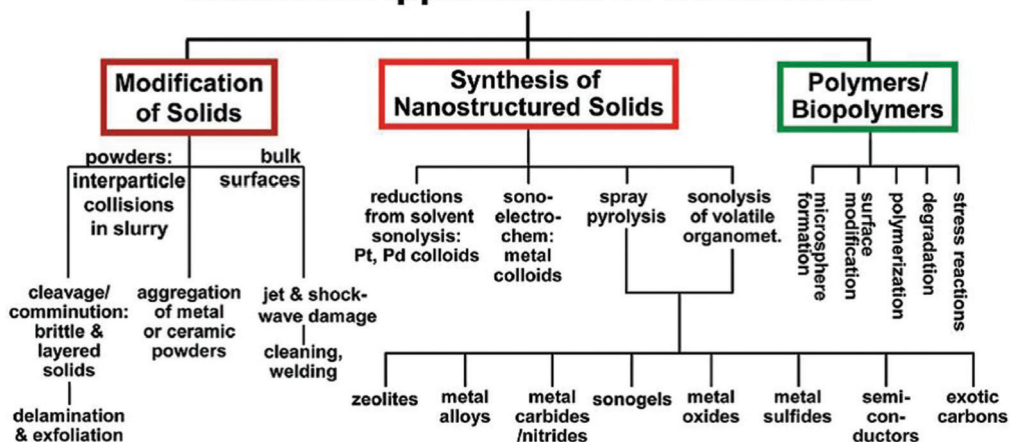


Figure 1.5 The application of ultrasound in the synthesis of nanomaterials. Reproduced from [23] with permission of The Royal Society of Chemistry.

In the graph below (Figure 1.6), it is seen that sonochemistry is a fast, high-energy, and high-pressure process in comparison with traditional synthesis methods. These conditions allow the synthesis of many materials that normally require high temperatures and pressures as well as long reaction times. Sonochemistry permits their synthesis on the benchtop in a room-temperature liquid [23].

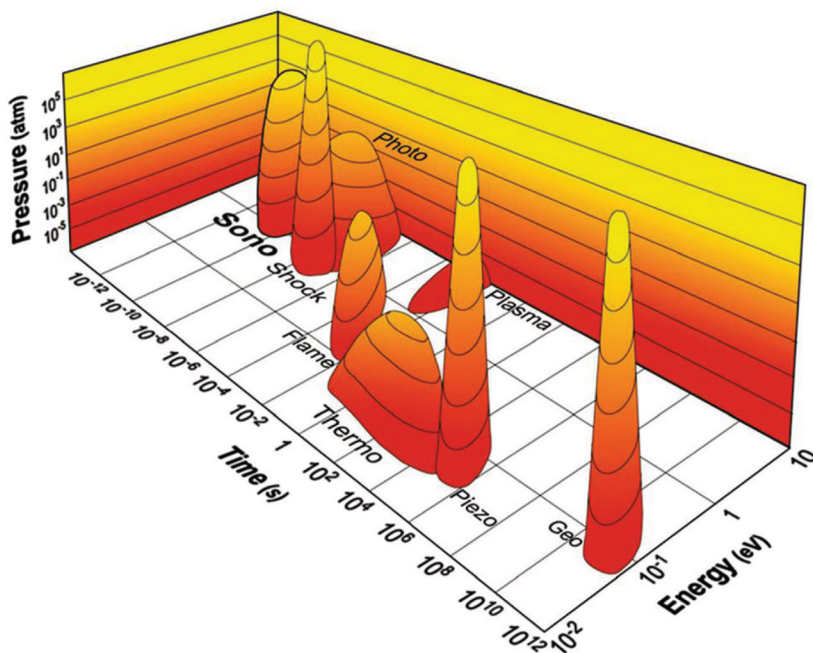


Figure 1.6 The chart presents the 'islands of chemistry' as a function of time, pressure and energy. Reproduced from [68] with permission of Annual Reviews.

In the synthesis of nanostructured materials, such chemical and physical effects of ultrasound are used, which provides a wide range of possibilities in their compositions and structures [4]. According to the type of the effect exploited in the formation of nanomaterials, they could be classified into four groups, as proposed in the review work done by the Suslick's group [23]. The first group includes materials prepared from volatile precursors in non-volatile solvents in the reactions initiated in the hot-spot nuclei of the bubble (primary sonochemistry). The harsh conditions inside the bubble favor dissociation of metal-carbonyl bonds in volatile organometallic compounds (e.g., $\text{Fe}(\text{CO})_5$), releasing metal nanoparticles. The short cavitation time can result in the formation of amorphous nanoparticles, because of too-rapid cooling and a short crystallization period [69]. Such obtained metal atoms are very reactive, and adding surfactants, supports, or other reactants to the reaction mixture leads to the formation of a variety of metallic nanomaterials (see Figure 1.7) [70].

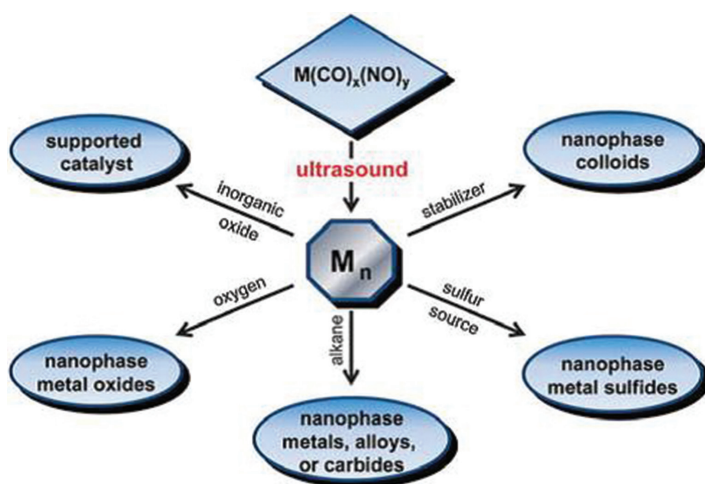
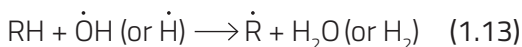
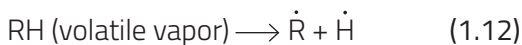


Figure 1.7 A variety of nanostructured materials that can be obtained from sonication of volatile organometallics. Reproduced from [70] with permission of Annual Reviews.

In the second group, a different type of nanomaterials can be prepared from non-volatile precursors dissolved in volatile solvents [23]. Herein, highly reactive species with reductive properties are produced in cavitation events from volatile solvents. Next, they can react in the liquid phase with non-volatile species, according to the following reactions 1.12–1.15 (secondary sonochemistry) [4]:



Such reactions have some advantages in comparison with traditional processes, including fast reduction rates, no need to add strong reducing agents, and the formation of small nanoclusters when appropriate stabilizers are present [23]. This method usually leads to the formation of well-crystallized materials. The literature provides many examples of sonochemical reduction of noble metals precursors, including the formation of monometallic as well as bimetallic core-shell nanostructures [71-74]. However, it is not only limited to the noble class of materials. Various metal oxides, hydroxide nanoparticles, and metal chalcogenides were also prepared using this method by adding oxygen or chalcogen source to the sonicated solution [75-79]. The use of structuring agents makes it possible to produce not only spherical, but also differently-shaped materials, e.g., nanowires, nanocubes, nanorods or hollow spheres etc. [75, 80-83].

The third group includes materials formed under the physical effects of ultrasound. The high-speed jets and shockwaves, as well as other effects deriving from them, can significantly influence the formation of nanomaterials [23]. Some examples of how the physical effects can be exploited in the synthesis procedure are listed below. Both single- and few-layered materials can be exfoliated in the liquid phase by sonication, and the reaction rate of intercalation of guest substances into layered materials can be significantly increased under ultrasonic irradiation [84-88]. The schematic illustration of this process is presented in Figure 1.8. Similarly, diffusion of dopant ions into the spherical nanoparticles can also be promoted by ultrasound [89, 90].

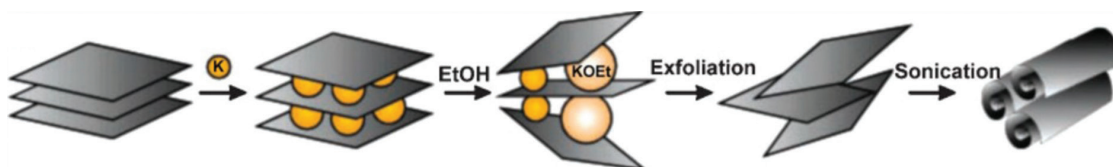


Figure 1.8 Schematic illustration of intercalation and exfoliation process in preparation of carbon scrolls. Adapted from [85]. Reprinted with permission from AAAS.

Collisions provoked by ultrasound between particles suspended in liquid slurries are able to improve the properties of the resulting materials (e.g., superconductors) because of the enhancement of intergrain coupling [91-93]. An improvement of anticorrosion surface coatings is a result of direct physical change on the surface of solid materials provoked by ultrasound effects [94]. Sonication is often coupled with traditional synthesis methods in order to improve them. For example, in sol-gel synthesis, ultrasound is able to accelerate the hydrolysis, which results in the formation of metal oxides with narrower size distributions, higher surface areas, and improved phase purity [95, 96]. There are reports showing the effects of ultrasound on the crystallization process; however, the formation of crystals on the micron scale is more common *via* sonochemistry than on the nanoscale [97-99]. Sonication can enhance the crystallization process through increased nucleation, enhanced mass transport to the crystal surface, or the sonofragmentation of larger crystals. The power of ultrasound

can also initiate some mechanochemical reactions in polymers, such as covalent bond scission or the incorporation of chemical groups, so called 'mechanophores', into a polymer chain [100, 101]. The application of sonochemical deposition in the fabrication of homogeneous coatings [102-105] and core-shell nanocomposites [75, 106, 107] has also been widely reported in the literature. The physical effects in this sonochemical process help to obtain a uniform coating, as well as to reduce the reaction time. Manipulating with the sonication time enables tuning of the properties of coatings [106]. Also, *in situ* deposition of nanoparticles onto different substrates (e.g., silica particles, carbon nanotubes, polymer matrix, titania particles, metal oxides, etc.) was successfully done by using this sonochemical approach [108-116]. However, such application is an example of preparation of materials influenced by both physical and chemical effects [23, 117]. Chemical effects (sonochemically formed radicals) cause the reduction of noble metal nanoparticles, whereas physical effects influence the mechanical properties of the deposits and accelerate deposition time. Another example in which the synergistic role of ultrasound effects was exploited is the preparation of graphene, schematically represented in Figure 1.9 [118]. The physical effects are useful in the formation of single- or few-layered graphene, whereas the chemical effects (radicals derived from the reactive solvent, e.g., styrene) can functionalize these layers.

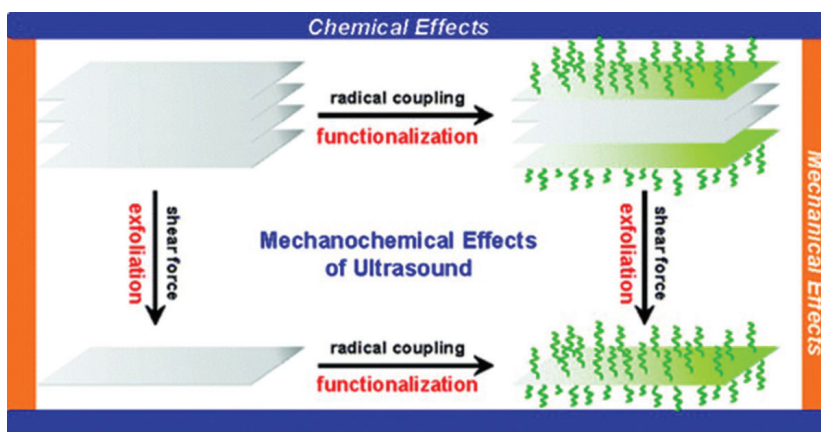


Figure 1.9 A schematic illustration of mechano-chemical effects of ultrasound for the synthesis of polymer-functionalized graphene. Reprinted with permission from [118]. Copyright (2011) American Chemical Society.

Also, in the preparation of protein microspheres, both effects can be used. The combination of the emulsification process (physical effect) with the bonds cross-linking induced by radicals derived from the sonolysis of water (chemical effects) results in the formation of a stable protein microsphere [119]. An interesting—and well-performed in aromatization of methane to benzene—egg-shell structure consisting of $\text{Mo}_2\text{C}/\text{ZSM-5}$ was synthesized by Suslick and Dantsin [120]. In this approach, well-dispersed Mo_2C nanoparticles on the ZSM-5 surface were obtained due to combining physical and chemical effects of ultrasound.

1.5 Principles of photochemistry (photocatalysis), with emphasis on the process of metal (oxide) photodeposition on semiconductor surfaces

Photochemistry describes chemical processes that are initiated by light absorption in liquids [121]. Light-induced chemical reactions, including photosynthesis, are the basis of our life. As a general rule, after absorption of light, a molecule is transformed into the excited state by the movement of an electron from a lower energy orbital to a higher energy orbital. The amount of energy delivered in the quantum of light can be high enough (up to 150 kcal mol⁻¹ for $\lambda = 200$ nm) to provoke a homolytic bond-breaking of C-N, C-C or C-H bonds leading to the formation of new molecular species. The Beer-Lambert law describes the amount of energy that can be absorbed by the molecule, according to formula 1.16:

$$A(\lambda) = \varepsilon(\lambda)cl \quad (1.16)$$

where A is the absorbance, λ is the wavelength, $\varepsilon(\lambda)$ is the molar absorption coefficient at specified λ , c is the molar concentration, and l is the absorption path length. The absorption of light initiates different processes that the molecule in the excited state can undergo. For example, the basic photochemical and photophysical processes for the molecule containing a C-H bond are depicted in Figure 1.10 [121].

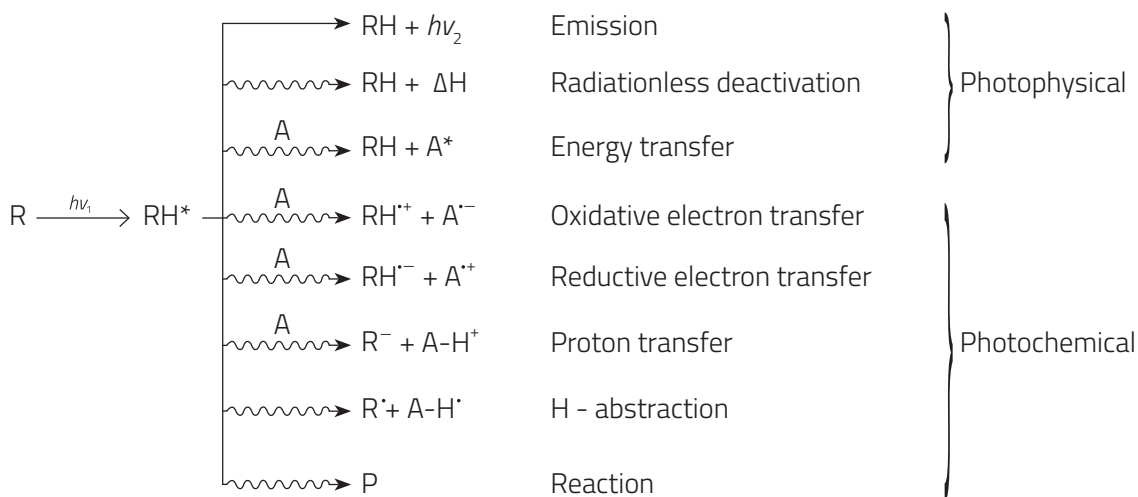


Figure 1.10 Basic primary processes of an electronically excited molecule (wavy arrows indicate non-radiative processes). Reproduced from [121] with permission of John Wiley & Sons, Inc.

The main difference, and also advantage, of the photochemical reaction over the thermal reaction is a low activation energy, E_a , which needs to be supplied in order to convert the substrate into the product. This is directly related to the light absorption and the formation of the excited state of the substrate, as shown in the diagram in Figure 1.11(1). Then, the final product can be formed in two different ways: (i) diabatic, following the thermal potential curve

(the moment of passing from the photochemical to the thermal potential curve is indicated by dotted lines), and (ii) adiabatic, with the formation of the product in its excited state followed by radiative or non-radiative deactivation to the ground state. Similarly, in photocatalytic reaction, light is absorbed by the substance called the photocatalyst, which is involved in the chemical transformation of the reaction partners without being consumed in the process, according to the definition of IUPAC [122]. However, as seen in the reaction diagram presented in Figure 1.11(2), the substrate (R) or a weak substrate–photocatalyst surface complex (R+PC) can also act as an absorbing species. The photocatalytic reaction can also follow diabatic as well as adiabatic reaction pathways, but generally the diabatic path is more common [121].

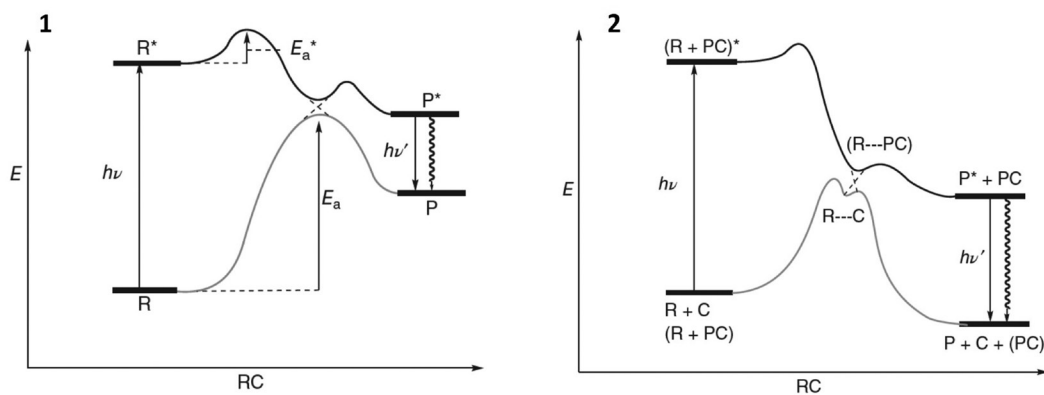
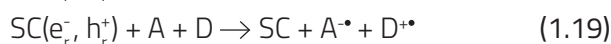


Figure 1.11 Potential energy diagrams of thermal and photochemical reactions of substrate R to product P: (1) stoichiometric, and (2) catalytic, where C and PC symbolize a thermal catalyst and photocatalyst, respectively. Reproduced from [121] with permission of John Wiley & Sons, Inc.

The term semiconductor photocatalysis describes a heterogeneous system in which photosensitization is realized by a solid photocatalyst [121]. The basic reactions taking place after light absorption by semiconductor (SC) particles are summarized in equations 1.17–1.19. First, the reactive electron-hole pair trapped at the surface must be formed (1.17) in order to perform the interfacial electron transfer reactions (IFET) with adsorbed substrates (1.19). Nevertheless, the charge recombination process (1.18) must be slow enough to allow the IFET to proceed.



Generally, the reactions photocatalyzed by the semiconductor proceed with the formation of reduced and oxidized products (1.20), but there is also a rare possibility that these primary redox products can follow intermolecular bond formation to an addition product (1.21 and 1.22) [121].



A pictorial view of photocatalytic reactions on a semiconductor surface is shown below in Figure 1.12 [121]. There are two possible reaction pathways of semiconductor photocatalysis: direct ($h\nu_1$) and indirect ($h\nu_2$). The direct route occurs on the semiconductor surface and is generally a standard mechanism. However, the substrate (when is a dye) can also get excited, injecting the electron into the conduction band (1.12a) or, in rare cases, the hole into the valence band (1.12b). This is possible when the reduction potential of the excited state is equal to or more negative than the conduction band edge or more positive than the valence band edge, respectively [123, 124].

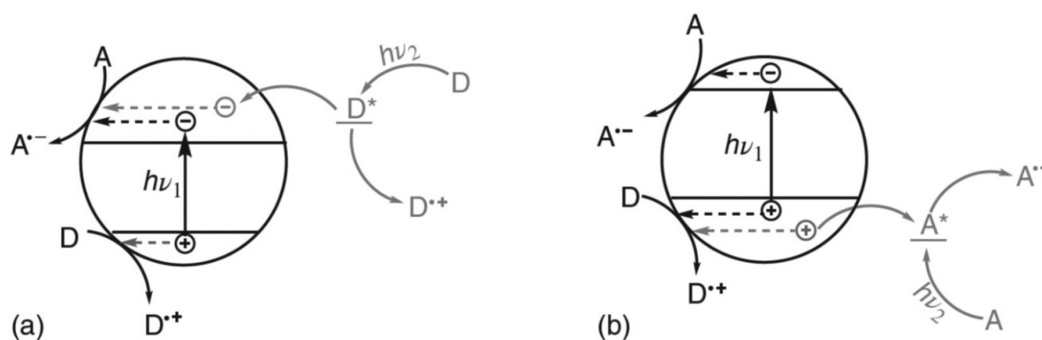


Figure 1.12 (a, b) Direct and indirect semiconductor photocatalysis. Reproduced from [121] with permission of John Wiley & Sons, Inc.

Semiconductor photocatalysis (e.g., with TiO_2) is principally identified with environmental applications, such as water and air treatment processes [125-127]. Meanwhile, this procedure can also be used in the synthesis of materials. Photochemical deposition (photodeposition) is a process that makes it possible to obtain metal or metal oxide nanoparticles on the surface of a semiconducting material (photocatalyst). In order to achieve this, the semiconductor particles need to be illuminated in the aqueous phase solution of metal salt [128]. The use of this method for deposition of metals or metal oxides started to expand intensively since deposition of platinum nanoparticles on the anatase surface was reported by Kraeutler and Bard around 40 years ago [129]. There are two mechanisms, reductive and oxidative, according to which photodeposition can proceed (both are presented in Figure 1.13).

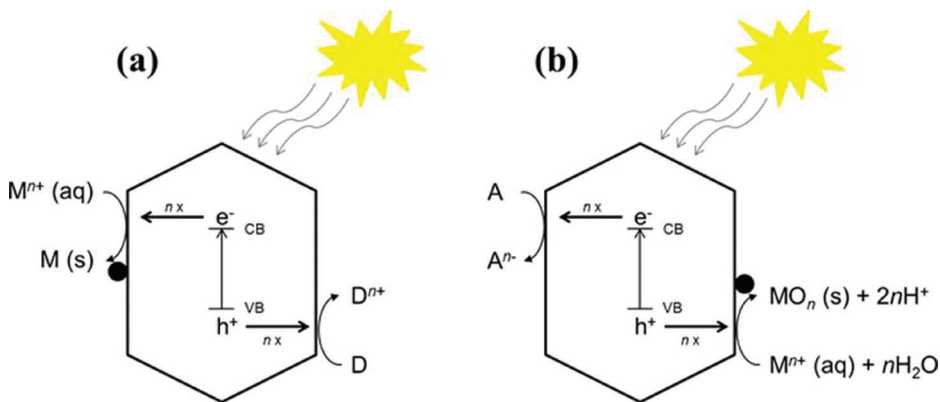


Figure 1.13 Schematic overview of (a) reductive photodeposition and (b) oxidative photodeposition. Reprinted with permission from [128]. Copyright (2016) American Chemical Society.

In reductive photodeposition, metal nanoparticles are deposited on the surface of the semiconductor (following equation 1.23), whereas in oxidative photodeposition, metal oxide nanoparticles are formed (following equation 1.24):



Generally, photodeposition can proceed when two conditions are fulfilled: (i) an adequate value of the reduction/oxidation potential of the metal/metal oxide, referring to the energy band positions of the semiconductor (in detail, a more negative value of the conduction band with regard to the reduction potential of metals, and a more positive value of the valence band with regard to the oxidative potential of metal oxide; some examples of band gap positions of the most common semiconductors and redox potentials for several metals are presented in Figure 1.14); (ii) the rules of carrying out a semiconductor photocatalytic reaction must be completed (energy of photons high enough to promote the photons from the VB to the CB, efficient charge separation, an adequate amount of active sites) [128].

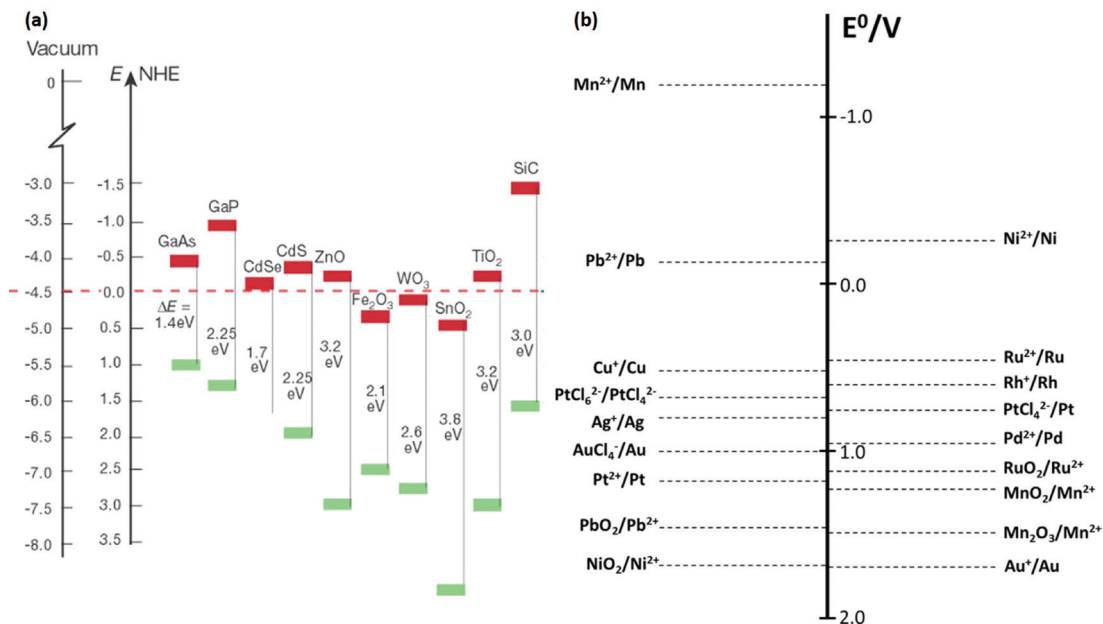


Figure 1.14 (a) Band positions of several semiconductors in contact with aqueous electrolyte at pH 1. The lower edge of the conduction band (red color) and upper edge of the valence band (green color) are presented along with the band gap in electron volts. The energy scale is indicated in electron volts, using either the normal hydrogen electrode (NHE) or the vacuum level as a reference. Adapted by permission from Macmillan Publishers Ltd: Nature [130], copyright (2001); (b) Schematic overview of redox potentials of several aqueous metal solutions relevant for photodeposition [131].

Deposition of metal/metal oxide nanoparticles on the surfaces of semiconductors performed using other methods (e.g., impregnation, electrodeposition, sputtering, atomic layer deposition) often requires elevated temperatures or an applied potential [132-135]. In this sense, photodeposition presents an attractive alternative, because the formation of well-defined nanoparticles is performed under illumination alone. Additionally, a possibility of controlling the geometrical distribution, size, and oxidation state of deposited nanoparticles is often mentioned as an advantage of photodeposition [128]. However, it is not difficult to find in the literature reports indicating the superiority of other methods over photodeposition, reflected in lower photocatalytic activity [136-139]. Such reports show that photodeposition, despite undeniable advantages, still requires some improvements.

Materials obtained *via* photodeposition of metals/metal oxides on semiconductor surfaces are principally used in photocatalysis, e.g., solar fuel cells, the elimination of hazardous substances from water and air, or selective organic transformations [128]. Their performance in these processes is often enhanced just by the presence of metal/metal oxide nanoparticles, often described as co-catalysts. Particularly, these deposits are able to retard electron/hole recombination, enhance light absorption, or provide active sites for charge transfer reactions. There are many possibilities in combinations between metals and semiconductors; therefore, the number of reports dedicated to this topic and available in the literature is enormous. One of the latest review article with many examples therein is the work of Wenderich and Mul [128].

1.6 The synergism between sono- and photochemical irradiation

In view of the above short introduction to photochemistry, it is seen that sonochemistry and photochemistry rely on very different physical phenomena; however, in both processes, the excited-state species are produced [140, 141]. Therefore, studies have appeared that compared the photochemical and sonochemical pathways in the same reactions. The first comparative study was done by Suslick's group with metal carbonyl complexes [142, 143]. Sonochemical and photochemical treatment of $\text{Fe}(\text{CO})_5$ in decalin resulted in different end-products— $\text{Fe}_3(\text{CO})_{12}$ in sonolysis and $\text{Fe}_2(\text{CO})_9$ in photolysis—showing differences between sonochemical and photochemical activation. On the other hand, Reyman et al. observed that the same products were formed in sono- and photo-irradiation of β -carboline in halomethane media, although the mechanisms of these processes were different [144]. In the context of many examples showing different results of such comparative studies, no obvious analogy was found between sonochemical and photochemical activation [141]. Thus, the results of their simultaneous use were rather difficult to predict in a different than experimental way.

A detailed analysis of how sonochemical effects can influence photochemical reactions is presented in Figure 1.15 [140]. Most often, the enhancement of mass transfer induced by ultrasound improves light absorption and results in modifying the photochemical reaction rates and pathways. The formation of hot spots and generation of free radicals leads to energy transfer between sonochemically excited species and photoexcited solutes, sometimes ending in some new chemistry routes. It is known that in a pure photochemical system, transfer of photoexcited species is not homogeneous, because it strictly depends on the propagation of light through an absorbing medium [141]. However, the photochemical reaction rate depends on the concentration of the photoexcited states, and adding ultrasound to the photochemical reaction system can significantly influence their distribution, resulting in more or less the same reaction rates in each point of the solution. It was also observed that an intense ultrasound streaming can provoke quenching of long-lived photoexcited states by collisional activation.

Sonophotochemistry was applied thus in homogeneous as well as in heterogeneous liquid systems ([140, 141] and references therein). In works that studied homogeneous reactions, the role of ultrasound was often attributed to a better mixing enhancing light absorption and, as a result, accelerating the reaction rates. In several works of Gaplovsky et al. dedicated to photoisomerization reactions, it was found that ultrasound could quench the triplet excited states of some products, which finally resulted in a modified reaction pathway [145-147]. In photocatalytic destruction of hazardous chemicals, ultrasound was supposed to enhance the photocatalytic activity in different ways: (i) by dislodging the solid particles and increasing the active surface area of a catalyst; (ii) by eroding and cleaning the surface of the solid by micro-jetting and preventing its deactivation; (iii) by increasing the bulk and localized mass transport, improving the molecular contact; and (iv) by providing an extra

source of hydroxyl radicals [140]. Some of these assumptions and expectations were reported in experimental works. For example, an enhancement in the photodechlorination process, studied by Compton et al. [148], was explained by an enhanced mass transport at the semiconductor–solution interface. A higher number of oxidizing species resulting from ultrasound-favored H₂O₂ bond scission was a main reason for the enhanced degradation rate of several modelled water pollutants reported by Mrowetz et al. [149]. Activation of the photocatalytic surface by ultrasound and an enhancement of mass transport were indicated by Kado et al. to be mostly responsible for the increased photo-oxidation rate of aliphatic alcohols [150]. These examples prove the existence of a synergistic effect between sound and light, which was reflected in greater rate constants of sonophotocatalytic reactions when compared with sonolysis or photolysis or the sum of these individual processes. Nevertheless, there is a lack of examples applying sonophotochemistry in the synthesis of materials. One can find reports in which photodeposition of metals was preceded by treatment of ultrasonication [151–153]. In this methodology, sonication and photochemical deposition were applied one by one. Herein, ultrasound was used in order to ensure good disaggregation of nanoparticles and better mass transfer between reagents. A weak point of such a two-step procedure is a prolonged synthesis time compared with a one-step simultaneous application of sonication and photochemistry.

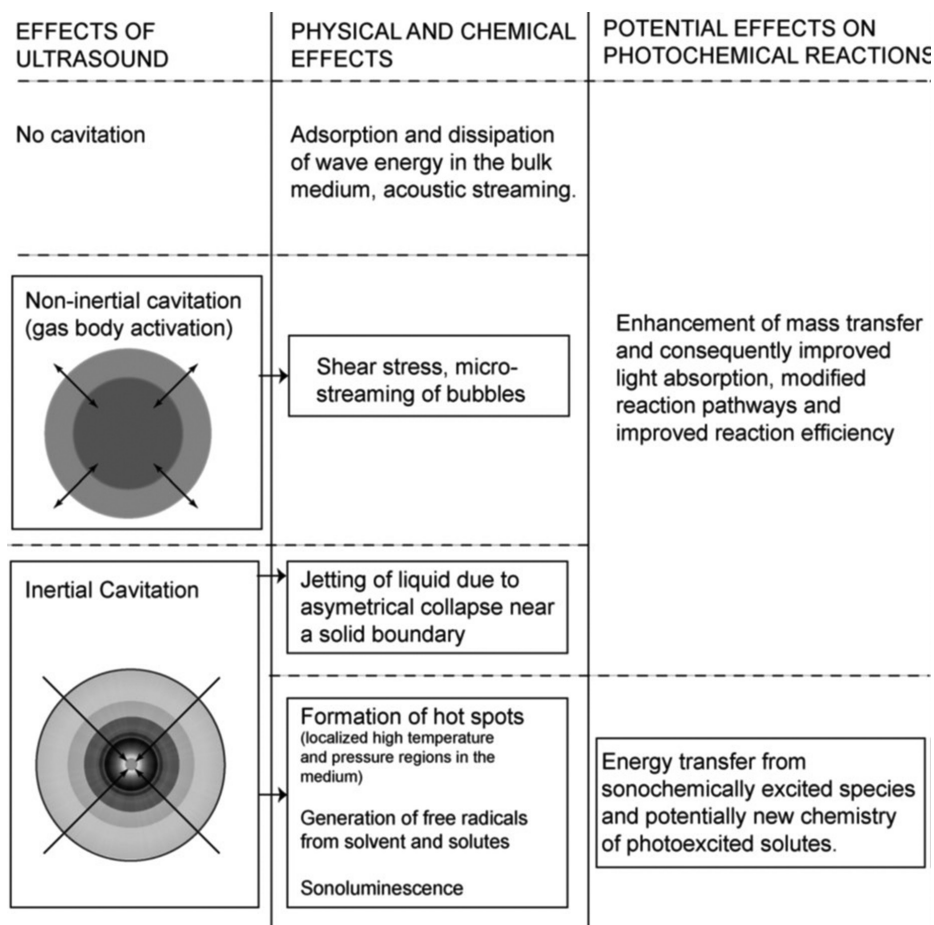


Figure 1.15 Interaction of ultrasound effects with photochemical reactions. Reprinted from [140] with permission of Springer.

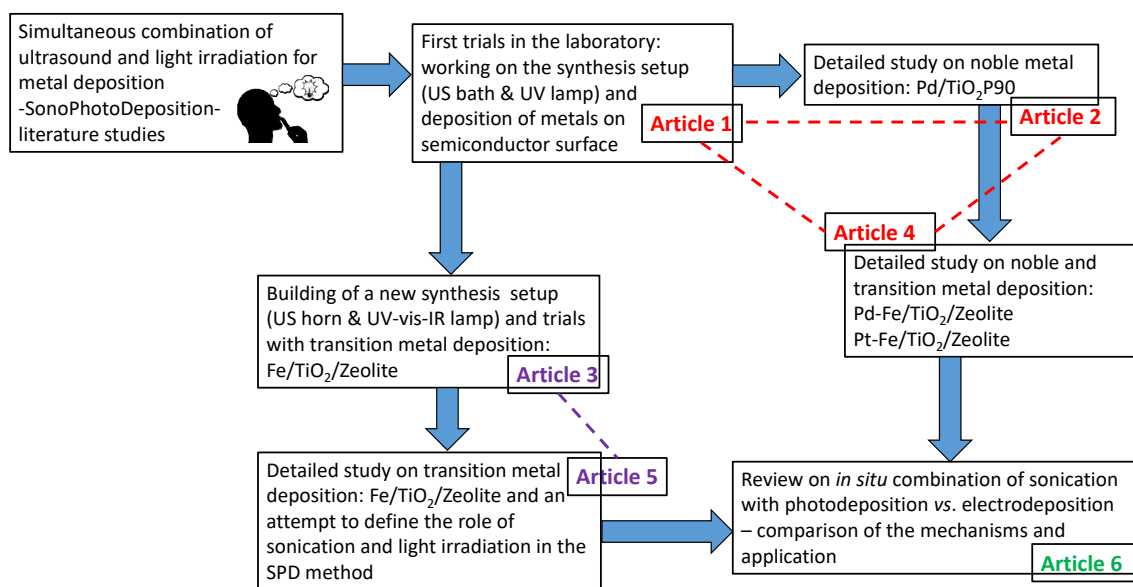
2. Research goals

A properly chosen synthesis method is crucial for the properties and future application of the prepared material. Therefore, searching for new ones or improving the commonly known methods is still a demanding area in the field of materials synthesis. In this context, development of an improved methodology based on simultaneous application of photodeposition and sonication for the synthesis of photoactive materials was the main aim of this dissertation. Sonophotochemistry was already studied thus in homogeneous as well as in heterogeneous systems, but attempts to synthesize materials have not yet been reported in the literature. We truly believed that in situ combination of these powerful methods would result in the formation of very interesting and promising materials with some unique properties. The particular research goals were the following:

- ▶ to design and build the reaction setup consisting of a light source and an ultrasound source, enabling the synthesis of solid materials;
- ▶ to synthesize several photoactive materials based on a semiconductor (TiO_2) with deposited mono- or bimetallic structures (Me^0 or Me_xO_y forms of palladium, platinum, and iron), applying the sonophotodeposition procedure;
- ▶ to characterize the prepared materials by several techniques in order to determine their properties (light absorption, structural and textural properties, morphology, chemical composition on the surface and in the bulk, etc.);
- ▶ to investigate the efficiency of these materials in different photocatalytic reactions: liquid and gas phase, mineralization of hazardous chemicals and selective organic transformations, and showing the multitasking of the sonophotodeposition methodology;
- ▶ to understand the specific role of photochemical and sonochemical processes occurring during sonophotodeposition on the properties of the synthesized materials.

3. Thesis development: introduction to the articles

As mentioned in the Abstract, this dissertation is composed of six published works. In this part, I present a development of the research from the moment when the idea of coupling ultrasound and light irradiation for application in the synthesis of materials was born. To facilitate a discussion of these works, summarizing schemes and tables are provided. Schemes 3.1 and 3.3 help to understand the linkage between articles, and Scheme 3.1 provides me a template on which to build my research story. Table 3.1 collects information about all photocatalytic test reactions performed in the works and Scheme 3.2 shows all setups used in these reactions. Table 3.2 provides a list of experimental techniques employed for characterization of the materials with a brief explanation of each one. Technical description of these methods is available in the texts of articles. The articles will not be discussed in the order of their appearance (as presented in the List of Papers), but following Scheme 3.1.



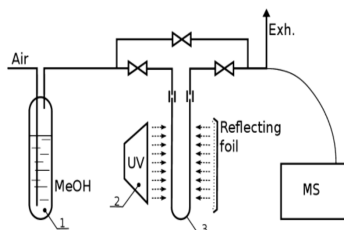
Scheme 3.1 The steps followed in my research (dotted lines connect articles belonging to the same case studies; see also Scheme 3.3).

| Article number | Article title | Photocatalyst | Test reaction | Reaction results (for the best photocatalyst) |
|----------------|---|--|---|--|
| 2 | A new photocatalytic tool in VOCs abatement: Effective synergetic combination of sonication and light for the synthesis of monometallic palladium-containing TiO ₂ | Pd/TiO ₂ P90 | Gas-phase methanol oxidation under UV lamp ($\lambda_{\text{max}} = 365 \text{ nm}$), reaction time = 3h | 1% Pd/P90/SPD: Conversion of methanol = 91 % after 60 min of illumination. Mineralization to carbon dioxide = 83 % after 40 min of illumination. Trapping of e ⁻ by Pd ⁰ enhances oxidation of methanol on free h ⁺ and initiates formation of other oxidative species. |
| 3 | Iron-containing titania photocatalyst prepared by the sonophotodeposition method for the oxidation of benzyl alcohol | ¹ Fe/TiO ₂ /Zeolite | Liquid-phase selective benzyl alcohol (BA) oxidation under UV-Vis-IR lamp ($\lambda = 240\text{--}2000 \text{ nm}$), reaction time = 8h | 1% Fe/TiO ₂ /ZeSPD: Conversion of benzyl alcohol = 48 %. Yield of benzaldehyde = 46 %. High selectivity to BHA was a result of enhanced absorption properties in the visible range and adequate Fe/Ti surface ratio. |
| 4 | Sonication and light irradiation as green energy sources simultaneously implemented in the synthesis of Pd-Fe- and Pt-Fe-doped TiO ₂ -based photocatalysts | Pt-Fe/TiO ₂ /Zeolite Pd-Fe/TiO ₂ /Zeolite | Liquid-phase phenol oxidation under UV lamp ($\lambda_{\text{max}} = 365 \text{ nm}$), reaction time = 4h | Pt-Fe/TiO ₂ /ZeSPD: Phenol degradation = 46 %, $r_0 = 11.17 \times 10^{-3} \text{ mM min}^{-1}$. The formation of a Schottky junction (Pt ⁰ -TiO ₂) and trapping e ⁻ by Fe ₂ O ₃ enhanced the photocatalytic efficiency. |
| 5 | Insight into the synthesis procedure of Fe ³⁺ /TiO ₂ -based photocatalyst applied in the selective photo-oxidation of benzyl alcohol under sun-imitating lamp | ² Fe/TiO ₂ /Zeolite | Liquid-phase selective benzyl alcohol (BA) oxidation under UV-Vis-IR lamp ($\lambda = 240\text{--}2000 \text{ nm}$), reaction time = 8h | 2% Fe/TiO ₂ /ZeSPD: Conversion of benzyl alcohol = 57 %. Selectivity to benzaldehyde = 90 %. The Fe ³⁺ form acted as both e ⁻ and h ⁺ acceptor enhancing the charge separation. Any iron leaching was observed in the liquid after reaction pointed out good stability of this photocatalyst. |

Table 3.1 Photocatalytic test reactions reported in particular articles (^{1,2}: materials described in Articles 3 and 5 have been denominated with the same symbol, Fe/TiO₂/Zeolite, but it is important to mention that they were prepared using different ultrasound powers—25 % and 10 % respectively—and they differ in Fe loading; SPD: sonophotodeposition method).

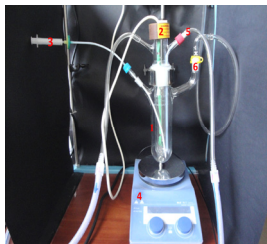
PHOTOCATALYTIC TEST REACTIONS SETUPS

(A) Gas-phase oxidation of methanol
(Article 2)



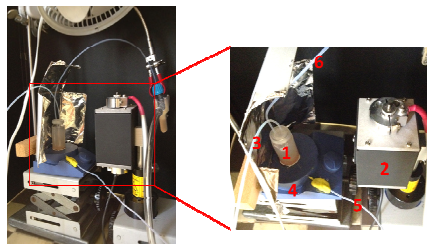
1- methanol, 2- 125 W UV lamp, 3-reactor with photocatalyst

(B) Liquid-phase oxidation of phenol (Article 4)



1- phenol water solution with photocatalyst, 2- 125 W UV lamp, 3-sampling, 4-magnetic stirrer, 5-water recirculation, 6-venting

(C) Liquid-phase selective oxidation of benzyl alcohol (Article 3 and Article 5)



1- benzyl alcohol acetonitrile solution with photocatalyst, 2- 150 W UV-Vis-IR lamp, 3-sampling, 4-magnetic stirrer, 5-thermocouple, 6-venting

Scheme 3.2 Graphic representation of test reactions setups applied in the particular works. Pictures (A) and (B) adapted from [154] copyright (2014) and [155] copyright (2011) with permissions from Elsevier, respectively.

US bath & UV lamp ($\lambda_{max} = 254 \text{ nm}$)



Article 1

Method of depositing metal nanoparticles on the surface of semiconductor materials and surface obtained by this process

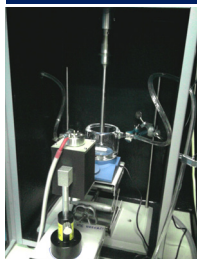
Article 2

A new photocatalytic tool in VOCs abatement: Effective synergetic combination of sonication and light for the synthesis of monometallic palladium-containing TiO_2

Article 4

Sonication and light irradiation as green energy sources simultaneously implemented in the synthesis of Pd-Fe- and Pt-Fe-doped TiO_2 -based photocatalysts

US horn & UV-vis-IR lamp (240-2000 nm)



Article 3

Iron-containing titania photocatalyst prepared by the sonophotodeposition method for the oxidation of benzyl alcohol

Article 5

Insight into the synthesis procedure of $\text{Fe}^{3+}/\text{TiO}_2$ -based photocatalyst applied in the selective photo-oxidation of benzyl alcohol under sun-imitating lamp

Scheme 3.3 Groups of articles according to the applied setup used in the synthesis of photocatalysts.

| Entry | Characterization technique (acronym) | Key information about the technique in the context of my studies | Applied in Article |
|-------|--|---|--------------------|
| 1 | Diffuse reflectance UV-vis spectroscopy (DRUV-vis) | Enables to estimate the optical properties of the material in the ultraviolet-visible spectral region based on the analysis of the shape of the spectrum. | 2, 3, 4, 5 |
| 2 | X-ray photoelectron spectroscopy (XPS) | Enables to determine the elemental composition of the surface of the material, empirical formula and chemical/electronic state of the elements. The spectrum is recorded by analysis of the energy of photoelectrons emitted from the surface up to 10 nm in depth. | 2, 3, 4, 5 |
| 3 | X-ray diffraction (XRD) | Enables to determine the structure of chemical compounds forming the crystals of the material based on the diffraction patterns of X-rays, which are formed as a result of interaction between a beam of X-rays and atoms. | 2 |
| 4 | Energy dispersive X-ray fluorescence (EDXRF) | Enables to determine the elemental composition of materials using X-ray fluorescent emission of the elements presented in the sample. | 3 |
| 5 | ⁵⁷ Fe Mössbauer spectroscopy | Enables to study the local interactions in the material applying the nuclear probe (isotopes). It can detect phases invisible for other techniques and determine the magnetic arrangement. | 5 |
| 6 | High resolution transmission electron microscopy with energy dispersive spectroscopy (HRTEM-EDS) | Enables to image the sample with a very high resolution providing details about internal composition, morphology, crystallography, stress, or even magnetic domains. | 2, 3, 4, 5 |
| 7 | Scanning electron microscopy with energy dispersive spectroscopy (SEM-EDS) | Enables to specify the surface topography of the material as well as to identify qualitatively and quantitatively the elements in the sample. | 1 |
| 8 | N ₂ physisorption | Enables to determine surface area and other textural properties of the material, such as pore size and pore size distribution. | 2, 4 |
| 9 | Inductively coupled plasma mass spectrometry (ICP-MS) | Enables to determine elemental composition of the material with a very high sensitivity and a rapid sample processing. | 4 |

Table 3.2 Techniques applied for characterization study of the synthesized materials in each article.

Going back to the beginning of this research, the idea of simultaneous coupling of ultrasound and light irradiation with the aim of metal deposition appeared after a careful study of the literature (please follow Scheme 3.1). As mentioned in the introduction, there was no such research reported at that time. Therefore, my first efforts were put into elaborating the reaction setup, which allowed a simultaneous emission of light and ultrasonic waves. For this purpose, I used a commonly available ultrasonic bath (Bandelin, 35 kHz, 140 W) and 6W Hg UV lamp emitting at $\lambda_{\max} = 254$ nm. As depicted in the top image in Scheme 3.2, it was as simple as inserting the photoreactor with the lamp into the ultrasonic bath. However, in such a system, the possibility of mechanical mixing (e.g., magnetic stirring) inside the photoreactor was eliminated. Even though action of ultrasound (cavitation) ensures mixing of the liquids, the possibility of formation of standing waves inside the reactors was reported by Suslick et al. [117]. To avoid it, the reaction setup should be equipped with some external mixing. Therefore, the photoreactor used in this setup was provided with a sintered glass disc fitted to the bottom of the flask, which permitted gas agitation of the reaction mixture. Its shape was inspired by reactors often used in photocatalytic reactions. More pictures of this setup are available in **Article 1**. The first trials using this setup were focused on the determination of several technical parameters, namely, a good mixing of the reaction solution, a gas flow, the composition and pH of the reaction mixture, the time of ultrasound and light exposure, the type of light irradiation and ultrasound, etc. The most important parameters are discussed more carefully below:

- i. Dissolved gas. Argon was bubbled through the reaction mixture in order to ensure good mixing of the reagents (flow 70 mL min^{-1}). Additionally, it is known that dissolved gases facilitate the formation of cavitation bubbles [2]. The specific heat ratio, solubility, and thermal conductivity are the main physical characteristics of the gases that influence the bubbles' nucleation. As a rule, a high specific heat ratio of the gas guarantees a high cavitation effect; therefore, the monoatomic gases, argon and helium, should produce more cavitation bubbles than do diatomic gases. However, this is not the case of every system. A study conducted by Entezari et al. showed that it depends on the studied system, in which other factors can be predominant [156].
- ii. Composition of the reaction mixture. A liquid phase was composed of water and organic solvent. A higher amount of organic solvent was used to create a more selective environment for the reaction, to decrease the rate of formation of $\dot{\text{O}}\text{H}$ radicals, and to minimize or eliminate the leaching effect of metals often observed in aqueous solutions. Different solvents were considered, but in the end, acetonitrile was used. Although it was not considered a completely green solvent [157], it presented some attractive properties for this process: stability and no absorption of UVA and UVB light, as well as easy reuse and distillation after the reaction. Similarly, no absorption in the UV range was a requirement while selecting acetylacetonate as an organic salt precursor of the deposited metal. An added advantage of the organic

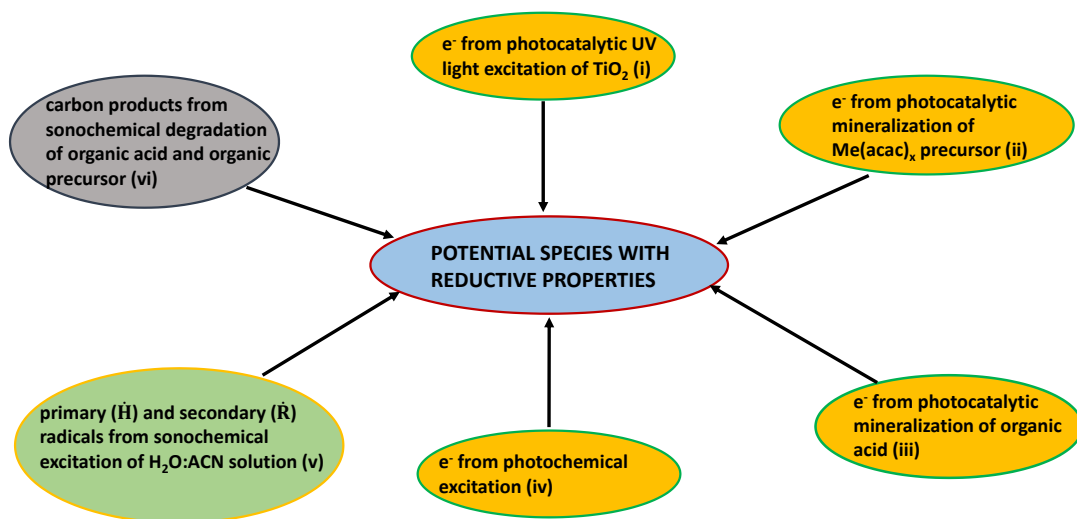
precursors over their inorganic equivalents is their easy elimination from the reaction mixture, e.g., by mineralization under the photocatalytic conditions of the SPD process (by photo-induced holes and radicals with oxidative properties). Continuing, an organic acid (oxalic acid) was added to the reaction mixture to be oxidized by photo-induced holes, leaving at the same time free electrons for the reduction process. Also, there were reports demonstrating that pH value can influence size, distribution, and oxidized state, as well as the kinetics of photodeposited nanoparticles [158-160]. Several researchers observed the formation of metallic platinum with better-dispersed nanoparticles on the TiO₂ surface at an acidic pH, which resulted in higher photocatalytic activity of these materials [159-161]. Photo-mineralization of all these organic components can be an additional source of electrons in the process of sonophotodeposition. Eventually, the reaction mixture formed a homogeneous and well-mixed suspension after adding an appropriate number of particles of semiconducting material.

- iii. Time of light and ultrasound exposure. This parameter could be variable and dependent on the reductive potential (E^0) of deposited metal. The metals with a high positive value of E^0 ('easily reduced') could be treated for a shorter time in comparison with those having a lower value. In any case, this method ensures a significant time-savings (60 minutes as a maximum treatment time) when compared with the application of ultrasound and light irradiation following each other in similar experiments.
- iv. Source of light irradiation and ultrasound. The type of the lamp was determined by the absorption properties of the semiconductor material applied in the synthesis. It is known that TiO₂ powder absorbs in the UV range (up to 380 nm); therefore, it requires the use of a lamp emitting in this range. An ultrasonic bath was used as the most suitable technical solution for the specific immersed-well photoreactor. Additionally, it is the most typical and universal source of ultrasonic irradiation available in many laboratories, which makes this setup easy to reproduce.

Having all these parameters specified, I made the first successful attempts with deposition of one noble metal (palladium) on the commercial TiO₂ P90 surface. After that, more complex systems consisting of noble–non-noble pairs of metals (selected from palladium, platinum, iron, and chromium) were deposited on self-prepared TiO₂/Zeolite Y material (the choice of zeolite Y as a support will be explained while discussing **Article 2**). The use of TiO₂ as a semiconductor was dictated by the application of these systems in the photocatalytic reactions and by the fact that TiO₂ is still a leading material in this area. After receiving some satisfactory results based on preliminary characterization a patent application concerned the sonophotodeposition method (SPD) was submitted to the Polish Patent Office, which

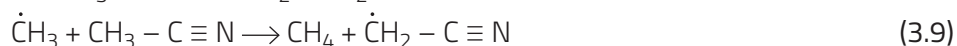
is presented herein as **Article 1**. A detailed study of these systems was then carried out in the next works, **Article 2** (noble metal deposition) and **Article 4** (noble–non-noble metals deposition), which therefore are strongly correlated with one another and are the continuation of the research started in the patent application.

Before moving on to the next publication, a brief analysis of the plausible sources of electrons and reductive species available in the sonophotodeposition method will be provided. Following Scheme 3.4, it is seen that coupled action of light and ultrasound irradiation on this specific reaction mixture can provide differentially-originated species with reductive properties.

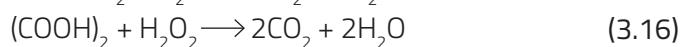
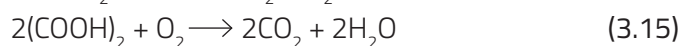
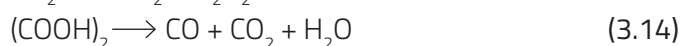


Scheme 3.4 Different reductive species that can be formed in the sonophotodeposition method.

Therefore, electrons could derive from (i) photocatalytic excitation of TiO_2 under UV light, (ii) photocatalytic mineralization of organic precursors of metals (acetylacetonate salts), (iii) photocatalytic mineralization of organic acid (oxalic acid), or (iv) photochemical excitation. Additionally, some primary ($\dot{\text{H}}$) and secondary ($\dot{\text{R}}$) radicals formed in the sonochemical processes are available (v), as are carbon products produced during sonochemical degradation of organic compounds (vi). These species could also have reductive properties and therefore could enhance the reduction rate of metal salt. The secondary radicals are generated in the reactions of primary radicals ($\dot{\text{H}}$ and $\dot{\text{O}}\text{H}$) with organic additives in the solution [23]. In the mixture of water and acetonitrile (30% H_2O /70% ACN), the overall processes with the competitive reactions (3.1–3.12) are quite complex and can be summarized as follows [162, 163]:



As indicated by the reactions above, the sonochemical treatment of aqueous solution of acetonitrile results in the formation of methyl radicals ($\dot{\text{C}}\text{H}_3$), which are formed by adding an H atom to the triple bond and scission of the C-C bond (reaction 3.7), as well as $\dot{\text{C}}\text{H}_2\text{CN}$ radicals, which can be formed in the thermal pyrolysis reaction (reaction 3.12) or following the abstraction reactions (reactions 3.8–3.11) [162, 163]. Methyl radicals have been reported as an unstable and reactive species, because their octet rule on the carbon is not filled. They present a double nature, as the carbon atom adopts a middle structure between the methyl cation and the methyl anion. Therefore, they can act either as strong oxidants or strong reductants, depending on the reaction environment. In water, they behave as strong reductants, forming methanol and hydrogen, which could act as an added reducing agent in the system [164]. Additionally, in the studied solution, sonochemical decomposition of oxalic acid should be taken into account. The results of sonolysis and photolysis of oxalic acid under high-frequency ultrasound (200 kHz) have been reported in the work of Tanaka et al. [165]. It is known that oxalic acid is a reducing agent with a non-volatile nature; therefore, neither oxalic acid nor oxalate ions can enter the cavitation bubbles. This fact determines the type of reactions that can occur with regards to cavitation: pyrolysis occurring close to the walls of cavitation bubbles and oxidation by active species produced from cavitation, in which mainly CO_2 and CO are formed (see reactions 3.13–3.17):



The authors claim pyrolysis to be the main reaction among them (reaction 3.14) because similar amounts of CO_2 and CO were obtained in this process. Interestingly, higher yields of the above-mentioned carbon products were received in the case of the combined photolysis system

than after summarizing the results of sonolysis and photolysis separately. This observation proved the occurrence of the synergistic effect of combining ultrasound and light irradiation on the degradation of oxalic acid. Based on the performed studies, they concluded that in their reaction system, degradation of oxalic acid was promoted by active species derived from H_2O_2 produced during sonolysis of water, and enhanced production of CO_2 was promoted by photo-irradiation (reaction 3.17).

As mentioned before, the research presented in **Articles 2** and **4** continues and deepens the investigation announced in **Article 1**. Therefore, in these works, the same reaction setup was used, consisting of an ultrasonic bath and a UV lamp (please follow Scheme 3.3). Thus, **Article 2** describes in detail the characterization studies of palladium deposited on commercial TiO_2 P90 material. Three different loadings of palladium—0.5, 1, and 2 wt% Pd—were studied and compared with 1 wt% Pd photodeposited on TiO_2 P90. The results obtained in all characterization techniques were complementary to one another and allowed me to formulate the following conclusions:

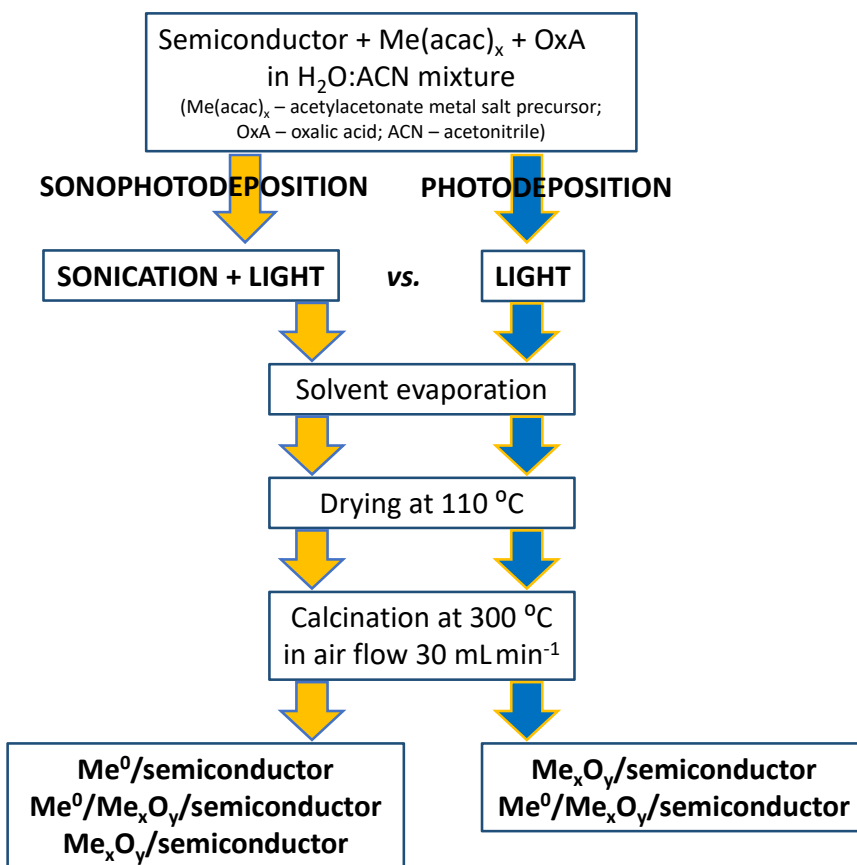
- i. Complete reduction of palladium after the sonophotodeposition (SPD) method was proved by studying the crystalline form of palladium. Among all materials prepared by SPD, only metallic form Pd^0 was registered, which was confirmed by several techniques: X-ray diffraction (XRD), X-ray photoelectron spectroscopy (XPS), high resolution transmission electron microscopy with energy dispersive spectroscopy (HRTEM-EDS), and UV-vis diffuse reflectance spectroscopy (DRUV-vis). In contrast, photodeposition of palladium resulted in the formation of two crystalline structures, Pd^0 and PdO , and only the oxidized form was identified at the surface by XPS measurements.
- ii. The tendency of palladium to form aggregations (up to 100 nm) was observed in TEM images. They were built of nanoparticles sized at approximately 24 nm, as estimated from Scherrer 's equation (XRD). Generally, a higher amount of small-sized aggregations (below 50 nm) was found in the materials prepared by the SPD method, especially in the case of the 2% Pd/P90/SPD sample.
- iii. A plausible position of palladium particles within the TiO_2 matrix was estimated on the basis of N_2 physisorption, XRD, and XPS results. The pore size of TiO_2 was not big enough (14 nm average, N_2 physisorption) to let the Pd particles (24 nm, XRD) enter inside. The Pd/Ti ratio on the surface was low (XPS). Also, there were no changes in peak positions in the XRD profile, suggesting that after deposition, palladium particles were rather physically dissolved in the TiO_2 matrix.
- iv. A significant improvement of absorption properties, increasing with Pd loading, was observed, as expected. In the case of the 1% Pd/P90/PD sample, prepared by photodeposition, a band between 450 and 550 nm was seen, suggesting the

presence of PdO particles. Interestingly, a small improvement of absorption properties under the visible light was also observed for the TiO₂ P90 material exposed to conditions of sonophotodeposition (P90/SPD) in comparison with a bare TiO₂ P90. The enhancement of absorption properties of TiO₂ was also observed after 6 h of low-frequency ultrasound treatment by Osorio-Vargas et al. [166]. Besides optical, they also found morphological and surface changes in TiO₂ P25 nanoparticles, being consequences of high-speed inter-particle collisions and shockwaves induced by the action of ultrasound [93]. These changes were mainly seen as particle aggregation and surface damage responsible for oxygen vacancies (*V_o*) formation. It is known that oxygen vacancy states are formed between the valence and conduction bands in the TiO₂ band structure, allowing visible light absorption [167].

v. All Pd-containing materials prepared by the SPD method showed better performance in the gas phase photocatalytic oxidation of methanol under UV light irradiation ($\lambda_{\text{max}} = 365 \text{ nm}$) than did photocatalysts prepared by photodeposition or bare TiO₂ P90. The fastest (40 min) methanol degradation was obtained by 2% Pd/P90/SPD, but a very fast degradation rate (> 90 % degradation in 60 min) was also achieved by 1% Pd/P90/SPD. Additionally, both photocatalysts showed very similar mineralization (80 %) to CO₂ after 40 min of illumination. These results as well as economic reasons led to my choosing 1% wt Pd as the optimal loading for this reaction. The activity of the photocatalyst prepared by the photodeposition method (1% Pd/P90/PD) was three times lower. Turnover frequency values (TOF) calculated for 1% Pd/P90/SPD and 1% Pd/P90/PD photocatalysts showed almost nine times faster conversion of CH₃OH into CO₂ in the case of photocatalyst prepared by the sonophotodeposition method (43.2 mmol CO₂ mmol⁻¹ Pd⁻¹ s⁻¹ vs. 4.9 mmol CO₂ mmol⁻¹ Pd⁻¹ s⁻¹). This means that the Pd⁰-TiO₂ system is more active in this reaction than is PdO-TiO₂. It was often reported that the metallic form of palladium was a better acceptor of electrons in photocatalytic reactions when compared with the oxidized forms [168, 169]. When photo-excited electrons are trapped by Pd⁰, the recombination probability between electrons (e^{-_{cb}} or e^{-_{tr}}) and holes is reduced, and the oxidation process is enhanced on the more accessible holes [170, 171]. In the air Pd⁰ serves also as the active site on which the trapped electrons are transferred to the molecular O₂, reducing it to O₂^{•-} [172].

vi. A comparison of the structural properties and the revealed differences between the materials synthesized by the SPD and PD methods made me think that somehow the ultrasound had a crucial role in the reduction of palladium. Having only the metallic Pd⁰ form detected after SPD was even more intriguing, because after the 'sonophoto' as well as after the 'photo' treatment, all materials were exposed to the high-temperature air treatment (30 mL min⁻¹ air flow, 300 °C) in order to eliminate the organic residues from the samples (please follow Scheme 3.5). Therefore, partial

oxidation of the photo-reduced palladium into PdO and the co-existence of two crystal phases (Pd⁰ and surface PdO) in the photocatalyst prepared by photodeposition was rather natural and expected. No detection of the oxidized palladium phase in the photocatalyst prepared by sonophotodeposition was, in turn, a bit surprising. The plausible explanation of such different behavior should be linked with the action of ultrasound during the SPD experiment (as it was the only difference between SPD and PD methods). We suspect that under SPD conditions, sono-radicals could interact with the Pd(acac)₂ precursor through the oxygen atoms, reducing the ligand selectively. If this was the case, oxygen available during air calcination was not consumed for Pd⁰ oxidation, but was combined with carbon remaining from the precursor, forming CO₂. On the other hand, the organic (acac)₂ ligand remaining after photodeposition was removed by high-temperature treatment and the oxygen from the air flow could be consumed for the oxidation of palladium. This explanation was formulated on some theoretical basis of ultrasound theory.



Scheme 3.5 Sonophotodeposition vs. photodeposition reaction procedure.

The next step in my research plan was sonophotodeposition of two metals: noble metal together with transition metal (see Scheme 3.1), which was described in **Article 4**. Deposition of Pd-Fe and Pt-Fe pairs on self-prepared TiO₂/Zeolite Y material was carried out in the same reaction setup as reported in **Articles 1** and **2** (see Scheme 3.3). There were various reasons for using such combination of metals. Noble metals (Pd, Pt) are very attractive dopants in photocatalysis, because their interaction with TiO₂ can result in the formation of a Schottky junction or localized surface plasmon resonance (LSPR) [173]. These effects are able to retard electron–hole recombination or activate large-band gap photocatalyst towards visible light [174]. Nevertheless, their high price restricts their use in large amounts. It is possible to reduce this cost by combining the noble metal with a low-cost second metal, forming an active bimetallic structure [175-177]. Careful analysis of the literature pointed out that iron could be successfully used in this context [178-180]. It is a cheap and abundant metal with very attractive properties [181]. Nevertheless, one can find many controversies about its activity in the literature, examples of positive [180-185] as well as detrimental [178, 186-188] effects on photocatalytic activity. Agreeing with my own research experience, a detrimental effect of iron doping on phenol degradation was reported in one of the previous works [189]. It seems the choice of doping method determines whether iron's presence is favorable [190]. In view of the above comments, combining noble metals with iron might be beneficial for both of them by minimizing or eliminating their drawbacks and creating some new active structures. In this research, I decided to change semiconducting material and support TiO₂ on the high-surface area zeolite material in order to avoid aggregations of TiO₂ nanoparticles, as reported in **Article 2** [191, 192]. Zeolite Y was chosen as a support because of its transparency, necessary for the synthesis conditions and for the photocatalytic test reaction [193]. Its good pollutant adsorption and diffusion properties were also not meaningless. Additionally, it was reported that when the surface of zeolite was charged, it could trap electrons from the semiconductor electron–hole separation [194, 195]. The most relevant findings of this work are listed below:

- i. Different forms of deposited metals were obtained after SPD treatment. The XPS studies revealed that the surface was composed of Pd²⁺, Pd⁰, and Fe³⁺ in the case of Pd-Fe/TiO₂/ZeSPD, and Pt⁰, Pt²⁺, and Fe³⁺ in the case of Pt-Fe/TiO₂/ZeSPD materials. The strong domination of the Pd²⁺ form (84 % fraction state) and almost complete reduction of platinum to Pt⁰ (92 % fraction state) showed different behaviors of these noble metals under the SPD conditions, because they differ in the values of their reduction potentials. Interestingly, in the previously discussed **Article 2**, palladium was totally reduced under the same experimental conditions. This could be related to the presence of a second metal and competition in trapping electrons. However, in comparison with the noble metals, Fe³⁺ reduction would be a very difficult task given its negative reduction potential value. In our experimental conditions, its partial reduction to Fe²⁺ is more probable. Then, in the last air treatment step, iron ions could

be easily re-oxidized to the Fe^{3+} form. These results forced me to analyze an additional sample containing a single iron ($\text{Fe}/\text{TiO}_2/\text{ZeSPD}$). In this sample, besides Fe^{3+} , the Fe^+ form was also detected. This observation supports the above mentioned hypothesis that only partial reduction of iron is possible when mild SPD reduction conditions are applied, even though there is no second metal present.

- ii. Almost all forms of deposited metals identified in the surface were confirmed by TEM studies, except Pt^{2+} . An excellent dispersion of small (2–3 nm) platinum particles and bigger aggregations (20–30 nm) of palladium/palladium oxide particles were seen on the zeolite blocks. Also, the nano-sized iron particles in the form of $\alpha\text{-Fe}_2\text{O}_3$ accurately covered some zeolite rods in the $\text{Pt-Fe}/\text{TiO}_2/\text{ZeSPD}$ as well as in the $\text{Pd-Fe}/\text{TiO}_2/\text{ZeSPD}$ photocatalyst. A detailed analysis of TEM images showed that deposited metals can be in close vicinity with TiO_2 particles or each other; therefore, the formation of some specific heterostructures cannot be totally excluded. Unfortunately, I could not find any evidence supporting this hypothesis in other techniques.
- iii. The liquid phase phenol degradation under UV light was a test reaction for the synthesized photocatalysts. I wanted to verify whether the detrimental effect of iron doping in this reaction, observed in my previous work, would be reduced by adding a noble metal. An enhancement of photocatalytic activity was observed only in the case of Pt-Fe combination. Several reasons might contribute to this enhancement; however, the most important ones seemed to be the formation of a Schottky barrier between the metallic Pt^0 and TiO_2 that enables trapping of e^- , retarding the recombination of charges, as well as the excellent dispersion and small size of Pt^0 particles. Also, Fe_2O_3 can serve as an electron relay to Pt^0 , thus reducing its detrimental role in this reaction. At the same time, no improvement in the case of the Pd-Fe metals combination was probably mainly a result of PdO formation's preventing the creation of a Schottky barrier.
- iv. Photocatalytic efficiency of the Pt-Fe material prepared by SPD was higher in comparison with the analogue Pt-Fe prepared by PD, thus proving again the positive results of the 'sonophoto' combination over a single 'photo'.

In fact, one can say that photocatalytic activities obtained in this reaction were not very high, even for the best-performing $\text{Pt-Fe}/\text{TiO}_2/\text{ZeSPD}$ material (46 % of PhOH degradation after 4 h of UV illumination). Here it is worth mentioning that an appropriate amount of deposited metal is an important parameter in catalysis [196]. However, optimization studies were not performed in this work, and this fact could have influenced the results obtained in photocatalytic phenol degradation. The importance of metals' optimization in the bimetallic structure synthesized by the SPD method was shown in two other works done by our group. Although they are not a part of this dissertation, I feel obligated to briefly mention the results

obtained therein because they perfectly match with a discussed topic. My colleagues studied sonophotodeposition of Pd-Cu [197] and Pd-Au [198] pairs of metals on TiO₂ P90 material, using the same reaction setup as I used in the articles described so far in this dissertation (UV light and US bath). Interestingly, they also observed that palladium was not fully reduced such during sonophotodeposition of Pd-Cu, nor in the case of Pd-Au. These results are in agreement with my observation regarding the Pd-Fe sample and confirm that the presence of a second metal can have a retarding effect on the total reduction process of palladium during the SPD method. They also noticed that a strong metal–support interaction effect (SMSI) was formed between randomly appearing Pd-Au alloys and TiO₂ particles. This SMSI effect was explained as a probable result of shockwaves and inter-particle collisions produced by cavitation. It is important to realize that such behavior was observed for only one sample with a specific metal composition (1wt% Pd₅₀-Au₅₀/TiO₂P90) [198]. Similarly, the SMSI effect was also seen in only one sample after Pd-Cu sonophotodeposition (1wt% Pd-Cu(1-1)/TiO₂P90) [197]. These above-mentioned samples were the best-performing photocatalysts in the gas phase selective conversion of methanol to methyl formate.

Article 3 and **Article 5** can be considered as a second group, since both of them include studies on the sonophotodeposition of iron oxide carried out in the new reaction setup, consisting of a UV-Vis-IR lamp and a sonication horn. As presented in Scheme 3.3, the sonication horn was immersed in the reaction vessel, which was externally illuminated by a 150 W Xe lamp. **Article 3** communicates a successful deposition of iron oxide performed by a lamp emitting mainly UV-visible light during the SPD experiment (IR was cut off by water flowing through the sonoreactor jacket) and a US horn working at the amplitude of 30 μm. The reaction setup was modified in order to broaden its operating possibilities, especially with regard to the ultrasound emitter. The use of a regular cleaning bath presents a number of disadvantages, such as working toward a fixed nominal frequency and ultrasonic power, defective distribution of a sonic field, or absorption of the sonic waves by glass walls, among others [199]. In this context, the use of the sonication horn with an operational power mode gives more opportunities as well as enabling it to operate inside the reaction solution. It is worth mentioning that nowadays it is a conventional laboratory tool, often applied as homogenizer. Also, the use of a wide-range (sun-imitating) lamp allowed me to go beyond the rigid frames of UV lamps used in the photodeposition processes so far and to follow a worldwide trend of replacing UV with solar light [121, 200]. Phenol degradation results (not too promising in fact, although without optimization studies) reported in **Article 4** prompted me to verify the efficiency of the SPD photocatalysts in another liquid test reaction. It was of scientific interest and relevant to the present tendency in photocatalysis to test SPD photocatalysts in some selective organic transformations and driven under visible light. This kind of reaction usually requires a lower oxidation power to oxidize some selected functional groups. When iron was

used in the selective photo-oxidation processes, the catalytic systems were most often composed with or based on oxidized iron forms according to the actual publications [201-204]. Therefore, my goal in **Article 3** was to deposit iron oxide on a self-prepared TiO₂/Zeolite Y semiconductor designed for photo-oxidation of benzyl alcohol into benzaldehyde. The most relevant findings of this work are listed below:

- i. According to XPS studies, only the oxidized forms of iron (Fe³⁺) were found on the surface of the material synthesized by the SPD method. The main peak was identified as the hematite form, and this form was also recognized in TEM measurements. Interestingly, the same iron forms were recognized on the XPS spectrum after introducing iron by the wet-impregnation method (UI), which was used as a control experiment. However, a clear difference in the UV-vis absorption spectrum between these two samples suggested that they could differ in structural iron features. Two separated bands in the spectrum of the sample prepared by the SPD method could indicate the co-existence of two semiconducting oxides, TiO₂ and Fe₂O₃. On the other hand, a red shift of the band in the spectrum of the sample prepared by the UI method could suggest the incorporation of Fe³⁺ ions into the TiO₂ lattice [183]. However, more experimental evidence is required to support this hypothesis.
- ii. The use of different ultrasound emitters in the SPD and UI methods was reflected in the iron distribution in the samples. In the UI method, the ultrasound operating zone outside the reactor (less ultrasound power delivered to the reaction system) resulted in the evident surface enrichment with Fe³⁺. In contrast, during the SPD method, operating with ultrasound inside the sonoreactor (more ultrasound power delivered to the reaction system) caused less Fe³⁺ to be located on the surface in comparison with the UI method.
- iii. Aggregations of fine (3–5 nm) iron oxide particles tightly covering some of the zeolite blocks with bigger (10 nm) spherically-shaped TiO₂ particles on them were seen in TEM images for the SPD sample. The closeness between TiO₂ and Fe₂O₃ could not preclude the possibility of forming a kind of junction between them. Interestingly, iron particles were not visible by this technique in the case of the material prepared by the UI method. This observation could support the conclusion drawn on the basis of the UV-vis spectrum about Fe³⁺ incorporation into the TiO₂ lattice.
- iv. Selective photo-oxidation of benzyl alcohol (BA) into benzaldehyde (BHA) under the same sun-imitating lamp as was used during the synthesis experiment was a test reaction for these materials. Conversion of BA using the photocatalyst prepared by the SPD procedure was nearly five times higher than that obtained with the photocatalyst synthesized according to the UI method. We were looking for the explanation of such result in structural and morphological differences between these

materials. Better visible light response, lower Fe/Ti surface atomic ratio, and different morphology were found to be the main reasons for the enhanced performance of the SPD photocatalyst in this reaction.

This successful sonophotodeposition of non-noble metal using a UV-Vis-IR lamp and a sonication horn prompted me to gain an insight into the synthesis procedure. Therefore, the next experiments I described in **Article 5** were focused on understanding the roles of sonication and light irradiation while they were simultaneously applied during the sonophotodeposition procedure. However, before I go into a detailed discussion of the results, a short comment on the optimization of the sonication horn should be added. After calorimetric studies, the working amplitude was set to 12 μm , while the maximum amplitude of the horn was 120 μm . This obviously means that the acoustic power ($P_L = 15 \text{ W}$) delivered to this system and thus the cavitation effect in the reaction solution did not reach the maximum possible value for this device. However, we have observed that the efficiency of the transducer decreased with increasing amplitude, gaining the highest value for 12 μm precisely. The same observation was reported by Kobus et al. [205]. The explanation of this phenomenon they found in dielectric and mechanical power losses in the transducer as well as in changes of its loading, which all increased with the amplitude [206, 207]. Additionally, the efficiency test (photocatalytic oxidation of benzyl alcohol) of the materials prepared under different ultrasonic amplitudes showed the best results for the material prepared with 12 μm of amplitude. This could mean that the sonophotodeposition method does not require high electric power to be employed and a high cavitation effect to be produced. Thus, less energy delivered to the system makes this method economically attractive. The second important parameter of the sonication horn was to decide between the continuous and the pulse working modes. The pulse mode was chosen (3 sec on/2 sec off) to avoid heating up the reaction solution, which could have happened while working on continuous mode. Additionally, it has been reported that under certain pulse conditions, more nucleation sites can be produced [208, 209]. In order to explore the way ultrasound and light irradiation influence the properties of the material exposed on their simultaneous treatment during sonophotodeposition (SPD), I prepared the corresponding materials by simple sonodeposition (SD) and photodeposition (PD). Comparing the physical properties and photocatalytic activity of these materials allowed me to draw the following conclusions (for the sake of brevity I am using the acronyms of these methods):

- i. In all samples, only the oxidized surface forms of iron were identified by XPS measurements. The main signal of Fe^{3+} was ascribed to the hematite form in each sample, no matter which synthesis method was used. However, more detailed information about the exact chemical nature of Fe^{3+} was provided by the Mössbauer technique. Interestingly, the same components, three sextets and one doublet, were found in the spectrum of materials prepared by the SPD and PD methods.

This means that they contained four different Fe^{3+} forms, namely: stoichiometric hematite, defected hematite, nano-hematite, and dispersed Fe^{3+} [210]. Integration of peaks areas allowed us to determine the quantity of each form and showed some differences in composition between these samples, which might affect their photocatalytic properties, as discussed below. In contrast, the spectrum of the material prepared by the SD method presented mainly a doublet characteristic for highly dispersed Fe^{3+} forms [211].

- ii. Differences in morphology between SD and the other samples were clearly seen in TEM images. In the case of 2% $\text{Fe}/\text{TiO}_2/\text{ZeSD}$, highly dispersed Fe^{3+} oxide species were not seen in TEM images, and the presence of iron was confirmed by EDS analysis. On the other hand, hematite aggregations built of 4–5 nm sized particles were easy to detect on some zeolite blocks in the case of 2% $\text{Fe}/\text{TiO}_2/\text{ZePD}$. Similar hematite aggregations, but decorated with bigger TiO_2 particles, were also seen in the images of 2% $\text{Fe}/\text{TiO}_2/\text{ZeSPD}$. Such morphology was probably reflected in the band seen on UV-vis absorption spectra centered at 500 nm for PD and SPD samples [212, 213].
- iii. All results obtained from the applied characterization techniques contributed to the final observation that the chemical nature of iron was mainly determined by light-induced reactions, whereas its distribution and dispersion depended on ultrasound action during sonophotodeposition. The chemical effects of ultrasound were probably diminished in the solution consisting of 30% $\text{H}_2\text{O}/70\%$ ACN. The advantage of acetonitrile resulted in increased sonochemical production of radicals derived from acetonitrile bond scission, which means that this solution contained more radicals with a reductive power lower than hydrogen radicals. Therefore, the physical action of ultrasound and the effects, such as acoustic streaming, shockwaves, and microjets, at the liquid-solid interface were most pronounced in this particular reaction system.
- iv. The results of the selective photo-oxidation of benzyl alcohol into benzaldehyde showed the best photocatalytic performance (57 % BA conversion, 90 % selectivity to BHA) for the sample prepared by the SPD method. The activity in this reaction of the control samples (PD and SD) was lower, although 2% $\text{Fe}/\text{TiO}_2/\text{ZePD}$ contained the same iron forms as 2% $\text{Fe}/\text{TiO}_2/\text{ZeSPD}$. In the case of this photocatalyst, the lower activity was probably related to the high surface concentration of aggregated iron forms, which could act as recombination centers. On the other hand, the 2% $\text{Fe}/\text{TiO}_2/\text{ZeSD}$ material presented worse absorption properties under visible light, while the sun-range Xe lamp was used in this reaction. Therefore, the enhanced activity of the 2% $\text{Fe}/\text{TiO}_2/\text{ZeSPD}$ photocatalyst was the result of the compilation of several properties, such as a high visible light absorption threshold, an adequate distribution of iron forms with low Fe^{3+} surface concentration, and the composition of iron forms

(more nano-Fe₂O₃, defected Fe₂O₃, and dispersed Fe³⁺ than in the corresponding PD photocatalyst). Iron forms in this reaction principally acted as electron or hole acceptors, reducing the charge recombination of the TiO₂ semiconductor. Additional XRF measurements of the liquid after reaction were performed showing good stability of the photocatalyst prepared by the SPD method.

After detailed experimental studies, I found it necessary to 'place sonophotodeposition' in the broader context of the related methods. Therefore, **Article 6**, which closes this dissertation, is a review work comparing sonophotodeposition with sonoelectrodeposition, which is another example of *in situ* coupling of ultrasound with chemical deposition. In both processes, the interaction between sonication and electrochemical or photochemical reactions is based mainly on the cavitation phenomenon. The mechanism can vary depending on the type of physical and chemical effects produced by ultrasound in the liquid [199, 214-216]. The influence of cavitation is mostly related to the enhanced mass transfer. In the case of the sonoelectrodeposition process, it is mainly seen as the increase in electrochemical current of the electrode. The resulting deposits of metals on the electrode surface present enhanced mechanical properties, such as increased hardness and brightness, greater adhesion, and enlarged film thickness, as well as improved deposition rates [217-219]. On the other hand, during sonophotodeposition, the enhanced mass transfer is able to increase the photochemical reaction rate or even modify the reaction pathway [140]. As a result, modification of some chemical properties of deposits can be observed. A comparison of these methods in the context of application clearly demonstrated an unambiguous advantage of sonoelectrodeposition over sonophotodeposition in the number of synthesized materials. The truth is that I was not able to find another researcher, who would have applied the simultaneous use of sonication and light for the synthesis of materials. The synergy of light irradiation with ultrasound was of course studied and applied in other processes, e.g., sonophotocatalytic decomposition of hazardous chemicals, but not in deposition of metals/metal oxides. This could mean that, with our research, we have filled a gap in this scientific area, showing that some interesting photo-active materials can be produced that simultaneously apply these two sources of energy. The sonophotodeposition methodology can be improved, along with developing sonochemistry (especially engineering of sonoreactors) and photochemistry, to reach the challenging goal of using solar energy in the production of photo-active materials. The sonophotodeposition method also presents some attractive features, which may be included in the frames of green chemistry principles: operating in mild reaction conditions (room temperature and pressure), a simple and time-saving procedure, and no need to use some strong reducing agents. The above make this method attractive in comparison to traditional synthesis methods, which are not always environmentally friendly.

4. Final comments on this work and future outlook

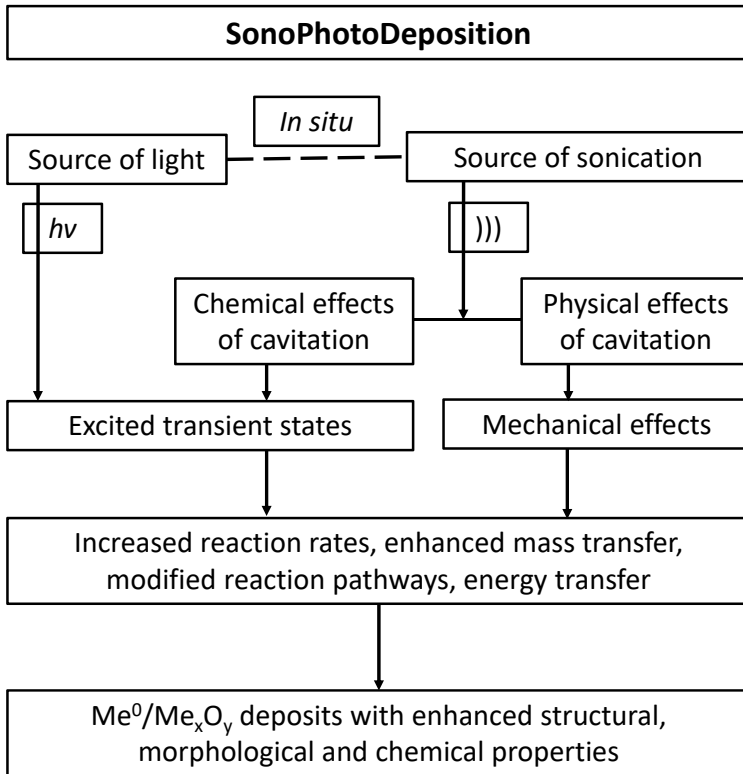
This compilation of six works—one patent application, four research articles, and one review—contains a full picture of my research on the sonophotodeposition method. In this part of my dissertation, possible directions for future studies are given. These have arisen together with the thesis development, e.g., during the literature review and as a result of the experimental measurements. Typically, for experimental basic research studies, it is difficult to impose rigid limits on laboratory works, because one discovery often creates many new questions and ideas.

At the beginning of this research period in my PhD studies, I found it surprising and at the same time interesting that simultaneous combination of light irradiation and ultrasound, intensively studied in different scientific aspects (e.g., homo- and heterogeneous liquid systems, photocatalytic decomposition of hazardous substances, sonoluminescence [140, 141, 220]) were not attempted in the synthesis of materials. My research studies revealed that deposition of metals/metal oxides can be achieved using the sonophotodeposition procedure, applying even ordinary ultrasonic baths with UV lamps typically used in photodeposition processes. This means that simultaneous combination of ultrasound with light irradiation does not require any sophisticated laboratory equipment. However, the simplest setup solution imposes some restrictions regarding the possibility of adjusting synthesis parameters, e.g., a fixed nominal frequency and ultrasonic power and the use of wide band gap semiconductors absorbing UV light, such as TiO_2 . In this context, a sonication horn with a power mode (nowadays also a conventional laboratory tool) in combination with a wide sun-range lamp (UV-vis-IR) gives more opportunities, such as adjusting the power of ultrasound or using different light-absorbing semiconducting materials. Therefore, further studies might benefit from investigating the deposition of metals/metal oxides on semiconducting materials absorbing visible light such as $\alpha\text{-Fe}_2\text{O}_3$, CdS or Ta_3N_5 . The results could be relevant for a worldwide trend of wider use of solar light [200, 221]. Generally, the sonophotodeposition method gives different possibilities regarding the combination of ultrasound and light irradiation sources in the setup and composition of the materials, depending on their application. The use of specific sources of ultrasound (power, frequency) and light irradiation (power, operating wavelength) determines the role they have in the sonophotodeposition process. In our second reaction system, composed of a 150 W UV-vis-IR Xe lamp and a 20 kHz sonication horn, the chemical role of light irradiation and the mechanical role of ultrasound during iron deposition were mainly found.

All materials I have synthesized using sonophotodeposition method were intended to be used in photocatalysis, although this is not the only possible application. They could also have been tested in other disciplines based on semiconducting materials, such as

optoelectronics. Herein, their possible applications in photocatalysis were checked in different processes: in gas and liquid phases, and in selective and non-selective reactions. In view of the results obtained from these reactions, it is seen that the combination of sono- and photochemistry during the preparation of the materials is appropriate for their photocatalytic features. High photocatalytic efficiencies in the selective organic transformation of benzyl alcohol into benzaldehyde, reported in **Article 3** and in **Article 5** (please follow Table 3.1), are definitely the most promising results. Selective photocatalytic processes are at present a very attractive and in-demand research topic studied by an increasing number of researchers [222]. Selective photocatalytic reactions are more difficult to conduct in comparison with non-selective reactions; however, their successful application can replace more complex synthesis procedures with a simple and environmentally-friendly photocatalytic method [223–225]. However, the real applications of these materials in the studied processes must be preceded by careful studies of metals/metal oxides loading on the surface of semiconducting material (I have underlined this issue discussing the results of **Article 4** and **Article 5**, especially). In this context, I have performed some preliminary studies regarding the optimal composition of Pd-Fe and Pt-Fe on TiO₂/Zeolite Y (continuation of the studies started in **Article 4**) as well as Fe loading on TiO₂/Zeolite Y (continuation of the studies presented in **Article 5**). Besides the 2 wt% of Fe discussed in **Article 5** (2%Fe/TiO₂/ZeSPD) lower loadings—1 wt% Fe and 0.5 wt% Fe—were checked in the photo-oxidation of benzyl alcohol. Higher conversions of benzyl alcohol with high selectivity to benzaldehyde were obtained for 1 wt% Fe ($C = 68 \%$, $S = 82 \%$) as well as for 0.5 wt% Fe conversion of BA ($C = 64 \%$, $S = 86 \%$) in comparison with 2 wt% Fe ($C = 56 \%$, $S = 90 \%$). The lower activity of the 2% Fe/TiO₂/ZeSPD photocatalyst could be partially explained by decreasing distance between the trapping sites in the particles with high iron content, which enhances the recombination activity. In the case of low iron content, fewer trapping sites are available, and the recombination activity is reduced [183]. Based on the above results and dealing with economic issues, I used the amount of 0.5 wt% Fe in the systems composed of two metals, Pd-Fe and Pt-Fe. The results of the selective photo-oxidation of benzyl alcohol showed that the highest conversion into benzaldehyde, with the selectivity above 80 %, was registered for the samples composed of 0.05 wt% Pt–0.5 wt% Fe ($C = 77 \%$, $S = 85 \%$) and 0.05 wt% Pd–0.5 wt% Fe ($C = 78 \%$, $S = 82 \%$). These preliminary results are quite promising, though some future characterization experiments should be continued in this topic, and the optimal amount should be checked in the reuse photocatalyst studies.

I would like to close this dissertation with the scheme below presenting the idea of sonophotodeposition and summarizing the method.



Scheme 4.1 The schematic summary of the sonophotodeposition method.

References

- [1] S.K. Bhangu, M. Ashokkumar, *Theory of sonochemistry*, Topics in Current Chemistry, **374**, (2016).
- [2] L.H. Thompson, L.K. Doraiswamy, *Sonochemistry: Science and engineering*, Industrial & Engineering Chemistry Research, **38**, 1215-1249, (1999).
- [3] Y.G. Adewuyi, *Sonochemistry: Environmental science and engineering applications*, Industrial & Engineering Chemistry Research, **40**, 4681-4715, (2001).
- [4] J.J. Hinman, K.S. Suslick, *Nanostructured materials synthesis using ultrasound*, Topics in Current Chemistry, **375**, (2017).
- [5] S.G. Babu, M. Ashokkumar, B. Neppolian, *The role of ultrasound on advanced oxidation processes*, Topics in Current Chemistry, **374**, (2016).
- [6] M. Draye, N. Kardos, *Advances in green organic sonochemistry*, Topics in Current Chemistry, **374**, (2016).
- [7] N. Pokhrel, P.K. Vabbina, N. Pala, *Sonochemistry: Science and engineering*, Ultrasonics Sonochemistry, **29**, 104-128, (2016).
- [8] J. Thornycroft, S. Barnaby, *Torpedo-boat destroyers*, in: Minutes of the proceedings of the institution of civil engineers, Thomas Telford-ICE Virtual Library, 51-69, (1895).
- [9] L. Rayleigh, *On the pressure developed in a liquid during the collapse of a spherical cavity*, London, Edinburgh, and Dublin Philosophical Magazine, **34**, 94-98, (1917).
- [10] W.T. Richards, A.L. Loomis, *The chemical effects of high frequency sound waves I. A preliminary study*, Journal of the American Chemical Society, **49**, 3086-3100, (1927).
- [11] R.W. Wood, A.L. Loomis, *The physical and biological effects of high frequency sound waves of great intensity*, Philosophical Magazine Series 7, **4**, 417-436, (1927).
- [12] S. Brohult, *Splitting of the haemocyanin molecule by ultrasonic waves*, Nature, **140**, 805 (1937).
- [13] J. Weiss, *Radiochemistry of aqueous solutions*, Nature, **153**, 48-50, (1944).
- [14] B.E. Noltingk, E.A. Neppiras, *Cavitation produced by ultrasonics*, Proceedings of the Physical Society of London Section B, **63**, 674-685, (1950).
- [15] A. Henglein, R. Schultz, *Der einfluss organischer verbindungen auf einige chemische wirkungen des ultraschalls*, Zeitschrift Fur Naturforschung Section B-A Journal of Chemical Sciences, **8**, 277-284, (1953).
- [16] S.A. Elder, J. Kolb, W.L. Nyborg, *Small-scale acoustic streaming effects in liquids*, Journal of the Acoustical Society of America, **26**, 933-933, (1954).
- [17] S.A. Elder, J. Kolb, W.L. Nyborg, *Physical factors involved in sonic irradiation of liquids*, Physical Review, **93**, 364-364, (1954).
- [18] E.A. Neppiras, *Acoustic cavitation*, Physics Reports-Review Section of Physics Letters, **61**, 159-251, (1980).

- [19] K. Makino, M.M. Mossoba, P. Riesz, *Chemical effects of ultrasound on aqueous-solutions - formation of hydroxyl radicals and hydrogen-atoms*, Journal of Physical Chemistry, **87**, 1369-1377, (1983).
- [20] K. Makino, M.M. Mossoba, P. Riesz, *Chemical effects of ultrasound on aqueous-solutions - evidence for $\cdot\text{OH}$ and $\cdot\text{H}$ by spin trapping*, Journal of the American Chemical Society, **104**, 3537-3539, (1982).
- [21] M.S. Plesset, A. Prosperetti, *Bubble dynamics and cavitation*, Annual Review of Fluid Mechanics, **9**, 145-185, (1977).
- [22] K.S. Suslick, *The chemical effects of ultrasound*, Scientific American, **260**, 80-86, (1989).
- [23] H. Xu, B.W. Zeiger, K.S. Suslick, *Sonochemical synthesis of nanomaterials*, Chemical Society Reviews, **42**, 2555-2567, (2013).
- [24] Pankaj, M. Ashokkumar, *Theoretical and experimental sonochemistry involving inorganic systems*, Springer, Berlin, Germany 2011.
- [25] D.E. Yount, *Skins of varying permeability - stabilization mechanism for gas cavitation nuclei*, Journal of the Acoustical Society of America, **65**, 1429-1439, (1979).
- [26] K. Yasui, T. Tuziuti, W. Kanematsu, K. Kato, *Dynamic equilibrium model for a bulk nanobubble and a microbubble partly covered with hydrophobic material*, Langmuir, **32**, 11101-11110, (2016).
- [27] W.J. Wang, W.Z. Chen, M.J. Lu, R.J. Wei, *Bubble oscillations driven by aspherical ultrasound in liquid*, Journal of the Acoustical Society of America, **114**, 1898-1904, (2003).
- [28] D.E. Yount, E.W. Gillary, D.C. Hoffman, *A microscopic investigation of bubble formation nuclei*, Journal of the Acoustical Society of America, **76**, 1511-1521, (1984).
- [29] J.P. Lorimer, T.J. Mason, *Sonochemistry part 1-the physical aspects*, Chemical Society Reviews, **16**, 239-274, (1987).
- [30] M. Ashokkumar, *Ultrasonic synthesis of functional materials*, in: Springerbriefs in green chemistry for sustainability Springer, Cham, 17-40, (2016).
- [31] F. Grieser, M. Ashokkumar, *Sonochemical synthesis of inorganic and organic colloids.*, in: F. Caruso (Ed.) Colloids and colloid assemblies: Synthesis, modification, organization and utilization of colloid particles, Wiley-VCH, Weinheim, 120-149, (2006).
- [32] T. Leong, S.H. Wu, S. Kentish, M. Ashokkumar, *Growth of bubbles by rectified diffusion in aqueous surfactant solutions*, Journal of Physical Chemistry C, **114**, 20141-20145, (2010).
- [33] F.R. Young, *Cavitation* McGraw-Hill, New York, 1989.
- [34] G.J. Price, M. Ashokkumar, F. Grieser, *Sonoluminescence quenching of organic compounds in aqueous solution: Frequency effects and implications for sonochemistry*, Journal of the American Chemical Society, **126**, 2755-2762, (2004).
- [35] M.H. Entezari, P. Kruus, *Effect of frequency on sonochemical reactions 2. Temperature and intensity effects*, Ultrasonics Sonochemistry, **3**, 19-24, (1996).

- [36] A. Francony, C. Petrier, *Sonochemical degradation of carbon tetrachloride in aqueous solution at two frequencies: 20 kHz and 500 kHz*, *Ultrasonics Sonochemistry*, **3**, S77-S82, (1996).
- [37] C. Petrier, A. Jeunet, J.L. Luche, G. Reverdy, *Unexpected frequency-effects on the rate of oxidative processes induced by ultrasound*, *Journal of the American Chemical Society*, **114**, 3148-3150, (1992).
- [38] L.A. Crum, *Comments on the evolving field of sonochemistry by a cavitation physicist*, *Ultrasonics Sonochemistry*, **2**, S147-S152, (1995).
- [39] T.J. Mason, J.P. Lorimer, D.M. Bates, Y. Zhao, *Dosimetry in sonochemistry - the use of aqueous terephthalate ion as a fluorescence monitor*, *Ultrasonics Sonochemistry*, **1**, S91-S95, (1994).
- [40] R.F. Contamine, A.M. Wilhelm, J. Berlan, H. Delmas, *Power measurement in sonochemistry*, *Ultrasonics Sonochemistry*, **2**, S43-S47, (1995).
- [41] F. Contamine, F. Faid, A.M. Wilhelm, J. Berlan, H. Delmas, *Chemical reactions under ultrasound: Discrimination of chemical and physical effects*, *Chemical Engineering Science*, **49**, 5865-5873, (1994).
- [42] S. Merouani, O. Hamdaoui, Y. Rezgui, M. Guemini, *Effects of ultrasound frequency and acoustic amplitude on the size of sonochemically active bubbles - theoretical study*, *Ultrasonics Sonochemistry*, **20**, 815-819, (2013).
- [43] A. Brotchie, F. Grieser, M. Ashokkumar, *Effect of power and frequency on bubble-size distributions in acoustic cavitation*, *Physical Review Letters*, **102**, (2009).
- [44] M. Ibsi, B. Brown, *Variation of relative intensity of cavitation with temperature*, *Journal of the Acoustical Society of America*, **41**, 568-572, (1967).
- [45] C.M. Sehgal, S.Y. Wang, *Threshold intensities and kinetics of sonoreaction of thymine in aqueous-solutions at low ultrasonic intensities*, *Journal of the American Chemical Society*, **103**, 6606-6611, (1981).
- [46] K.J. Moulton, S. Koritala, E.N. Frankel, *Ultrasonic hydrogenation of soybean oil*, *Journal of the American Oil Chemists Society*, **60**, 1257-1258, (1983).
- [47] K.J. Moulton, S. Koritala, K. Warner, E.N. Frankel, *Continuous ultrasonic hydrogenation of soybean oil 2. Operating-conditions and oil quality*, *Journal of the American Oil Chemists Society*, **64**, 542-547, (1987).
- [48] A. Gedanken, *Sonochemistry and its application to nanochemistry*, *Current Science*, **85**, 1720-1722, (2003).
- [49] P. Riesz, T. Kondo, C.M. Krishna, *Sonochemistry of volatile and nonvolatile solutes in aqueous-solutions - EPR and spin trapping studies*, *Ultrasonics*, **28**, 295-303, (1990).
- [50] P. Riesz, D. Berdahl, C.L. Christman, *Free-radical generation by ultrasound in aqueous and nonaqueous solutions*, *Environmental Health Perspectives*, **64**, 233-252, (1985).
- [51] K.S. Suslick, J.J. Gawienowski, P.F. Schubert, H.H. Wang, *Sonochemistry in non-aqueous liquids*, *Ultrasonics*, **22**, 33-36, (1984).

- [52] K.S. Suslick, J.J. Gawienowski, P.F. Schubert, H.H. Wang, *Alkane sonochemistry*, Journal of Physical Chemistry, **87**, 2299-2301, (1983).
- [53] N. Serpone, P. Colarusso, *Sonochemistry 1. Effects of ultrasounds on heterogeneous chemical-reactions - a useful tool to generate radicals and to examine reaction-mechanisms*, Research on Chemical Intermediates, **20**, 635-679, (1994).
- [54] M. Ashokkumar, J. Lee, S. Kentish, F. Grieser, *Bubbles in an acoustic field: An overview*, Ultrasonics Sonochemistry, **14**, 470-475, (2007).
- [55] K.S. Suslick, L.A. Crum, *Sonochemistry and sonoluminescence*, in: M.J. Crocker (Ed.) Handbook of acoustics, Wiley-Interscience, New York 243-253, (1998).
- [56] C.C. Wu, P.H. Roberts, *Shock-wave propagation in a sonoluminescing gas bubble*, Physical Review Letters, **70**, 3424-3427, (1993).
- [57] K. Yasui, *Alternative model of single-bubble sonoluminescence*, Physical Review E, **56**, 6750-6760, (1997).
- [58] K. Yasui, *Single-bubble and multibubble sonoluminescence*, Physical Review Letters, **83**, 4297-4300, (1999).
- [59] M. Ashokkumar, *The characterization of acoustic cavitation bubbles - an overview*, Ultrasonics Sonochemistry, **18**, 864-872, (2011).
- [60] S. Hatanaka, H. Mitome, K. Yasui, S. Hayashi, *Single-bubble sonochemiluminescence in aqueous luminol solutions*, Journal of the American Chemical Society, **124**, 10250-10251, (2002).
- [61] C.D. Ohl, T. Kurz, R. Geisler, O. Lindau, W. Lauterborn, *Bubble dynamics, shock waves and sonoluminescence*, Philosophical Transactions of the Royal Society A: Mathematical Physical and Engineering Sciences, **357**, 269-294, (1999).
- [62] L.A. Crum, *Sonoluminescence, sonochemistry, and sonophysics*, Journal of the Acoustical Society of America, **95**, 559-562, (1994).
- [63] T.J. Mason, D. Peters, *Practical sonochemistry: Power ultrasound uses and applications*, Woodhead, Cambridge, 2002.
- [64] M.A. Margulis, *Fundamental aspects of sonochemistry*, Ultrasonics, **30**, 152-155, (1992).
- [65] M.A. Margulis, *Sonoluminescence and sonochemical reactions in cavitation fields - a review*, Ultrasonics, **23**, 157-169, (1985).
- [66] T. Lepoint, F. Mullie, *What exactly is cavitation chemistry*, Ultrasonics Sonochemistry, **1**, S13-S22, (1994).
- [67] I. Hua, R.H. Hochemer, M.R. Hoffmann, *Sonolytic hydrolysis of p-nitrophenyl acetate - the role of supercritical water*, Journal of Physical Chemistry, **99**, 2335-2342, (1995).
- [68] K.S. Suslick, D.J. Flannigan, *Inside a collapsing bubble: Sonoluminescence and the conditions during cavitation*, Annual Review of Physical Chemistry, **59**, 659-683, (2008).
- [69] K.S. Suslick, S.B. Choe, A.A. Cichowlas, M.W. Grinstaff, *Sonochemical synthesis of amorphous iron*, Nature, **353**, 414-416, (1991).

- [70] K.S. Suslick, G.J. Price, *Applications of ultrasound to materials chemistry*, Annual Review of Materials Science, **29**, 295-326, (1999).
- [71] D.G. Shchukin, D. Radziuk, H. Mohwald, *Ultrasonic fabrication of metallic nanomaterial and nanoalloys*, in: D.R. Clarke, M. Ruhle, F. Zok (Eds.) Annual Review of Materials Research, **40**, 345-362, (2010).
- [72] Y. Mizukoshi, K. Okitsu, Y. Maeda, T.A. Yamamoto, R. Oshima, Y. Nagata, *Sonochemical preparation of bimetallic nanoparticles of gold/palladium in aqueous solution*, Journal of Physical Chemistry B, **101**, 7033-7037, (1997).
- [73] K. Vinodgopal, Y.H. He, M. Ashokkumar, F. Grieser, *Sonochemically prepared platinum-ruthenium bimetallic nanoparticles*, Journal of Physical Chemistry B, **110**, 3849-3852, (2006).
- [74] A. Godinez-Garcia, J.F. Perez-Robles, H.V. Martinez-Tejada, O. Solorza-Feria, *Characterization and electrocatalytic properties of sonochemical synthesized PdAg nanoparticles*, Materials Chemistry and Physics, **134**, 1013-1019, (2012).
- [75] T. Gao, T.H. Wang, *Sonochemical synthesis of SnO₂ nanobelt/CdS nanoparticle core/shell heterostructures*, Chemical Communications, **22**, 2558-2559, (2004).
- [76] P. Hasin, Y.Y. Wu, *Sonochemical synthesis of copper hydride (CuH)*, Chemical Communications, **48**, 1302-1304, (2012).
- [77] M.A. Alavi, A. Morsali, *Syntheses and characterization of Mg(OH)₂ and MgO nanostructures by ultrasonic method*, Ultrasonics Sonochemistry, **17**, 441-446, (2010).
- [78] M.A. Alavi, A. Morsali, *Ultrasonic-assisted synthesis of Ca(OH)₂ and CaO nanostructures*, Journal of Experimental Nanoscience, **5**, 93-105, (2010).
- [79] M.A. Alavi, A. Morsali, *Syntheses and characterization of Sr(OH)₂ and SrCO₃ nanostructures by ultrasonic method*, Ultrasonics Sonochemistry, **17**, 132-138, (2010).
- [80] J.J. Zhu, S. Xu, H. Wang, J.M. Zhu, H.Y. Chen, *Sonochemical synthesis of CdSe hollow spherical assemblies via an in-situ template route*, Advanced Materials, **15**, 156-159, (2003).
- [81] X. Zhang, H.L. Zhao, X.J. Tao, Y.B. Zhao, Z.J. Zhang, *Sonochemical method for the preparation of ZnO nanorods and trigonal-shaped ultrafine particles*, Materials Letters, **59**, 1745-1747, (2005).
- [82] D.L. Chen, S.H. Yoo, Q.S. Huang, G. Ali, S.O. Cho, *Sonochemical synthesis of Ag/AgCl nanocubes and their efficient visible-light-driven photocatalytic performance*, Chemistry - A European Journal, **18**, 5192-5200, (2012).
- [83] R. Wahab, S.G. Ansari, Y.S. Kim, H.K. Seo, H.S. Shin, *Room temperature synthesis of needle-shaped ZnO nanorods via sonochemical method*, Applied Surface Science, **253**, 7622-7626, (2007).
- [84] K. Chatakondur, M.L.H. Green, M.E. Thompson, K.S. Suslick, *The enhancement of intercalation reactions by ultrasound*, Journal of the Chemical Society, Chemical Communications, **12**, 900-901, (1987).
- [85] L.M. Viculis, J.J. Mack, R.B. Kaner, *A chemical route to carbon nanoscrolls*, Science, **299**, 1361-1361, (2003).

- [86] J. Walter, M. Nishioka, S. Hara, *Ultrathin platinum nanoparticles encapsulated in a graphite lattice-prepared by a sonochemical approach*, Chemistry of Materials, **13**, 1828-1833, (2001).
- [87] J.E. Jones, M.C. Cheshire, D.J. Casadonte, C.C. Phifer, *Facile sonochemical synthesis of graphite intercalation compounds*, Organic Letters, **6**, 1915-1917, (2004).
- [88] Y. Hernandez, V. Nicolosi, M. Lotya, F.M. Blighe, Z.Y. Sun, S. De, I.T. McGovern, B. Holland, M. Byrne, Y.K. Gun'ko, J.J. Boland, P. Niraj, G. Duesberg, S. Krishnamurthy, R. Goodhue, J. Hutchison, V. Scardaci, A.C. Ferrari, J.N. Coleman, *High-yield production of graphene by liquid-phase exfoliation of graphite*, Nature Nanotechnology, **3**, 563-568, (2008).
- [89] V. Belova, T. Borodina, H. Mohwald, D.G. Shchukin, *The effect of high intensity ultrasound on the loading of Au nanoparticles into titanium dioxide*, Ultrasonics Sonochemistry, **18**, 310-317, (2011).
- [90] H.M. Xiong, D.G. Shchukin, H. Mohwald, Y. Xu, Y.Y. Xia, *Sonochemical synthesis of highly luminescent zinc oxide nanoparticles doped with magnesium (II)*, Angewandte Chemie International Edition, **48**, 2727-2731, (2009).
- [91] T. Prozorov, B. McCarty, Z. Cai, R. Prozorov, K.S. Suslick, *Effects of high-intensity ultrasound on $\text{Bi}_2\text{Sr}_2\text{CaCu}_2\text{O}_{8+x}$ superconductor*, Applied Physics Letters, **85**, 3513-3515, (2004).
- [92] T. Prozorov, R. Prozorov, A. Snezhko, K.S. Suslick, *Sonochemical modification of the superconducting properties of MgB_2* , Applied Physics Letters, **83**, 2019-2021, (2003).
- [93] T. Prozorov, R. Prozorov, K.S. Suslick, *High velocity interparticle collisions driven by ultrasound*, Journal of the American Chemical Society, **126**, 13890-13891, (2004).
- [94] D.V. Andreeva, D. Fix, H. Mohwald, D.G. Shchukin, *Self-healing anticorrosion coatings based on pH-sensitive polyelectrolyte/inhibitor sandwichlike nanostructures*, Advanced Materials, **20**, 2789-2794, (2008).
- [95] J.C. Yu, J.G. Yu, W.K. Ho, L.Z. Zhang, *Preparation of highly photocatalytic active nano-sized TiO_2 particles via ultrasonic irradiation*, Chemical Communications, **19**, 1942-1943, (2001).
- [96] D. Qian, J.Z. Jiang, P.L. Hansen, *Preparation of ZnO nanocrystals via ultrasonic irradiation*, Chemical Communications, **9**, 1078-1079, (2003).
- [97] B.W. Zeiger, K.S. Suslick, *Sonofragmentation of molecular crystals*, Journal of the American Chemical Society, **133**, 14530-14533, (2011).
- [98] D.K. Bucar, L.R. MacGillivray, *Preparation and reactivity of nanocrystalline cocrystals formed via sonocrystallization*, Journal of the American Chemical Society, **129**, 32-33, (2007).
- [99] J.R.G. Sander, D.K. Bucar, J. Baltrusaitis, L.R. MacGillivray, *Organic nanocrystals of the resorcinarene hexamer via sonochemistry: Evidence of reversed crystal growth involving hollow morphologies*, Journal of the American Chemical Society, **134**, 6900-6903, (2012).
- [100] C.R. Hickenboth, J.S. Moore, S.R. White, N.R. Sottos, J. Baudry, S.R. Wilson, *Biasing reaction pathways with mechanical force*, Nature, **446**, 423-427, (2007).
- [101] M.J. Kryger, M.T. Ong, S.A. Odom, N.R. Sottos, S.R. White, T.J. Martinez, J.S. Moore, *Masked cyanoacrylates unveiled by mechanical force*, Journal of the American Chemical Society, **132**, 4558-4559, (2010).

- [102] K. Shafi, A. Ulman, A. Dyal, X.Z. Yan, N.L. Yang, C. Estournes, L. Fournes, A. Wattiaux, H. White, M. Rafailovich, *Magnetic enhancement of γ -Fe₂O₃ nanoparticles by sonochemical coating*, Chemistry of Materials, **14**, 1778-1787, (2002).
- [103] K. Shafi, A. Ulman, X.Z. Yan, N.L. Yang, M. Himmelhaus, M. Grunze, *Sonochemical preparation of silane-coated titania particles*, Langmuir, **17**, 1726-1730, (2001).
- [104] Q. Chen, C. Boothroyd, G.H. Tan, N. Sutanto, A.M. Soutar, M.T. Zeng, *Silica coating of nanoparticles by the sonogel process*, Langmuir, **24**, 650-653, (2008).
- [105] J.E. Park, M. Saikawa, M. Atobe, T. Fuchigami, *Highly-regulated nanocoatings of polymer films on carbon nanofibers using ultrasonic irradiation*, Chemical Communications, **25**, 2708-2710, (2006).
- [106] A.L. Morel, S.I. Nikitenko, K. Gionnet, A. Wattiaux, J. Lai-Kee-Him, C. Labrugere, B. Chevalier, G. Deleris, C. Petibois, A. Brisson, M. Simonoff, *Sonochemical approach to the synthesis of Fe₃O₄@SiO₂ core-shell nanoparticles with tunable properties*, ACS Nano, **2**, 847-856, (2008).
- [107] T. Gao, Q.H. Li, T.H. Wang, *Sonochemical synthesis, optical properties, and electrical properties of core/shell-type ZnO nanorod/CdS nanoparticle composites*, Chemistry of Materials, **17**, 887-892, (2005).
- [108] V.G. Pol, H. Grisar, A. Gedanken, *Coating noble metal nanocrystals (Ag, Au, Pd, and Pt) on polystyrene spheres via ultrasound irradiation*, Langmuir, **21**, 3635-3640, (2005).
- [109] V.G. Pol, M. Motiei, A. Gedanken, J. Calderon-Moreno, Y. Mastai, *Sonochemical deposition of air-stable iron nanoparticles on monodispersed carbon spherules*, Chemistry of Materials, **15**, 1378-1384, (2003).
- [110] V.G. Pol, G. Wildermuth, J. Felsche, A. Gedanken, J. Calderon-Moreno, *Sonochemical deposition of Au nanoparticles on titania and the significant decrease in the melting point of gold*, Journal of Nanoscience and Nanotechnology, **5**, 975-979, (2005).
- [111] V.G. Pol, A. Gedanken, J. Calderon-Moreno, V. Palchik, M.A. Slifkin, A.M. Weiss, *Deposition of gold nanoparticles on silica spheres: A sonochemical approach*, Chemistry of Materials, **15**, 3402-3402, (2003).
- [112] H.B. Pan, C.M. Wai, *Facile sonochemical synthesis of carbon nanotube-supported bimetallic Pt-Rh nanoparticles for room temperature hydrogenation of arenes*, New Journal of Chemistry, **35**, 1649-1660, (2011).
- [113] Y. Mizukoshi, Y. Tsuru, A. Tominaga, S. Seino, N. Masahashi, S. Tanabe, T.A. Yamamoto, *Sonochemical immobilization of noble metal nanoparticles on the surface of maghemite: Mechanism and morphological control of the products*, Ultrasonics Sonochemistry, **15**, 875-880, (2008).
- [114] Y. Mizukoshi, Y. Makise, T. Shuto, J. Hu, A. Tominaga, S. Shironita, S. Tanabe, *Immobilization of noble metal nanoparticles on the surface of TiO₂ by the sonochemical method: Photocatalytic production of hydrogen from an aqueous solution of ethanol*, Ultrasonics Sonochemistry, **14**, 387-392, (2007).

- [115] D. Yang, S.W. Lee, *Photocatalytic activity of Ag, Au-deposited TiO₂ nanoparticles prepared by sonochemical reduction method*, Surface Review and Letters, **17**, 21-26, (2010).
- [116] D. Yang, S.E. Park, J.K. Lee, S.W. Lee, *Sonochemical deposition of nanosized Au on titanium oxides with different surface coverage and their photocatalytic activity*, Journal of Crystal Growth, **311**, 508-511, (2009).
- [117] J.H. Bang, K.S. Suslick, *Applications of ultrasound to the synthesis of nanostructured materials*, Advanced Materials, **22**, 1039-1059, (2010).
- [118] H.X. Xu, K.S. Suslick, *Sonochemical preparation of functionalized graphenes*, Journal of the American Chemical Society, **133**, 9148-9151, (2011).
- [119] K.S. Suslick, M.W. Grinstaff, *Protein microencapsulation of nonaqueous liquids*, Journal of the American Chemical Society, **112**, 7807-7809, (1990).
- [120] G. Dantsin, K.S. Suslick, *Sonochemical preparation of a nanostructured bifunctional catalyst*, Journal of the American Chemical Society, **122**, 5214-5215, (2000).
- [121] H. Kisch, *Semiconductor photocatalysis: Principles and applications*, Wiley-VCH Verlag GmbH & Co. KGaA, Weinheim, Germany, 2015.
- [122] S.E. Braslavsky, A.M. Braun, A.E. Cassano, A.V. Emeline, M.I. Litter, L. Palmisano, V.N. Parmon, N. Serpone, O.M. Alfano, M. Anpo, V. Augugliaro, C. Bohne, S. Esplugas, E. Oliveros, C. von Sonntag, R.G. Weiss, M. Schiavello, *Glossary of terms used in photocatalysis and radiation catalysis (IUPAC recommendations 2011)*, Pure and Applied Chemistry, **83**, 931-1014, (2011).
- [123] T. Sakata, K. Hashimoto, M. Hiramoto, *New aspects of electron-transfer on semiconductor surface - dye-sensitization system*, Journal of Physical Chemistry, **94**, 3040-3045, (1990).
- [124] M. Buchalska, J. Kuncewicz, E. Swietek, P. Labuz, T. Baran, G. Stochel, W. Macyk, *Photoinduced hole injection in semiconductor-coordination compound systems*, Coordination Chemistry Reviews, **257**, 767-775, (2013).
- [125] M.R. Hoffmann, S.T. Martin, W.Y. Choi, D.W. Bahnemann, *Environmental applications of semiconductor photocatalysis*, Chemical Reviews, **95**, 69-96, (1995).
- [126] S. Chaturvedi, P.N. Dave, *Environmental application of photocatalysis*, in: R.J. Tayade (Ed.) Photocatalytic Materials & Surfaces for Environmental Cleanup-II, **734**, 273-294, (2013).
- [127] P. Pichat, *Fundamentals of TiO₂ photocatalysis. Consequences for some environmental applications*, in: J.C. Colmenares, Y.J. Xu (Eds.) Heterogeneous photocatalysis: From fundamentals to green applications, Green Chemistry and Sustainable Technology. Springer, Berlin, Heidelberg, 321-359, (2016).
- [128] K. Wenderich, G. Mul, *Methods, mechanism, and applications of photodeposition in photocatalysis: A review*, Chemical Reviews, **116**, 14587-14619, (2016).
- [129] B. Kraeutler, A.J. Bard, *Heterogeneous photocatalytic preparation of supported catalysts - photodeposition of platinum on TiO₂ powder and other substrates*, Journal of the American Chemical Society, **100**, 4317-4318, (1978).

- [130] M. Gratzel, *Photoelectrochemical cells*, Nature, **414**, 338-344, (2001).
- [131] D.R. Lidle, *CRC handbook of chemistry and physics*, 86th ed., 2005.
- [132] K. Maeda, R. Abe, K. Domen, *Role and function of ruthenium species as promoters with TaON-based photocatalysts for oxygen evolution in two-step water splitting under visible light*, Journal of Physical Chemistry C, **115**, 3057-3064, (2011).
- [133] L.L. Ma, Z.D. Cui, Z.Y. Li, S.L. Zhu, Y.Q. Liang, Q.W. Yin, X.J. Yang, *The fabrication of SnSe/Ag nanoparticles on TiO₂ nanotubes*, Materials Science and Engineering B: Advanced Functional Solid-State Materials, **178**, 77-82, (2013).
- [134] N.P. Dasgupta, C. Liu, S. Andrews, F.B. Prinz, P.D. Yang, *Atomic layer deposition of platinum catalysts on nanowire surfaces for photoelectrochemical water reduction*, Journal of the American Chemical Society, **135**, 12932-12935, (2013).
- [135] A. Murata, N. Oka, S. Nakamura, Y. Shigesato, *Visible-light active photocatalytic WO₃ films loaded with Pt nanoparticles deposited by sputtering*, Journal of Nanoscience and Nanotechnology, **12**, 5082-5086, (2012).
- [136] K. Iizuka, T. Wato, Y. Miseki, K. Saito, A. Kudo, *Photocatalytic reduction of carbon dioxide over Ag cocatalyst-loaded Al₄Ti₄O₁₅ (A = Ca, Sr, and Ba) using water as a reducing reagent*, Journal of the American Chemical Society, **133**, 20863-20868, (2011).
- [137] J.X. Li, J.H. Xu, W.L. Dai, K.N. Fan, *Dependence of Ag deposition methods on the photocatalytic activity and surface state of TiO₂ with twistlike helix structure*, Journal of Physical Chemistry C, **113**, 8343-8349, (2009).
- [138] M.C. Hidalgo, J.J. Murcia, J.A. Navio, G. Colon, *Photodeposition of gold on titanium dioxide for photocatalytic phenol oxidation*, Applied Catalysis A: General, **397**, 112-120, (2011).
- [139] S.A.C. Carabineiro, B.F. Machado, R.R. Bacsá, P. Serp, G. Drazic, J.L. Faria, J.L. Figueiredo, *Catalytic performance of Au/ZnO nanocatalysts for Co oxidation*, Journal of Catalysis, **273**, 191-198, (2010).
- [140] I. Rosenthal, J.Z. Sostaric, P. Riesz, *Enlightened sonochemistry*, Research on Chemical Intermediates, **30**, 685-701, (2004).
- [141] S. Toma, A. Gaplovsky, J.L. Luche, *The effect of ultrasound on photochemical reactions*, Ultrasonics Sonochemistry, **8**, 201-207, (2001).
- [142] K.S. Suslick, J.W. Goodale, P.F. Schubert, H.H. Wang, *Sonochemistry and sonocatalysis of metal-carbonyls*, Journal of the American Chemical Society, **105**, 5781-5785, (1983).
- [143] K.S. Suslick, P.F. Schubert, *Sonochemistry of Mn₂(CO)₁₀ and Re₂(CO)₁₀*, Journal of the American Chemical Society, **105**, 6042-6044, (1983).
- [144] D. Reyman, A. Pardo, J.M.L. Poyato, J.G. Rodriguez, *Photochemical and sonochemical reactions of norharmane*, Journal of Photochemistry and Photobiology A: Chemistry, **98**, 39-44, (1996).
- [145] A. Gaplovsky, J. Donovalova, S. Toma, R. Kubinec, *Ultrasound effects on photochemical reactions 1. Photochemical reactions of ketones with alkenes*, Ultrasonics Sonochemistry, **4**, 109-115, (1997).

- [146] A. Gaplovsky, J. Donovalova, S. Toma, R. Kubinec, *Ultrasound effects on photochemical reactions 2. A study of ultrasound effects on some monomolecular and bimolecular photochemical reactions*, Journal of Photochemistry and Photobiology A: Chemistry, **115**, 13-19, (1998).
- [147] A. Gaplovsky, M. Gaplovsky, S. Toma, J.L. Luche, *Ultrasound effects on the photopinacolization of benzophenone*, Journal of Organic Chemistry, **65**, 8444-8447, (2000).
- [148] R.G. Compton, R.P. Akkermans, B.A. Coles, F. Marken, *Ultrasound in photoelectrochemistry: A new approach to the enhancement of the efficiency of semiconductor electrode processes*, Ultrasonics Sonochemistry, **4**, 223-228, (1997).
- [149] M. Mrowetz, C. Pirola, E. Selli, *Degradation of organic water pollutants through sonophotocatalysis in the presence of TiO₂*, Ultrasonics Sonochemistry, **10**, 247-254, (2003).
- [150] Y. Kado, M. Atobe, T. Nonaka, *Ultrasonic effects on electroorganic processes - part 20. Photocatalytic oxidation of aliphatic alcohols in aqueous suspension of TiO₂ powder*, Ultrasonics Sonochemistry, **8**, 69-74, (2001).
- [151] L. Sun, J. Li, C. Wang, S. Li, Y. Lai, H. Chen, C. Lin, *Ultrasound aided photochemical synthesis of Ag loaded TiO₂ nanotube arrays to enhance photocatalytic activity*, Journal of Hazardous Materials, **171**, 1045-1050, (2009).
- [152] S.W. Lee, S. Obregón-Alfaro, V. Rodríguez-González, *Photocatalytic coatings of silver-TiO₂ nanocomposites on foamed waste-glass prepared by sonochemical process*, Journal of Photochemistry and Photobiology A: Chemistry, **221**, 71-76, (2011).
- [153] J.C. Yu, X.C. Wang, L. Wu, W.K. Ho, L.Z. Zhang, G.T. Zhou, *Sono- and photochemical routes for the formation of highly dispersed gold nanoclusters in mesoporous titania films*, Advanced Functional Materials, **14**, 1178-1183, (2004).
- [154] J.C. Colmenares, A. Magdziarz, D. Lomot, O. Chernyayeva, D. Lisovytskiy, *A new photocatalytic tool in VOCs abatement: Effective synergetic combination of sonication and light for the synthesis of monometallic palladium-containing TiO₂*, Applied Catalysis B: Environmental, **147**, 624-632, (2014).
- [155] J.C. Colmenares, A. Magdziarz, A. Bielejewska, *High-value chemicals obtained from selective photo-oxidation of glucose in the presence of nanostructured titanium photocatalysts*, Bioresource Technology, **102**, 11254-11257, (2011).
- [156] M.H. Entezari, P. Kruus, R. Otson, *The effect of frequency on sonochemical reactions III: Dissociation of carbon disulfide*, Ultrasonics Sonochemistry, **4**, 49-54, (1997).
- [157] F.P. Byrne, S. Jin, G. Paggiola, T.H.M. Petchey, J.H. Clark, T.J. Farmer, A.J. Hunt, C. Robert McElroy, J. Sherwood, *Tools and techniques for solvent selection: Green solvent selection guides*, Sustainable Chemical Processes, **4**, 7-31, (2016).
- [158] C.J. Xi, Z.S. Chen, Q.L. Li, Z.S. Jin, *Effects of H⁺, Cl⁻ and CH₃COOH on the photocatalytic conversion of PtCl₆²⁻ in aqueous TiO₂ dispersion*, Journal of Photochemistry and Photobiology A: Chemistry, **87**, 249-255, (1995).

- [159] F.X. Zhang, J.X. Chen, X. Zhang, W.L. Gao, R.C. Jin, N.J. Guan, Y.Z. Li, *Synthesis of titania-supported platinum catalyst: The effect of pH on morphology control and valence state during photodeposition*, *Langmuir*, **20**, 9329–9334, (2004).
- [160] M. Qamar, A.K. Ganguli, *Self-assembling behaviour of Pt nanoparticles onto surface of TiO₂ and their resulting photocatalytic activity*, *Bulletin of Materials Science*, **36**, 945–951, (2013).
- [161] J.S. Lee, W.Y. Choi, *Photocatalytic reactivity of surface platinized TiO₂: Substrate specificity and the effect of Pt oxidation state*, *Journal of Physical Chemistry B*, **109**, 7399–7406, (2005).
- [162] P. Riesz, T. Kondo, A.J. Carmichael, *Sonochemistry of acetone and acetonitrile in aqueous-solutions- a spin-trapping study*, *Free Radical Research Communications*, **19**, S45–S53, (1993).
- [163] A. Lifshitz, A. Moran, S. Bidani, *Thermal-reactions of acetonitrile at high-temperatures - pyrolysis behind reflected shocks*, *International Journal of Chemical Kinetics*, **19**, 61–79, (1987).
- [164] H. Togo, *Advanced free radical reactions for organic synthesis*, Elsevier, 2004.
- [165] H. Tanaka, H. Harada, *Sonolysis of an oxalic acid solution under xenon lamp irradiation*, *Ultrasonics Sonochemistry*, **17**, 770–772, (2010).
- [166] P.A. Osorio-Vargas, C. Pulgarin, A. Sienkiewicz, L.R. Pizzio, M.N. Blanco, R.A. Torres-Palma, C. Petrier, J.A. Rengifo-Herrera, *Low-frequency ultrasound induces oxygen vacancies formation and visible light absorption in TiO₂P-25 nanoparticles*, *Ultrasonics Sonochemistry*, **19**, 383–386, (2012).
- [167] I. Nakamura, N. Negishi, S. Kutsuna, T. Ihara, S. Sugihara, E. Takeuchi, *Role of oxygen vacancy in the plasma-treated TiO₂ photocatalyst with visible light activity for no removal*, *Journal of Molecular Catalysis A: Chemical*, **161**, 205–212, (2000).
- [168] M.A. Aramendia, V. Borau, J.C. Colmenares, A. Marinas, J.M. Marinas, J.A. Navio, F.J. Urbano, *Modification of the photocatalytic activity of Pd/TiO₂ and Zn/TiO₂ systems through different oxidative and reductive calcination treatments*, *Applied Catalysis B: Environmental*, **80**, 88–97, (2008).
- [169] J.C. Colmenares, A. Magdziarz, M.A. Aramendia, A. Marinas, J.M. Marinas, F.J. Urbano, J.A. Navio, *Influence of the strong metal support interaction effect (SMSI) of Pt/TiO₂ and Pd/TiO₂ systems in the photocatalytic biohydrogen production from glucose solution*, *Catalysis Communications*, **16**, 1–6, (2011).
- [170] D. Bahnemann, A. Henglein, L. Spanhel, *Detection of the intermediates of colloidal TiO₂-catalyzed photoreactions*, *Faraday Discussions*, **78**, 151–163, (1984).
- [171] A.A. Ismail, D.W. Bahnemann, S.A. Al-Sayari, *Synthesis and photocatalytic properties of nanocrystalline Au, Pd and Pt photodeposited onto mesoporous RuO₂-TiO₂ nanocomposites*, *Applied Catalysis A: General*, **431**, 62–68, (2012).
- [172] A.A. Ismail, D.W. Bahnemann, *One-step synthesis of mesoporous platinum/titania nanocomposites as photocatalyst with enhanced photocatalytic activity for methanol oxidation*, *Green Chemistry*, **13**, 428–435, (2011).

- [173] Z. Wang, J. Liu, W. Chen, *Plasmonic Ag/AgBr nanohybrid: Synergistic effect of SPR with photographic sensitivity for enhanced photocatalytic activity and stability*, Dalton Transactions, **41**, 4866-4870, (2012).
- [174] R. Schasfoort, A. Tudos, *Handbook of surface plasmon resonance*, RSC Publishing, Cambridge, 2008.
- [175] M. Chen, J.P. Liu, S.H. Sun, *One-step synthesis of FePt nanoparticles with tunable size*, Journal of the American Chemical Society, **126**, 8394-8395, (2004).
- [176] C.-T. Hsieh, J.-Y. Lin, *Fabrication of bimetallic Pt-M (M=Fe, Co, and Ni) nanoparticle/carbon nanotube electrocatalysts for direct methanol fuel cells*, J. Power Sources, **188**, 347-352, (2009).
- [177] S. Hu, J. Hou, L. Xiong, K. Weng, X. Ren, Y. Luo, *Preparation and characterization of hydrophobic Pt-Fe catalysts with enhanced catalytic activities for interface hydrogen isotope separation*, Journal of Hazardous Materials, **209**, 478-483, (2012).
- [178] E. Piera, M.I. Tejedor-Tejedor, M.E. Zorn, M.A. Anderson, *Relationship concerning the nature and concentration of Fe (III) species on the surface of TiO₂ particles and photocatalytic activity of the catalyst*, Applied Catalysis, B: Environmental, **46**, 671-685, (2003).
- [179] V. Polshettiwar, R. Luque, A. Fihri, H.B. Zhu, M. Bouhrara, J.M. Bassett, *Magnetically recoverable nanocatalysts*, Chemical Reviews, **111**, 3036-3075, (2011).
- [180] J. Yu, Q. Xiang, M. Zhou, *Preparation, characterization and visible-light-driven photocatalytic activity of Fe-doped titania nanorods and first-principles study for electronic structures*, Applied Catalysis, B: Environmental, **90**, 595-602, (2009).
- [181] C. Adan, A. Bahamonde, I. Oller, S. Malato, A. Martinez-Arias, *Influence of iron leaching and oxidizing agent employed on solar photodegradation of phenol over nanostructured iron-doped titania catalysts*, Applied Catalysis B: Environmental, **144**, 269-276, (2014).
- [182] J. Chen, F. Qiu, W. Xu, S. Cao, H. Zhu, *Recent progress in enhancing photocatalytic efficiency of TiO₂-based materials*, Applied Catalysis A: General, **495**, 131-140, (2015).
- [183] W.Y. Choi, A. Termin, M.R. Hoffmann, *The role of metal-ion dopants in quantum-sized TiO₂ - correlation between photoreactivity and charge-carrier recombination dynamics*, Journal of Physical Chemistry, **98**, 13669-13679, (1994).
- [184] A.N. Okte, S. Akalin, *Iron (Fe³⁺) loaded TiO₂ nanocatalysts: Characterization and photoreactivity*, Reaction Kinetics, Mechanisms and Catalysis, **100**, 55-70, (2010).
- [185] M.I. Litter, J.A. Navio, *Photocatalytic properties of iron-doped titania semiconductors*, Journal of Photochemistry and Photobiology, A: Chemistry, **98**, 171-181, (1996).
- [186] J.A. Navio, G. Colon, M.I. Litter, G.N. Bianco, *Synthesis, characterization and photocatalytic properties of iron-doped titania semiconductors prepared from TiO₂ and iron (III) acetylacetonate*, Journal of Molecular Catalysis A: Chemical, **106**, 267-276, (1996).
- [187] A. Di Paola, G. Marci, L. Palmisano, M. Schiavello, K. Uosaki, S. Ikeda, B. Ohtani, *Preparation of polycrystalline TiO₂ photocatalysts impregnated with various transition metal ions: Characterization and photocatalytic activity for the degradation of 4-nitrophenol*, Journal of Physical Chemistry B, **106**, 637-645, (2002).

- [188] N. Serpone, D. Lawless, J. Disdier, J.M. Herrmann, *Spectroscopic, photoconductivity, and photocatalytic studies on TiO₂ colloids - naked and with the lattice doped with Cr³⁺, Fe³⁺, and V⁵⁺ cations*, *Langmuir*, **10**, 643-652, (1994).
- [189] J.C. Colmenares, A. Magdziarz, O. Chernyayeva, D. Lisovytskiy, K. Kurzydowski, J. Grzonka, *Sonication-assisted low-temperature routes for the synthesis of supported Fe-TiO₂ nanomaterials: Partial photooxidation of glucose and phenol aqueous degradation*, *ChemCatChem*, **5**, 2270-2277, (2013).
- [190] J.A. Navio, J.J. Testa, P. Djedjeian, J.R. Padron, D. Rodriguez, M.I. Litter, *Iron-doped titania powders prepared by a sol-gel method. Part II: Photocatalytic properties*, *Applied Catalysis A: General*, **178**, 191-203, (1999).
- [191] X. Qian, K. Fuku, Y. Kuwahara, T. Kamegawa, K. Mori, H. Yamashita, *Design and functionalization of photocatalytic systems within mesoporous silica*, *ChemSusChem*, **7**, 1528-1536, (2014).
- [192] J. Mo, Y. Zhang, Q. Xu, R. Yang, *Effect of TiO₂/adsorbent hybrid photocatalysts for toluene decomposition in gas phase*, *Journal of Hazardous Materials*, **168**, 276-281, (2009).
- [193] M.V. Shankar, S. Anandan, N. Venkatachalam, B. Arabindoo, V. Murugesan, *Fine route for an efficient removal of 2,4-dichlorophenoxyacetic acid (2,4-D) by zeolite-supported TiO₂*, *Chemosphere*, **63**, 1014-1021, (2006).
- [194] S. Sankararaman, K.B. Yoon, T. Yabe, J.K. Kochi, *Control of back electron-transfer from charge-transfer ion-pairs by zeolite supercages*, *Journal of the American Chemical Society*, **113**, 1419-1421, (1991).
- [195] R. Sasikala, A.R. Shirole, V. Sudarsan, V.S. Kamble, C. Sudakar, R. Naik, R. Rao, S.R. Bharadwaj, *Role of support on the photocatalytic activity of titanium oxide*, *Applied Catalysis A: General*, **390**, 245-252, (2010).
- [196] P. Pichat, J.M. Herrmann, J. Disdier, M.N. Mozzanega, H. Courbon, *Modification of the TiO₂ electron density by ion doping or metal deposit and consequences for photoassisted reactions*, *Studies in Surface Science and Catalysis*, **19**, 319-326, (1984).
- [197] P. Lisowski, J.C. Colmenares, D. Lomot, O. Chernyayeva, D. Lisovytskiy, *Preparation by sonophotodeposition method of bimetallic photocatalysts Pd-Cu/TiO₂ for sustainable gaseous selective oxidation of methanol to methyl formate*, *Journal of Molecular Catalysis A: Chemical*, **411**, 247-256, (2016).
- [198] J.C. Colmenares, P. Lisowski, D. Lomot, O. Chernyayeva, D. Lisovytskiy, *Sonophotodeposition of bimetallic photocatalysts Pd-Au/TiO₂: Application to selective oxidation of methanol to methyl formate*, *ChemSusChem*, **8**, 1676-1685, (2015).
- [199] J. Gonzalez-Garcia, V. Saez, J.S. Iñiesta, V. Montiel, A. Aldaz, *Electrodeposition of PbO₂ on glassy electrodes: Influence of ultrasound carbon power*, *Electrochemistry Communications*, **4**, 370-373, (2002).
- [200] V. Balzani, A. Credi, M. Venturi, *Photochemical conversion of solar energy*, *ChemSusChem*, **1**, 26-58, (2008).

- [201] S. Higashimoto, R. Shirai, Y. Osano, M. Azuma, H. Ohue, Y. Sakata, H. Kobayashi, *Influence of metal ions on the photocatalytic activity: Selective oxidation of benzyl alcohol on iron (III) ion-modified TiO₂ using visible light*, Journal of Catalysis, **311**, 137-143, (2014).
- [202] X.Y. Li, P.L. Yue, C. Kotal, *Synthesis and photocatalytic oxidation properties of iron doped titanium dioxide nanosemiconductor particles*, New Journal of Chemistry, **27**, 1264-1269, (2003).
- [203] Y. Ide, H. Hattori, S. Ogo, M. Sadakane, T. Sano, *Highly efficient and selective sunlight-induced photocatalytic oxidation of cyclohexane on an eco-catalyst under a CO₂ atmosphere*, Green Chemistry, **14**, 1264-1267, (2012).
- [204] A. Maldotti, A. Molinari, *Design of heterogeneous photocatalysts based on metal oxides to control the selectivity of chemical reactions*, in: C.A. Bignozzi (Ed.) Photocatalysis, **303**, 185-216, (2011).
- [205] Z. Kobus, E. Kusińska, *Influence of physical properties of liquid on acoustic power of ultrasonic processor*, TEKA Kom. Mot. Energ. Roln. – OL PAN, **8 a**, 71-78, (2008).
- [206] S.Y. Lin, F.C. Zhang, *Measurement of ultrasonic power and electro-acoustic efficiency of high power transducers*, Ultrasonics, **37**, 549-554, (2000).
- [207] Z.Y. Yan, Q.P. Fang, J.L. Huang, B.X. He, Z.M. Lin, *The considerations and guides of the wattmeter method for measuring output acoustical power of langevin-type transducers - II: Experiment*, Ultrasonics, **35**, 543-546, (1997).
- [208] H.G. Flynn, C.C. Church, *A mechanism for the generation of cavitation maxima by pulsed ultrasound*, Journal of the Acoustical Society of America, **76**, 505-512, (1984).
- [209] A. Henglein, M. Gutierrez, *Chemical effects of continuous and pulsed ultrasound - a comparative-study of polymer degradation and iodide oxidation*, Journal of Physical Chemistry, **94**, 5169-5172, (1990).
- [210] N.N. Greenwood, *Mössbauer spectroscopy*, Springer Netherlands, 1971.
- [211] J.W. Niemantsverdriet, W.N. Delgass, *In situ mossbauer spectroscopy in catalysis*, Topics in Catalysis, **8**, 133-140, (1999).
- [212] C. Adan, J. Carbajo, A. Bahamonde, I. Oller, S. Malato, A. Martinez-Arias, *Solar light assisted photodegradation of phenol with hydrogen peroxide over iron-doped titania catalysts: Role of iron leached/readsorbed species*, Applied Catalysis B: Environmental, **108**, 168-176, (2011).
- [213] C. Adan, A. Bahamonde, M. Fernandez-Garcia, A. Martinez-Arias, *Structure and activity of nanosized iron-doped anatase TiO₂ catalysts for phenol photocatalytic degradation*, Applied Catalysis B: Environmental, **72**, 11-17, (2007).
- [214] J. Klima, *Application of ultrasound in electrochemistry. An overview of mechanisms and design of experimental arrangement*, Ultrasonics, **51**, 202-209, (2011).
- [215] J. Gonzalez-Garcia, J. Iniesta, A. Aldaz, V. Montiel, *Effects of ultrasound on the electrodeposition of lead dioxide on glassy carbon electrodes*, New Journal of Chemistry, **22**, 343-347, (1998).

- [216] V. Saez, J. Gonzalez-Garcia, J.D. Iniesta, A. Frias-Ferrer, A. Aldaz, *Electrodeposition of PbO₂ on glassy carbon electrodes: Influence of ultrasound frequency*, *Electrochemistry Communications*, **6**, 757-761, (2004).
- [217] P. Lorimer, T.J. Mason, *The applications of ultrasound in electroplating*, *Electrochemistry*, **67**, 924-930, (1999).
- [218] R. Walker, *Ultrasound and electroplating*, *Chemistry in Britain*, **26**, 251-254, (1990).
- [219] R. Walker, C.T. Walker, *New explanation for brightness of electrodeposits produced by ultrasound*, *Ultrasonics*, **13**, 79-82, (1975).
- [220] P.R. Gogate, *Treatment of wastewater streams containing phenolic compounds using hybrid techniques based on cavitation: A review of the current status and the way forward*, *Ultrasonics Sonochemistry*, **15**, 1-15, (2008).
- [221] H.B. Gray, *Powering the planet with solar fuel*, *Nature Chemistry*, **1**, 7-7, (2009).
- [222] S. Munir, D.D. Dionysiou, S.B. Khan, S.M. Shah, B. Adhikari, A. Shah, *Development of photocatalysts for selective and efficient organic transformations*, *Journal of Photochemistry and Photobiology B: Biology*, **148**, 209-222, (2015).
- [223] Y. Shiraishi, T. Hirai, *Selective organic transformations on titanium oxide-based photocatalysts*, *Journal of Photochemistry and Photobiology C: Photochemistry Reviews*, **9**, 157-170, (2008).
- [224] J.H. Kou, C.H. Lu, J. Wang, Y.K. Chen, Z.Z. Xu, R.S. Varma, *Selectivity enhancement in heterogeneous photocatalytic transformations*, *Chemical Reviews*, **117**, 1445-1514, (2017).
- [225] J.C. Colmenares, R. Luque, *Heterogeneous photocatalytic nanomaterials: Prospects and challenges in selective transformations of biomass-derived compounds*, *Chemical Society Reviews*, **43**, 765-778, (2014).

5. Texts of articles

Article 1 Patent

Method of depositing metal nanoparticles on the surface of semiconductor materials and surface obtained by this process

J.C. Colmenares and **A. Magdziarz**

Polish Patent PL222050 (submitted Nov 2012, accepted Nov 2015)

Title of the invention:

Method of depositing metal nanoparticles on the surface of semiconductor materials and surface obtained by this process

Inventors:

J. C. Colmenares Quintero, A. Magdziarz

Field:

Chemistry new materials, Chemical technology, Environmental chemistry

Summary:

The present invention is a method of depositing metal nanoparticles, especially mono- and bimetallic nanoparticles on semiconductor materials, using the synergistic effect of ultrasound and ultraviolet radiation. The invention also includes the surface of the semiconductor material covered with metallic nanoparticles, especially mono- or bimetallic ones, obtained by this procedure.

Advantages / innovative aspects:

- Very short time of different metals' nanoparticles supported onto semiconductor surface.
- This method allows the synthesis of hybrid materials with very good metals distribution on the surface of any type of semiconductor.
- Through this method it is possible to prepare supported alloys with very good degree of metals miscibility.
- This method takes use of the synergetic effect of two low-rate invasive energy sources (sonication and photons energy).

Keywords:

Catalysts, ultrasounds, light energy, mono- and bimetallic semiconductor films, photoactive materials

Use:

Micro and Nanotechnologies, Electronic nanoengineering, Environment, Semiconductors

State of the progress:

stage of research

Intellectual property rights:

Patent application P-401693 - 20.11.2012 - Poland

Expected cooperation:

contract of sale, licence agreement, cooperation agreement

Sposób osadzania nanocząstek metalicznych na powierzchni materiałów półprzewodnikowych oraz powierzchnia otrzymana tym sposobem.

Przedmiotem wynalazku jest metoda osadzania nanocząstek metalicznych, szczególnie mono- i bimetalicznych, na materiałach półprzewodnikowych, wykorzystująca synergetyczne działanie ultradźwięków i promieniowania ultrafioletowego.

Ultradźwięki są uznawane obecnie za jedno z najbardziej użytecznych narzędzi stosowanych w syntezie nanomateriałów (J. H. Bang et al., *Advanced Materials*, 2010, 22, 1039-1059). W porównaniu z tradycyjnymi źródłami energii, ultradźwięki zapewniają dość nietypowe warunki reakcyjne w układach ciekłych, takie jak krótkotrwałe stany niezwykle wysokiego ciśnienia i temperatury. Istotą wykorzystania ultradźwięków w syntezie materiałów jest proces kawitacji akustycznej. Zjawisko to, wywołane falami akustycznymi generowanymi w cieczy, polega na powstawaniu, wzroście i gwałtownym zaniku pęcherzyków lub innych obszarów zamkniętych (kawern) zawierających parę danej cieczy, rozpuszczone w niej gazy lub mieszaninę wodno-parową. Pęcherzyki powstają w cieczy na skutek naprzemiennego rozciągającego i ściskającego działania fal akustycznych. Oscylujące pęcherzyki powiększając się (zazwyczaj osiągają rozmiary mikrometrów) gromadzą energię ultradźwiękową. W odpowiednich warunkach pęcherzyki mogą urosnąć ponad miarę a następnie rozpaść się uwalniając energię zmagazynowaną w bardzo krótkim czasie (współczynnik grzania i chłodzenia $>10^{10} \text{ K s}^{-1}$). Ten kawitacyjny rozpad, miejscowy i krótkotrwały, zachodzi w temperaturze ok. 5000 K i pod ciśnieniem ok. 1000 bar. Chemicznym efektem działania ultradźwięków w wodzie jest powstawanie wolnych rodników o właściwościach redukujących i utleniających, $\cdot\text{H}$ i $\cdot\text{OH}$. Rodniki te mogą rekombinować do związku wyjściowego lub łączyć się tworząc H_2 , H_2O_2 oraz

$\cdot\text{HO}_2$ w wyniku reakcji z O_2 . Te silne reduktory i utleniacze są źródłem różnych sonochemicznych reakcji w roztworach wodnych. Sonochemiczna metoda redukcji w roztworach wodnych ma tę przewagę nad tradycyjnymi metodami redukcyjnymi, iż nie wymaga stosowania dodatkowych czynników redukujących. W tym przypadku sonochemicznie produkowane rodniki wodorowe występują w roli reduktorów. Szybkość reakcji zależy w tym przypadku od ilości rodników o właściwościach redukujących, dlatego często dodaje się związki organiczne, takie jak alkohole lub surfaktanty, w celu wytworzenia dodatkowych rodników. Ponadto w metodzie tej osiąga się znaczne szybkości reakcji i uzyskuje się cząstki o średnicach nanometrycznych. Metoda sonochemicznej redukcji jest szeroko omawiana w literaturze, ponieważ znajduje zastosowanie przy wytwarzaniu nanocząstek: mono- i bimetalicznych, tlenków metali, halogenków i węglików metali. Bimetaliczne nanocząstki cieszą się coraz większym zainteresowaniem, ponieważ znajdują coraz szersze zastosowanie zarówno w katalizie jak i w optoelektronice. Wiele grup badawczych zgłasza otrzymanie różnych bimetalicznych nanocząstek na drodze sonochemicznej redukcji, głównie z roztworów wodnych lub alkoholowych z dodatkiem surfaktantów lub stabilizatorów. W sonochemicznej syntezie tlenków metali działaniu ultradźwięków poddaje się wodne roztwory soli tych metali. Uzyskane w ten sposób tlenki metali charakteryzują się bardziej jednorodnym rozmiarem cząstek, większą powierzchnią właściwą, szybszym czasem reakcji oraz większą czystością fazy krystalicznej w porównaniu z tlenkami otrzymanymi klasycznymi metodami. Udowodniono także, iż zastosowanie ultradźwięków w klasycznej syntezie zol-żel skraca znacznie czas reakcji w wyniku przyspieszenia reakcji hydrolizy i kondensacji prekursora metalu. Wpływ na skrócenie czasu reakcji mają towarzyszące ultradźwiękom warunki niezmiernie wysokiej temperatury powstającej na granicy rozpadających się pęcherzyków i roztworu.

Metoda fotoosadzania polega na nanoszeniu cząstek metalu z roztworu jego soli na powierzchnię półprzewodnika przy użyciu światła. Proces

fotoosadzania obejmuje powstawanie fotoelektronów oraz fotodziur w półprzewodniku w wyniku absorpcji światła o energii fotonu równej lub większej od wartości przerwy energetycznej, redukcję zaadsorbowanych jonów metalu przez elektrony z pasma przewodnictwa oraz utlenianie wody przez dziury z pasma walencyjnego. Innymi słowy, w wyniku oświetlenia półprzewodnika światłem ultrafioletowym w roztworze soli metalu powstaje cząsteczkowy tlen, a na powierzchni półprzewodnika osadza się metal. Szybkość reakcji fotoosadzania może zostać zwiększona poprzez dodanie donora elektronów, który może zapewnić praktycznie nieskończoną liczbę elektronów. Mimo, iż metoda fotoosadzania jest prosta w realizacji, w literaturze można znaleźć wiele badań wskazujących na niższą aktywność otrzymanych tą metodą katalizatorów w porównaniu z tradycyjnymi metodami, np. w przypadku osadzania nanocząstek Au na TiO_2 (M.C. Hidalgo et al. *Applied Catalysis A: General* 397 (2011) 112–120). Według Carabineiro et al. (S.A.C. Carabineiro et al., *Journal of Catalysis*, 2010, 273, 191–198) powodem tej niższej aktywności mogą być morfologiczne i strukturalne właściwości otrzymanego w ten sposób katalizatora, a mianowicie wielkość i kształt cząstek.

Pomimo wielu doniesień literaturowych dotyczących metod syntezy nanomateriałów z wykorzystaniem ultradźwięków lub promieniowania ultrafioletowego nie są one pozbawione słabych punktów. Zazwyczaj metody te stosowane są albo osobno, albo w kombinacji następczej, co wydłuża czas syntezy. Koniecznym staje się także użycie dodatkowych reduktorów chemicznych. W metodzie fotoosadzania nanocząstek metalu na powierzchni półprzewodnika poprzedzonej działaniem ultradźwięków, traktowanie ultradźwiękami ma na celu dysagregację nanocząstek soli metalu w roztworze wodnym i lepszą wymianę masy między reagentami. Redukcja nanocząstek metalu zachodzi następnie pod wpływem promieniowania ultrafioletowego (Lee et al., *Journal of Photochemistry and*

Photobiology A: Chemistry 221 (2011) 71–76, L. Sun et al., Journal of Hazardous Materials 171 (2009) 1045–1050).

Zgodnie z wynalazkiem, sposób osadzania nanocząstek metalicznych na powierzchni materiału półprzewodnikowego, charakteryzuje się tym, że:

- a) w reaktorze umieszcza się materiał półprzewodnikowy w postaci rozdrobnionej w roztworze soli prekursora metalu w mieszaninie wody i rozpuszczalnika, który nie absorbuje promieniowania ultrafioletowego w obszarze UV A i UV B,
- b) miesza się zawiesinę półprzewodnikową w roztworze w reaktorze za pomocą przepływu gazu obojętnego przez reaktor, korzystnie przez czas od 5 do 60 minut, korzystniej przez czas około 30 minut,
- c) poddaje się zawiesinę półprzewodnikową w roztworze w reaktorze jednoczesnemu działaniu ultradźwięków i promieniowania ultrafioletowego, korzystnie przez czas od 5 do 60 minut, korzystniej przez czas od 15 do 30 minut,
- d) usuwa się fazę ciekłą z reaktora, korzystnie przez odparowanie, zaś powierzchnię materiału półprzewodnikowego suszy się.

Korzystnie, rozpuszczalnikiem, który nie absorbuje promieniowania ultrafioletowego w obszarze UV A i UV B, jest acetonitryl, dichlorometan lub ich mieszanina.

Korzystnie, sól prekursora metalu jest solą rozpuszczalną w wodzie i rozpuszczalniku, który nie absorbuje promieniowania ultrafioletowego w obszarze UV A i UV B, korzystniej solą organiczną, najkorzystniej jest to acetyloacetonian.

Korzystnie, w mieszaninie wody i rozpuszczalnika, który nie absorbuje promieniowania ultrafioletowego w obszarze UV A i UV B, stosuje się przewagę rozpuszczalnika, szczególnie w stosunku objętościowym

rozpuszczalnik:woda wynoszącym od 95:5 v/v do 50:50 v/v, korzystniej 70:30 v/v.

Korzystnie, roztwór w reaktorze ma odczyn kwaśny, korzystniej o pH wynoszącym od 1,5 do 4,5, a zwłaszcza około 2.

Korzystnie, roztwór w reaktorze zawiera kwas, szczególnie kwas organiczny, zwłaszcza prosty kwas organiczny, szczególnie kwas szczawiowy, mrówkowy lub octowy.

Korzystnie, stosuje się przepływ gazu obojętnego przez reaktor od 50 mL/min do 70 mL/min.

Korzystnie, gazem obojętnym jest argon lub azot.

Korzystnie, jako źródło ultradźwięków stosuje się łożnię ultradźwiękową.

Korzystnie, jako źródło promieniowania ultrafioletowego stosuje się lampę UV lub lampę emitującą światło słoneczne.

Korzystnie, powierzchnię materiału półprzewodnikowego suszy się w temperaturze od 50°C do 150°C, korzystnie około 110°C, przez czas od 1 do 15 godzin, korzystnie około 10 godzin.

Wynalazek obejmuje także powierzchnię materiału półprzewodnikowego pokrytą nanocząstkami metalicznymi, szczególnie mono- lub bimetalicznymi, otrzymaną powyższym sposobem.

Proponowana tutaj nowa, fizykochemiczna metoda osadzania nanocząstek metalu na powierzchni materiału półprzewodnikowego łączy *in situ* sonochemię z fotokatalityczną redukcją metalu. Agentami redukującymi są tutaj elektrony generowane w wyniku absorpcji promieniowania ultrafioletowego przez materiał półprzewodnikowy. Działanie ultradźwięków zapewnia głównie dysagregację nanocząstek w roztworze, dobrą wymianę masy między reagentami, a także wspomaga redukcję metalu, np. poprzez generowanie rodników wodorowych w roztworze wodnym. Fazę ciekłą stanowi mieszanina wody i rozpuszczalnika, który nie absorbuje

promieniowania ultrafioletowego w obszarze UV A i UV B, na przykład acetonitrylu, z korzystną przewagą rozpuszczalnika (np. w przypadku acetonitrylu – w stosunku objętościowym 30:70 v/v), który zapewnia bardziej selektywne środowisko reakcji (lepsza redukcja nanocząstek metali na półprzewodniku bez zjawiska ługowania metali). Materiał półprzewodnikowy, dodany do roztworu w postaci rozdrobnionej, np. proszku, tworzy w roztworze zawiesinę półprzewodnikową. Reakcja jest prowadzona w środowisku kwaśnym (pH=2). Zastosowano kwas organiczny (korzystnie kwas szczawiowy, korzystne stężenie 9mM), który jest fotodegradowany (fotomineralizowany przez półprzewodnik do dwutlenku węgla i wody) stając się w ten sposób dodatkowym źródłem elektronów. Sól prekursora metalu jest solą rozpuszczalną w mieszaninie wody i rozpuszczalnika, który nie absorbuje promieniowania ultrafioletowego w obszarze UV A i UV B, korzystnie acetonitrylu, korzystnie jest solą organiczną (w tym przypadku wspomnianą solą jest acetyloacetonian). Stosowanie prekursorów organicznych ułatwia ich usuwanie ze środowiska reakcji (usuwanie przez fotokatalityczną pełną mineralizację). Proces redukcji nanocząstek metalu prowadzi się w przepływie obojętnego gazu (np. argonu, ale każdy inny obojętny gaz może być stosowany), korzystnie od 50 mL/min do 70 mL/min. Jako źródło światła UV zastosowano lampę ultrafioletową, a jako źródło ultradźwięków zastosowano łaźnię ultradźwiękową. Proces prowadzono przez max. 60 min, przy czym najbardziej korzystny czas reakcji to 15-30 min.

Metoda według wynalazku pozwala otrzymać nanocząstki mono- i bimetaliczne o powtarzalnych rozmiarach, dobrze zmieszany stop metali, dobrze rozdypergowane na powierzchni i o sferycznym kształcie. Nie wymaga stosowania silnych chemicznie czynników redukujących i prowadzona jest w krótkim czasie.

Wynalazek obejmuje także powierzchnię pokrytą nanocząstkami, otrzymaną powyższym sposobem.

Metoda osadzania nanocząstek metali na materiałach półprzewodnikowych według obecnego wynalazku może być szczególnie przydatna w preparatyce fotokatalizatorów, mających zastosowanie zarówno w procesach fotodegradacji odpadów organicznych zanieczyszczających wodę i powietrze, jak i selektywnego fotoutleniania różnych związków organicznych (np. cukrów, alkoholi) do związków o dużej wartości dodanej (np. związków do produkcji leków). Materiały bimetaliczne otrzymane sposobem według wynalazku mogą mieć zastosowanie w optoelektronice. Dodatkową zaletą tej metody jest możliwość projektowania materiałów o różnych kombinacjach metali i nośników, w zależności od potrzeb projektującego i przeznaczenia materiału.

Wynalazek zostanie teraz bliżej przedstawiony w korzystnych przykładach wykonania, z odniesieniem do załączonego rysunku, na którym:

Fig. 1 przedstawia układ reakcyjny: reaktor z lampą podłączony do linii argonu, gdzie: 1 – reaktor z mieszaniną reakcyjną zawierającą: H_2O , acetonitryl, kwas szczawiowy, acetyloacetonian zredukowanego metalu i półprzewodnik (nanocząstki TiO_2); 2 – połączenie z linią argonu; 3 – lampa UV umieszczona w kwarcowym chłodzącym płaszczu,

fig. 2 przedstawia kompletny układ reakcyjny przed i w trakcie procesu, gdzie: 4 – łaźnia ultradźwiękowa; 5 – włączona lampa UV; 6 – chłodnica zwrotna; 7 – system chłodzenia lampy,

fig. 3 przedstawia zdjęcia materiałów bimetalicznych otrzymanych metodą osadzania nanocząstek metalu na powierzchni nośnika półprzewodnikowego wykonane skaningowym mikroskopem elektronowym: (1) rozkład wysp osadzonych metali na nośniku TiO_2 /Zeolit: Pd/Fe- TiO_2 /Zeolit, (2) wyspy osadzonych metali: Pt-Cr/ TiO_2 /Zeolit, (3) analiza punktowa EDS (rengentowska

spektroskopia z dyspersją energii, ang. *Energy-dispersive X-ray Spectroscopy*) dla materiału Pt-Fe/TiO₂/Zeolit, zaś

fig. 4 przedstawia rozkład wielkości nanocząstek palladu określony dla materiału zawierającego 0,5%Pd na TiO₂P90.

Aparatura

Reakcję syntezy prowadzono w reaktorze szklanym (szkło pyrex) w kształcie litery U o pojemności 150 cm³ wyposażonym w spiek i kran gazowy (fig. 1). Reaktor ten został wykonany w Pracowni Szkła Laboratoryjnego w Instytucie Chemii Fizycznej PAN. Rtęciową lampę ultrafioletową (emitującą główną długość fali $\lambda=254$ nm, model RQ 3006) o mocy 6W zakupiono od Photochemical Reactors Ltd. Stosowano łożnię ultradźwiękową Sonorex-Digital RC (Badelin) o następujących parametrach: częstotliwość 35 kHz, moc 560 W. Rozwiązanie aparaturowe jako całość jest oryginalnym pomysłem zespołu Twórców obecnego wynalazku.

Materiały użyte do syntezy nanomateriałów.

Osadzanie nanocząstek monometalicznych.

Dwutlenek tytanu (AEROXIDE TiO₂P90) kupiono od Evonik Industries. Kwas szczawiowy (98%) został zakupiony od Alfa Aesar a acetyloacetonian (II) palladu (35%) od Acros Organics. W eksperymentach używano acetonitrylu (POCH) oraz wody MiliPore.

Osadzanie nanocząstek bimetalicznych.

Dwutlenek tytanu nanoszony na zeolicie typu Y (firma Zeolyst Int., ale jako nośnik może być również stosowany jakikolwiek inny izolator) zsyntetyzowano metodą mokrej impregnacji sprzężonej z ultradźwiękami. Kwas szczawiowy (98%) został zakupiony od Alfa Aesar. Prekursory metali: acetyloacetonian (II) palladu (35%), acetyloacetonian (III) żelaza (99+%), acetyloacetonian (III) chromu (97%) zostały zakupione od Acros Organics,

natomiast acetyloacetonian (II) platyny (98%) dostarczył ABCR. W eksperymentach używano acetonitrylu (do HPLC, POCH) oraz wody MilliPore.

Przykład 1

Osadzanie nanocząstek palladu na TiO_2 .

W typowym eksperymencie 0,1 g kwasu szczawiowego oraz 0,0071 g acetyloacetonianu palladu (w celu uzyskania 0,5% wag. palladu) rozpuszczono w 120 mL mieszaniny $\text{H}_2\text{O}:\text{ACN}$ w stosunku objętościowym 30:70 v/v. Przygotowany roztwór przelano do reaktora połączzonego z linią argonu (fig. 1). Przepływ argonu ustawiono na 70 mL/min. Dodano 0,5 g $\text{TiO}_2\text{P90}$ i reaktor umieszczono w myjce ultradźwiękowej. Zawiesinę przez 30 min. mieszano strumieniem argonu w celu osiągnięcia równowagi adsorpcji. Jednocześnie przez ok. 15 min stabilizowano lampę UV, która umieszczona była w termostатовanym (temp. 20 °C) kwarcowym płaszczu. Kolejnym krokiem było umieszczenie lampy w reaktorze i jednoczesne włączenie łożni ultradźwiękowej (kompletny układ reakcyjny pokazano na fig. 2). Czas reakcji wynosił 60 minut. Temperatura podczas syntezy wewnątrz reaktora wynosiła ok. 35 °C. Po reakcji rozpuszczalniki odparowano za pomocą wyparki próżniowej (temp. ok. 50 °C) a uzyskany materiał suszono w temp. 110 °C przez 10 godzin.

Przykład 2

Osadzanie nanocząstek chromu, żelaza, palladu i platyny w różnych bimetalicznych kombinacjach na powierzchni TiO_2 naniesionego na nośnik zeolitowy.

Metodą według wynalazku zsyntetyzowano także bardziej złożone układy, w których dwutlenek tytanu osadzony na nośniku zeolitowym promowano dwoma metalami. Przykładowo, w celu wprowadzenia palladu i żelaza, najpierw 0,1 g kwasu szczawiowego rozpuszczono w 36 mL H_2O a

następnie dodano acetonitryl, tak aby uzyskać 120 mL mieszaniny H₂O:ACN w stosunku objętościowym 30:70 v/v. Następnie w tej mieszaninie rozpuszczono sole żelaza i palladu. Ilość acetyloacetonianu żelaza obliczono tak, aby żelazo stanowiło 1% wag. całego układu natomiast pallad wprowadzono w stosunku atomowym do żelaza 1:1. Tak przygotowany roztwór przelano do reaktora połączanego z linią argonu. Przepływ argonu ustawiono na 70 mL/min. Dodano 1,2 g spreparowanego wcześniej TiO₂ na zeolicie i reaktor umieszczono w myjce ultradźwiękowej. Dalej postępowano jak w przykładzie 1.

Charakterystyka otrzymanych materiałów.

Właściwości morfologiczne układów bimetalicznych osadzonych na dwutlenku tytanu na nośniku zeolitytowym określono na podstawie zdjęć (fig. 3) wykonanych na skaningowym mikroskopie elektronowym (JEOL JSM-7001F). Stosując metodę osadzania nanocząstek metalu według wynalazku otrzymuje się wyspy nanocząstek metalu osadzone na materiale nośnikowym (w omawianym przypadku na zeolicie). Wyspy te są równomiernie rozmieszczone na powierzchni nośnika i mają kształt sferyczny (fig. 3.1). Analiza punktowa EDS wykazała, iż wyspy te zbudowane są z nanocząstek zredukowanych metali oraz TiO₂, np. wyspa na materiale Pt-Fe/TiO₂/Zeolit (fig. 3.3) składa się z Pt, Fe i Ti. Średnią wielkość wysp na podstawie zdjęć ze skaningowego mikroskopu elektronowego (fig. 3.3) określono na 50-80 nm. Podobny rozkład wielkości nanocząstek metalu otrzymano w przypadku materiałów monometalicznych (fig. 4). Z fig. 4 wynika, iż 80% skupisk palladu ma wielkość mniejszą niż 75 nm przy czym rozmiar ponad 50% skupisk zawiera się w granicach 50-75 nm.

Podziękowania

Opłaty związane z ochroną wynalazku sfinansowano ze środków projektu Nanotechnology, Biomaterials and alternative Energy Source for ERA integration FP7-REGPOT-CT-2011-285949-NOBLESSE.

Badania te były wspierane przez Marie Curie International Reintegration Grant w ramach 7. Programu Ramowego Wspólnoty Europejskiej.

Praca naukowa finansowana ze środków finansowych na naukę w latach 2012-2014 przyznanych na realizację projektu międzynarodowego współfinansowanego (Projekt Nr. 473/7.PR/2012 MNiSW"

Ta praca została częściowo finansowana przez Narodowe Centrum Nauki (NCN) w Polsce w ramach projektu badawczego DEC-2011/01/B/ST5/03888.

Zastrzeżenia patentowe

1. Sposób osadzania nanocząstek metalicznych na powierzchni materiału półprzewodnikowego, **znamienny tym, że**:
 - a) w reaktorze umieszcza się materiał półprzewodnikowy w postaci rozdrobnionej w roztworze soli prekursora metalu w mieszaninie wody i rozpuszczalnika, który nie absorbuje promieniowania ultrafioletowego w obszarze UV A i UV B,
 - b) miesza się zawieszinę półprzewodnikową w roztworze w reaktorze za pomocą przepływu gazu obojętnego przez reaktor, korzystnie przez czas od 5 do 60 minut, korzystniej przez czas około 30 minut,
 - c) poddaje się zawieszinę półprzewodnikową w roztworze w reaktorze jednoczesnemu działaniu ultradźwięków i promieniowania ultrafioletowego, korzystnie przez czas od 5 do 60 minut, korzystniej przez czas od 15 do 30 minut,
 - d) usuwa się fazę ciekłą z reaktora, korzystnie przez odparowanie, zaś powierzchnię materiału półprzewodnikowego suszy się.
2. Sposób według zastrz. 1, **znamienny tym, że** rozpuszczalnikiem, który nie absorbuje promieniowania ultrafioletowego w obszarze UV A i UV B, jest acetonitryl, dichlorometan lub ich mieszanina.
3. Sposób według zastrz. 1 albo 2, **znamienny tym, że** sól prekursora metalu jest solą rozpuszczalną w wodzie i rozpuszczalniku, który nie absorbuje promieniowania ultrafioletowego w obszarze UV A i UV B, korzystnie solą organiczną, korzystniej jest to acetyloacetonian.
4. Sposób według zastrz. 1, 2 albo 3, **znamienny tym, że** w mieszaninie wody i rozpuszczalnika, który nie absorbuje promieniowania ultrafioletowego w obszarze UV A i UV B, stosuje się przewagę rozpuszczalnika, szczególnie w stosunku objętościowym

rozpuszczalnik:woda wynoszącym od 95:5 v/v do 50:50 v/v, korzystnie 70:30 v/v.

5. Sposób według dowolnego z poprzedzających zastrzeżeń, **znamienny tym, że** roztwór w reaktorze ma odczyn kwaśny, korzystnie o pH wynoszącym od 1,5 do 4,5, a zwłaszcza około 2.
6. Sposób według zastrz. 5, **znamienny tym, że** roztwór w reaktorze zawiera kwas, szczególnie kwas organiczny, zwłaszcza prosty kwas organiczny, szczególnie kwas szczawiowy, mrówkowy lub octowy.
7. Sposób według dowolnego z poprzedzających zastrzeżeń, **znamienny tym, że** stosuje się przepływ gazu obojętnego przez reaktor od 50 mL/min do 70 mL/min.
8. Sposób według dowolnego z poprzedzających zastrzeżeń, **znamienny tym, że** gazem obojętnym jest argon lub azot.
9. Sposób według dowolnego z poprzedzających zastrzeżeń, **znamienny tym, że** jako źródło ultradźwięków stosuje się łożnię ultradźwiękową.
10. Sposób według dowolnego z poprzedzających zastrzeżeń, **znamienny tym, że** jako źródło promieniowania ultrafioletowego stosuje się lampę UV lub lampę emitującą światło słoneczne.
11. Sposób według dowolnego z poprzedzających zastrzeżeń, **znamienny tym, że** powierzchnię materiału półprzewodnikowego suszy się w temperaturze od 50°C do 150°C, korzystnie około 110°C, przez czas od 1 do 15 godzin, korzystnie około 10 godzin.
12. Powierzchnia materiału półprzewodnikowego pokryta nanocząstkami metalicznymi, szczególnie mono- lub bimetalicznymi, otrzymana sposobem według któregośkolwiek z powyższych zastrzeżeń.

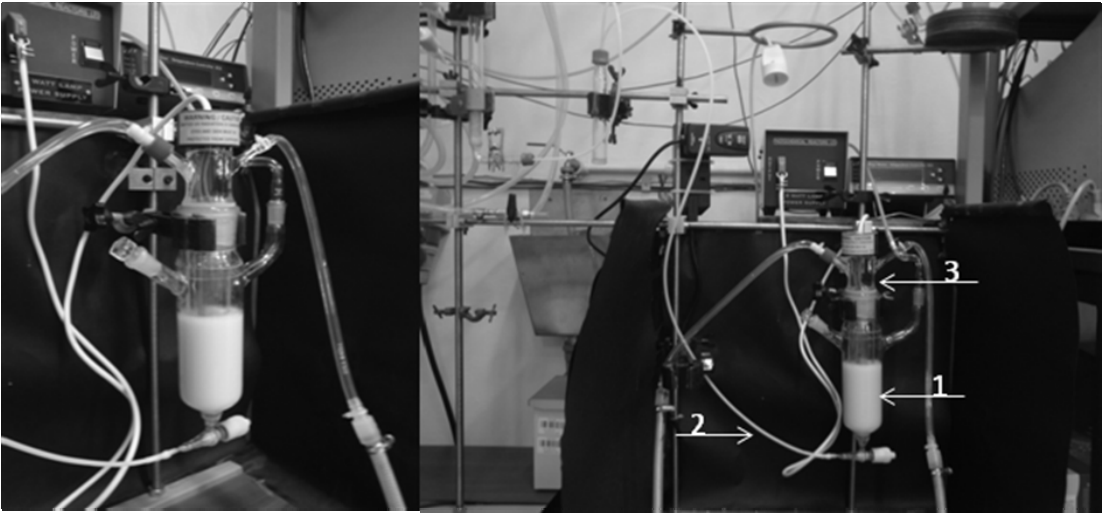
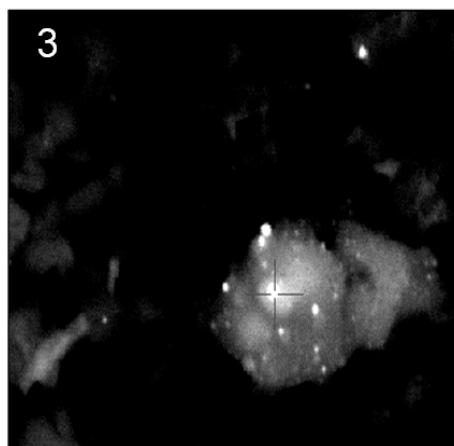
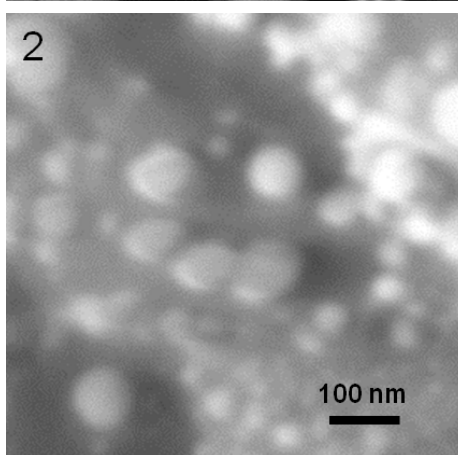
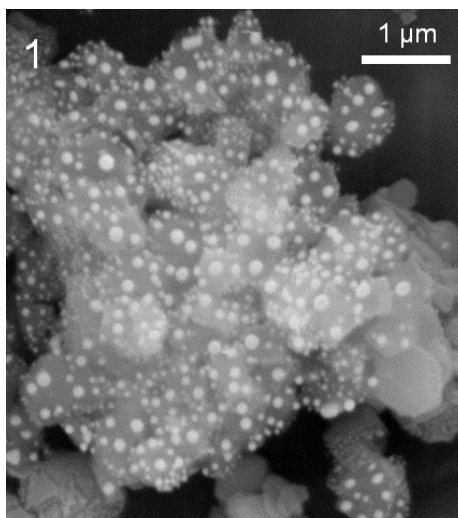


Fig. 1



Fig. 2



| EDS Quantitative Results | | |
|--------------------------|-------|-------|
| Element | Wt% | At% |
| Cl | 11.49 | 23.45 |
| Cl | 26.99 | 41.34 |
| Al | 0.61 | 0.55 |
| Si | 26.50 | 23.13 |
| PTM | 13.45 | 1.69 |
| Ti | 8.87 | 4.54 |
| Fe | 12.08 | 5.30 |

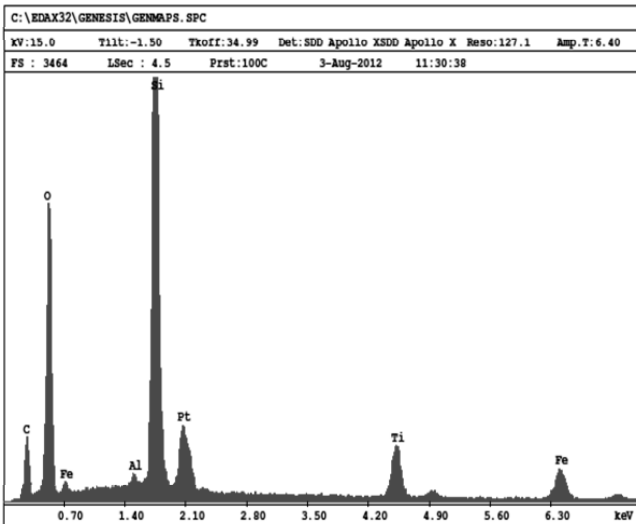


Fig. 3

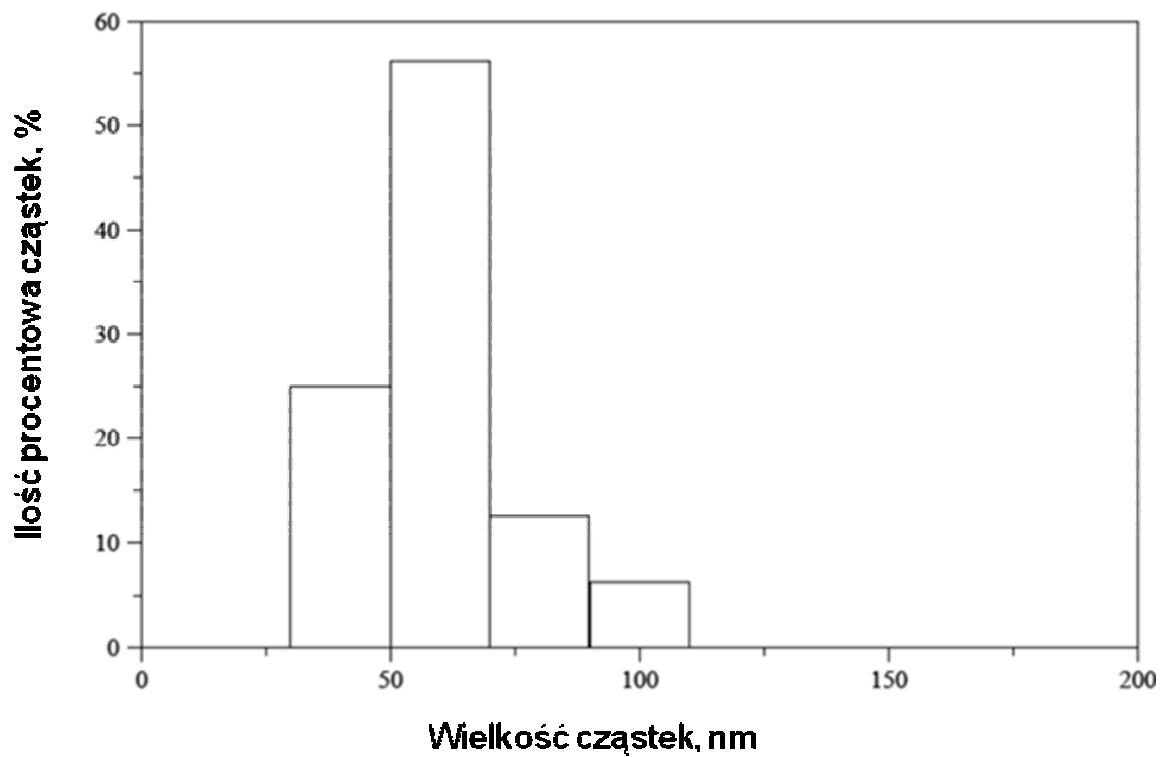


Fig. 4

Skrót opisu

Przedmiotem wynalazku Sposób osadzania nanocząstek metalicznych na powierzchni materiału półprzewodnikowego, **znamienny tym, że:**

- a) w reaktorze umieszcza się umieszcza się materiał półprzewodnikowy w postaci rozdrobnionej w roztworze soli prekursora metalu w mieszaninie wody i rozpuszczalnika, który nie absorbuje promieniowania ultrafioletowego w obszarze UV A i UV B,
- b) miesza się zawiesinę półprzewodnikową w roztworze w reaktorze za pomocą przepływu gazu obojętnego przez reaktor, korzystnie przez czas od 5 do 60 minut, korzystniej przez czas około 30 minut,
- c) poddaje się zawiesinę półprzewodnikową w roztworze w reaktorze jednoczesnemu działaniu ultradźwięków i promieniowania ultrafioletowego, korzystnie przez czas od 5 do 60 minut, korzystniej przez czas od 15 do 30 minut,
- d) usuwa się fazę ciekłą z reaktora, korzystnie przez odparowanie, zaś powierzchnię materiału półprzewodnikowego suszy się.

Wynalazek obejmuje także powierzchnię materiału półprzewodnikowego pokrytą nanocząstkami metalicznymi, szczególnie mono- lub bimetalicznymi, otrzymaną tym sposobem.

Fig. 1

(12 zastrzeżeń)

Article 2

A new photocatalytic tool in VOCs abatement: Effective synergetic combination of sonication and light for the synthesis of monometallic palladium-containing TiO₂

J.C. Colmenares, **A. Magdziarz**, D. Łomot, O. Chernyayeva, and D. Lisovytskiy

Applied Catalysis B: Environmental, 147, 624–632, 2014



A new photocatalytic tool in VOCs abatement: Effective synergetic combination of sonication and light for the synthesis of monometallic palladium-containing TiO₂



Juan C. Colmenares*, Agnieszka Magdziarz**, Dariusz Łomot, Olga Chernyayeva, Dmytro Lisovytskiy

Institute of Physical Chemistry PAS, Kasprzaka 44/52, 01-224 Warsaw, Poland

ARTICLE INFO

Article history:

Received 1 August 2013

Received in revised form

17 September 2013

Accepted 19 September 2013

Available online xxx

Keywords:

TiO₂

Palladium

Sonophotodeposition

Methanol photo-oxidation

Sonication

ABSTRACT

A new simultaneous combination of ultrasonication and ultraviolet irradiation was proposed to synthesize materials with photocatalytic properties. Different palladium modified TiO₂ systems were synthesized, using commercial TiO₂ P90 as a support. Morphological and surface characterization of the samples as well as photocatalytic activity for methanol photo-oxidation was studied. Among different characterization techniques X-ray diffraction, diffuse reflectance UV–vis spectroscopy, N₂ physisorption, X-ray photoelectron spectroscopy, high resolution transmission electron microscopy with X-ray microanalysis (HRTEM-EDS) were applied. Degradation of methanol was studied in the gas phase. The results of this study demonstrate that palladium in the reduced form was obtained in sonophotodeposition method (SPD), although the calcination step at 300 °C in air flow during 4 h was the last in the synthesis procedure. All Pd modified photocatalysts obtained by SPD method were very active (>90%) in gas phase methanol degradation and highly selective (>80%) to CO₂. The optimum palladium loading was fixed at 1 wt. %.

© 2013 Elsevier B.V. All rights reserved.

Article 3

Iron-containing titania photocatalyst prepared by the sonophotodeposition method for the oxidation of benzyl alcohol

A. Magdziarz, J.C. Colmenares, O. Chernyayeva, K. Kurzydłowski, and J. Grzonka

ChemCatChem, 8, 536–539, 2016

Iron-Containing Titania Photocatalyst Prepared by the Sonophotodeposition Method for the Oxidation of Benzyl Alcohol

Agnieszka Magdziarz,^{*,[a]} Juan C. Colmenares,^{*,[a]} Olga Chernyayeva,^[a]
Krzysztof Kurzydłowski,^[b] and Justyna Grzonka^[b]

Article 4

Sonication and light irradiation as green energy sources simultaneously implemented in the synthesis of Pd-Fe- and Pt-Fe-doped TiO₂-based photocatalysts

A. Magdziarz, J.C. Colmenares, O. Chernyayeva, D. Łomot, and K. Sobczak

Journal of Molecular Catalysis A, 425, 1–9, 2016



ELSEVIER

Contents lists available at ScienceDirect

Journal of Molecular Catalysis A: Chemical

journal homepage: www.elsevier.com/locate/molcata



Sonication and light irradiation as green energy sources simultaneously implemented in the synthesis of Pd-Fe- and Pt-Fe-doped TiO₂-based photocatalysts



Agnieszka Magdziarz^{a,*}, Juan C. Colmenares^{a,*}, Olga Chernyayeva^a, Dariusz Łomot^a, Kamil Sobczak^b

^a Institute of Physical Chemistry PAS, Kasprzaka 44/52, 01-224 Warsaw, Poland

^b Institute of Physics PAS, Aleja Lotników 32/46, 02-668 Warsaw, Poland

ARTICLE INFO

Article history:

Received 16 August 2016

Received in revised form

13 September 2016

Accepted 15 September 2016

Available online 15 September 2016

Keywords:

Sonophotodeposition

Titania

Iron

Phenol degradation

Bimetallic catalyst

ABSTRACT

Sono- and photochemical reactions were combined in the synthesis of Pd-Fe- and Pt-Fe-doped titania-based photocatalysts supported on zeolite Y. In the applied procedure, no harmful reducing agents were used. The resulting photocatalysts were characterized using diffuse reflectance UV–vis spectroscopy, high-resolution transmission electron microscopy (HRTEM), X-ray photoelectron spectroscopy (XPS), N₂ physisorption and inductively coupled plasma mass spectrometry (ICP-MS) techniques. The applied methodology leads to the formation of a mainly metallic form of platinum and oxidized forms of palladium and iron, with respect to different reduction potentials of metals. The photocatalytic degradation of phenol under UV light was applied as a test reaction. The photocatalyst containing Pt-Fe showed better results in this reaction in comparison with the Pd-Fe material, mainly because of the presence of the metallic form of platinum.

© 2016 Elsevier B.V. All rights reserved.

Article 5

Insight into the synthesis procedure of Fe³⁺/TiO₂-based photocatalyst applied in the selective photo-oxidation of benzyl alcohol under sun-imitating lamp

A. Magdziarz, J.C. Colmenares, O. Chernyayeva, D. Lisovytskiy, J. Grzonka,

K. Kurzydłowski, K. Freindl, and J. Korecki

Ultrasonics Sonochemistry, 38, 189–196, 2017



ELSEVIER

Contents lists available at ScienceDirect

Ultrasonics Sonochemistry

journal homepage: www.elsevier.com/locate/ultson



Insight into the synthesis procedure of Fe³⁺/TiO₂-based photocatalyst applied in the selective photo-oxidation of benzyl alcohol under sun-imitating lamp



Agnieszka Magdziarz^{a,*}, Juan C. Colmenares^{a,*}, Olga Chernyayeva^a, Dmytro Lisovytskiy^a, Justyna Grzonka^{b,c}, Krzysztof Kurzydłowski^b, Kinga Freindl^d, Józef Korecki^{d,e}

^aInstitute of Physical Chemistry, Polish Academy of Sciences, Kasprzaka 44/52, 01-224 Warsaw, Poland

^bFaculty of Materials Science and Engineering, Warsaw University of Technology, Woloska 141, 02-507 Warsaw, Poland

^cInstitute of Electronic Materials Technology, Wolczynska 133, 01-919 Warsaw, Poland

^dJerzy Haber Institute of Catalysis and Surface Chemistry PAS, Niezapominajek 8, 30-239 Cracow, Poland

^eFaculty of Physics and Applied Computer Science, AGH University of Science and Technology, Al. Mickiewicza 30, 30-059 Cracow, Poland

ARTICLE INFO

Article history:

Received 15 January 2017

Received in revised form 20 February 2017

Accepted 7 March 2017

Available online 9 March 2017

Keywords:

Ultrasounds

Light irradiation

Sonophotodeposition

Fe³⁺/TiO₂/Zeolite Y photocatalyst

Selective benzyl alcohol photooxidation

ABSTRACT

Fe³⁺/TiO₂/zeolite Y photocatalyst synthesized by using sonophotodeposition method was compared with photocatalysts prepared by simple photodeposition and sonodeposition methods in order to clarify the role of light irradiation and ultrasounds while they are used simultaneously. To gain an insight into the mechanism of this method a detailed characterization of the photocatalysts was carried out by means of the following techniques: UV–vis diffuse reflectance spectroscopy, X-ray photoelectron spectroscopy, transmission electron microscopy, Mössbauer measurements and photocatalytic test reaction. Basing on the results from these techniques the chemical role of light and mainly mechanical role of ultrasound were observed. The selective photocatalytic oxidation of benzyl alcohol into benzaldehyde in liquid phase was a test reaction verifying the utility of the prepared materials. The best photocatalytic efficiency in this reaction was performed by photocatalyst synthesized using compilation of ultrasound energy with photoexcitation.

© 2017 Elsevier B.V. All rights reserved.

Insight into the synthesis procedure of Fe³⁺/TiO₂-based photocatalyst applied in the selective photo-oxidation of benzyl alcohol under sun-imitating lamp

Agnieszka Magdziarz^{*1} amagdziarz@ichf.edu.pl, Juan C. Colmenares^{*1} icarloscolmenares@ichf.edu.pl, Olga Chernyayeva¹, Dmytro Lisovytskiy¹, Justyna Grzonka^{2,3}, Krzysztof Kurzydłowski², Kinga Freindl⁴ and Józef Korecki^{4,5}

¹Institute of Physical Chemistry Polish Academy of Sciences, Kasprzaka 44/52, 01-224 Warsaw, Poland

²Faculty of Materials Science and Engineering, Warsaw University of Technology, Woloska 141, 02-507 Warsaw, Poland

³Institute of Electronic Materials Technology, Wolczynska 133, 01-919 Warsaw, Poland

⁴Jerzy Haber Institute of Catalysis and Surface Chemistry PAS, Niezapominajek 8, 30-239 Cracow, Poland

⁵Faculty of Physics and Applied Computer Science, AGH University of Science and Technology, Al. Mickiewicza 30, 30-059 Cracow, Poland

*corresponding author

Characterization techniques

UV-vis diffuse reflectance spectra were recorded on a UV/VIS/NIR spectrophotometer Jasco V-570 equipped with an integrating sphere. The baseline was recorded using Spectralon™ (poly(tetrafluoroethylene) as a reference material. To determine the band gap of the powders (E_g), the Kubelka–Munk method based on the diffuse reflectance spectra was employed. The E_g of the powders was calculated from the $(f(R)hv)^{1/2}$ versus hv plots. The function $f(R)$ was calculated from the equation:

$$f(R) = (1-R)^2/2R.$$

XPS measurements were performed using a VG Scientific photoelectron spectrometer ESCALAB-210 using Al K α radiation (1486.6 eV) from an X-ray source operating at 15 kV and 20 mA. Survey spectra were recorded for all the samples in the energy range from 0 to 1350 eV with 0.4 eV step. High resolution spectra were recorded with 0.1 eV step, 100 ms dwell time and 25 eV pass energy. Ninety degrees take-off angle was used in all measurements. The curve fitting was performed using the AVANTAGE software provided by Thermo Electron, which describes each component of the complex envelope as a Gaussian–Lorentzian sum function; a constant 0.3(\pm 0.05) G/L ratio was used. The background was fitted using nonlinear Shirley model. Scofield sensitivity factors and measured transmission function were used for quantification. Ti 2p peak at 458.8 eV was used as reference of binding energy.

Structure characterization of the samples was carried out with high resolution Scanning Transmission Electron Microscope (STEM, Hitachi HD-2700, 200 kV, C_s corrected) equipped with Energy Dispersive X-ray spectrometer. The samples for STEM observations were prepared through dispersing powder in ethanol with using

ultrasonic bath. Then, a drop of suspension was deposited on copper grid covered with carbon film. After alcohol evaporation the samples were ready for analysis. The size of nanoparticles was calculated by image analyses, using dedicated MicroMeter computer software. For an image analysis a population of 100 of TiO₂ nanoparticles was used.

Mössbauer spectra were measured in a standard transmission geometry using a ⁵⁷Co source in the Rh matrix. All Mössbauer absorbers were prepared from powders with a density 250 mg/cm². The isomer shift (IS) is given relative to metallic iron, the quadrupole splitting (QS) is given as the distance between the doublet lines.

Additional Figures

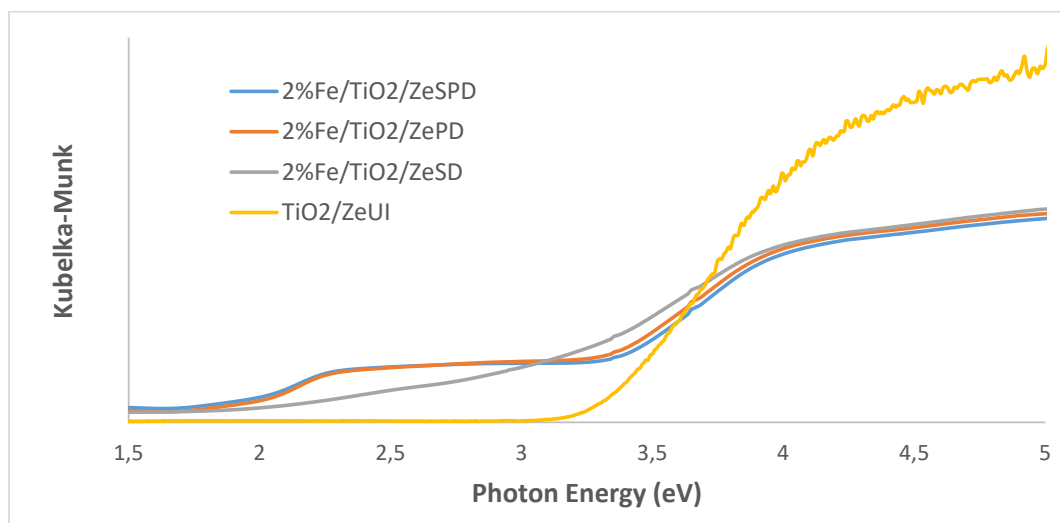


Figure S1. Kubelka-Munk plots of iron-containing photocatalysts prepared by sonophotodeposition (SPD), photodeposition (PD) and sonodeposition (SD) methods compared with TiO₂/ZeUI starting material.

| Photocatalyst | Temperature [K] | Spectral component | B_{hf} [T] | $\sigma(B_{hf})$ [T] | QS / ϵ [mm/s] | $\sigma(QS)$ [mm/s] | δ [mm/s] | Spectral area [%] (SA) |
|------------------------------|-----------------|--------------------|--------------|----------------------|------------------------|---------------------|-----------------|------------------------|
| 2%Fe/TiO ₂ /ZeSPD | 293 | NM | | | 0.87 | 0.49 | 0.39 | 11.7 |
| | | Mag1 | 50.6 | 0.9 | -0.1 | | 0.37 | 41.5 |
| | | Mag2 | 47.3 | 2.5 | -0.09 | | 0.37 | 14.9 |
| | | Mag3 | 32.5 | 17.1 | -0.05 | | 0.35 | 31.9 |
| 2%Fe/TiO ₂ /ZeSD | 293 | NM | | | 0.87 | 0.32 | 0.35 | 82.2 |
| | | Mag | 15.6 | 4.8 | | | 0.35 | 17.8 |
| 2%Fe/TiO ₂ /ZePD | 293 | NM | | | 0.56 | 0.3 | 0.34 | 9.0 |
| | | Mag1 | 49.4 | 1.1 | -0.11 | | 0.37 | 42.2 |
| | | Mag2 | 45.4 | 3.1 | -0.07 | | 0.4 | 24.4 |
| | | Mag3 | 22.5 | 14.3 | -0.03 | | 0.35 | 24.4 |

Table S1. The Mössbauer parameters: B_{hf} - hyperfine magnetic field, $\sigma(B_{hf})$ – distribution width of B_{hf} , QS – quadrupole splitting (non-magnetic spectra), ϵ – quadrupole shift (magnetic spectra), $\sigma(QS)$ – distribution width of QS, δ – isomer shift vs. α -Fe, NM-nonmagnetic, Mag-magnetic site.

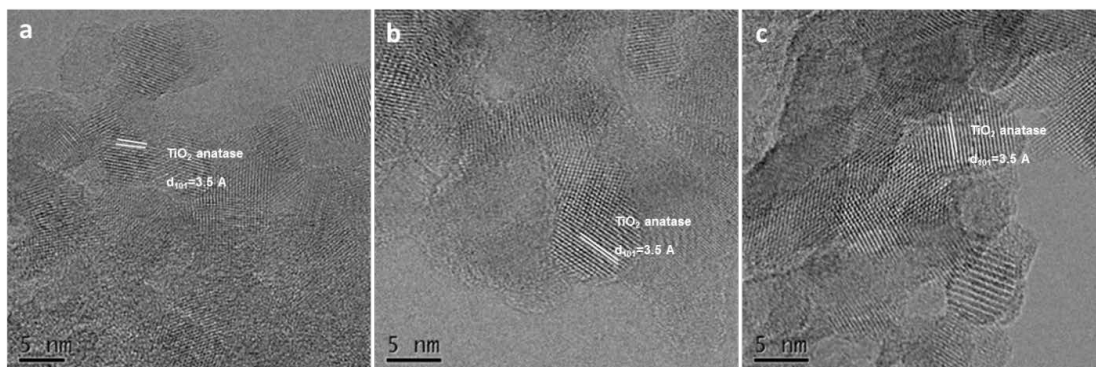


Figure S2. HR STEM image of TiO₂ nanoparticles for: (a) 2%Fe/TiO₂/ZePD, (b) 2%Fe/TiO₂/ZeSD, (c) 2%Fe/TiO₂/ZeSPD.

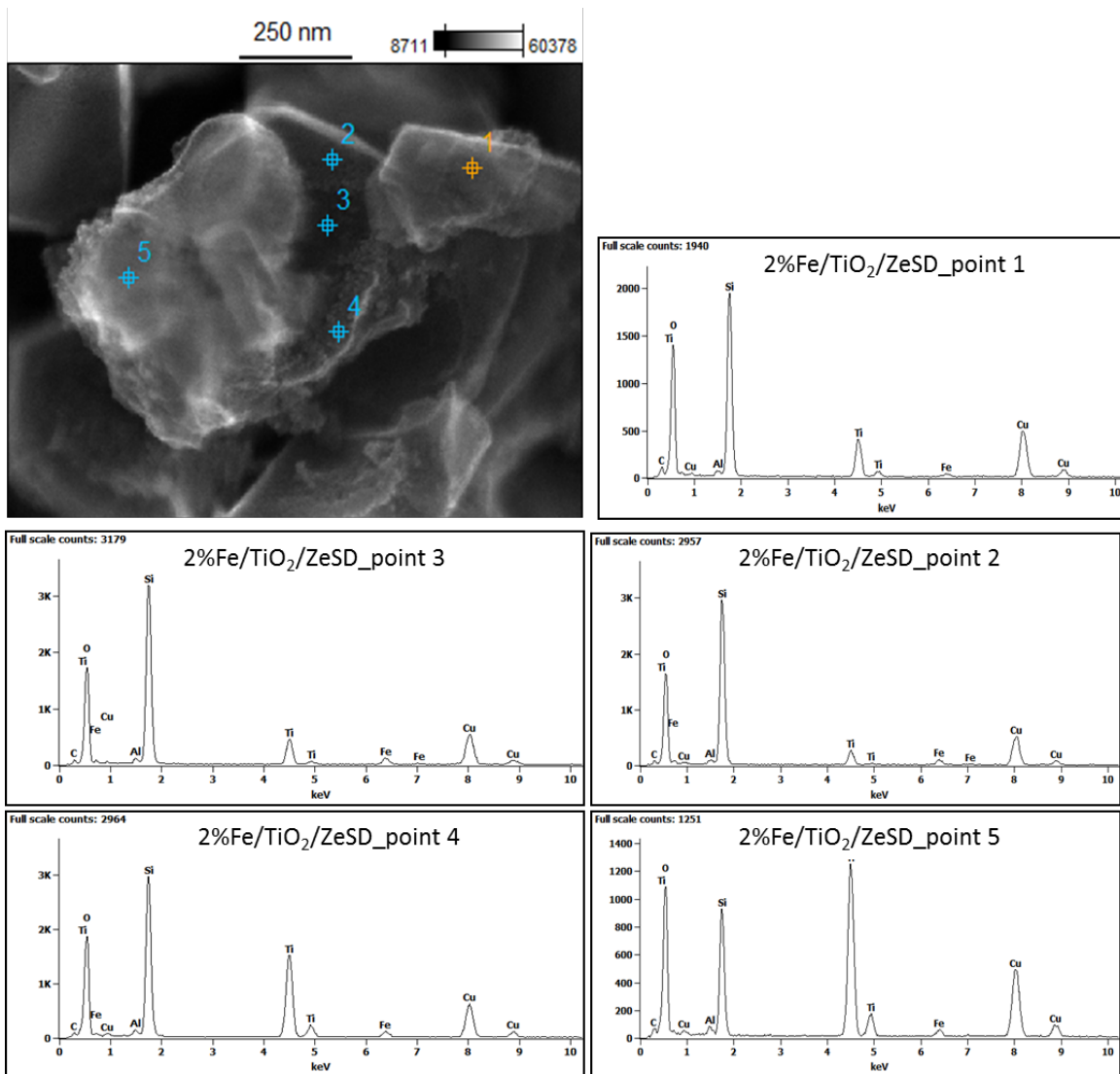


Figure S3. HAADF STEM image of 2%Fe/TiO₂/ZeSD with EDS chemical analysis.

Article 6

In situ coupling of ultrasound to electro- and photo-deposition methods for materials synthesis

A. Magdziarz and J.C. Colmenares

Molecules, 22, 216, 2017

Review

In Situ Coupling of Ultrasound to Electro- and Photo-Deposition Methods for Materials Synthesis

Agnieszka Magdziarz * and Juan C. Colmenares *

Institute of Physical Chemistry, Polish Academy of Sciences, Kasprzaka 44/52, 01-224 Warsaw, Poland

* Correspondence: amagdziarz@ichf.edu.pl (A.M.); jcarloscolmenares@ichf.edu.pl (J.C.C.);

Tel.: +48-22-343-3215 (J.C.C.)

Academic Editor: Gregory Chatel

Received: 20 December 2016; Accepted: 26 January 2017; Published: 31 January 2017

Abstract: This short review provides the current state-of-the-art of in situ coupling of ultrasound to chemical deposition methods. Synergetic action of ultrasound and light radiation or electrical fields may result in new powerful methodologies, which include sonophotodeposition and sonoelectrodeposition processes. The effect of ultrasound is explained on the basis of different physical mechanisms emerging from cavitation phenomenon. Some possible mechanisms of the interactions between ultrasound and photochemical and electrochemical processes are discussed here. The application of sonophotodeposition and sonoelectrodeposition as green energy sources in the syntheses of different nanomaterials is also reviewed.

Keywords: ultrasound; sonophotodeposition; sonoelectrodeposition; sonophotochemistry; sonoelectrochemistry; cavitation; current density

6. Contributions of Authors

My contributions to the articles:

1. Method of depositing metal nanoparticles on the surface of semiconductor materials and surface obtained by this process, J.C. Colmenares and A. Magdziarz, Polish Patent PL222050 (submitted Nov 2012, accepted Nov 2015)

I built the reaction setup for the sonophotodeposition process based on the idea of Prof. Colmenares (US bath and UV Hg lamp) and synthesized all photocatalysts. I performed photocatalytic test reactions, did some characterization measurements (e.g., DRUV-vis, N₂ physisorption), and analyzed the obtained data. I prepared most of the figures, and I wrote a report that was part of this patent application.

2. A new photocatalytic tool in VOCs abatement: Effective synergetic combination of sonication and light for the synthesis of monometallic palladium-containing TiO₂, J.C. Colmenares, A. Magdziarz, D. Łomot, O. Chernyayeva, and D. Lisovyskiy, *Applied Catalysis B: Environmental*, 147, 624–632, 2014

I synthesized all photocatalysts, performed DRUV-vis characterization and took part in some photocatalytic tests of gas phase methanol oxidation. I took part in the analysis of the experimental data obtained from other techniques as well as in the discussion of the results and in the survey of the literature. I prepared all the figures and wrote a part of the manuscript.

3. Iron-containing titania photocatalyst prepared by the sonophotodeposition method for the oxidation of benzyl alcohol, A. Magdziarz, J.C. Colmenares, O. Chernyayeva, K. Kurzydłowski, and J. Grzonka, *ChemCatChem*, 8, 536–539, 2016

I synthesized all photocatalysts studied in this work. For the photocatalyst prepared by the sonophotodeposition method, I built a new setup consisting of an ultrasonic probe and a UV-visible Xe lamp. I designed and optimized a new setup for photocatalytic selective oxidation of benzyl alcohol and performed all reactions and HPLC analysis. I carried out DRUV-vis experiments of the samples and analyzed the results. Most of the characterization were done by co-authors, but I took part in analysis of all data delivered by them. I designed the structure of this publication, did the literature review and prepared most of figures. I discussed the results, wrote the manuscript and prepared the replies to the reviewers' comments with some help of Prof Colmenares.

4. Sonication and light irradiation as green energy sources simultaneously implemented in the synthesis of Pd-Fe- and Pt-Fe-doped TiO₂-based photocatalysts, A. Magdziarz, J.C. Colmenares, O. Chernyayeva, D. Łomot, and K. Sobczak, *Journal of Molecular Catalysis A: Chemical*, 425, 1–9, 2016

I synthesized all photocatalysts studied in this work. I performed photocatalytic test reactions (phenol oxidation) and analyzed the results of HPLC measurements. I carried out DRUV-vis and N₂ physisorption experiments of the samples and analyzed them. I took part in the analysis of all data obtained from other characterization techniques, which were performed by co-authors. I designed the structure of this publication, did the literature review, prepared most of figures, and wrote the manuscript. I discussed the results and prepared the replies to the reviewers' comments with some help of Prof Colmenares.

5. Insight into the synthesis procedure of Fe³⁺/TiO₂-based photocatalyst applied in the selective photo-oxidation of benzyl alcohol under sun-imitating lamp, A. Magdziarz, J.C. Colmenares, O. Chernyayeva, D. Lisovytskiy, J. Grzonka, K. Kurzydłowski, K. Freindl, and J. Korecki, *Ultrasonics Sonochemistry*, 38, 189–196, 2017

I synthesized all photocatalysts studied in this work. I optimized the reaction system to determine the most appropriate conditions for the synthesis of the photocatalysts (the optimization studies are not included in this work, but they are an important contribution to the work in this publication). I performed photocatalytic test reactions (selective photo-oxidation of benzyl alcohol) and analyzed the results by HPLC technique. I carried out DRUV-vis experiments of the samples and analyzed them. I took part in analysis of all data obtained from other characterization techniques, which were performed by co-authors. I designed the structure of this publication, did the literature review, prepared most of figures, and wrote the manuscript. I discussed the results and prepared the replies to the reviewers' comments with help of Prof Colmenares.

6. In situ coupling of ultrasound to electro- and photo-deposition methods for materials synthesis, A. Magdziarz and J.C. Colmenares, *Molecules*, 22, 216, 2017

I designed the structure of this publication, did the literature review, prepared some figures and wrote the manuscript. I prepared the replies to the reviewers' comments with help of Prof Colmenares.

Contributions of the other authors of these publications are listed on the following pages.



Institute of Physical Chemistry Polish Academy of Sciences

Juan Carlos Colmenares Quintero, Ph.D. D.Sc.
Associate Professor
Research group leader
“Catalysis for sustainable energy production and
environmental protection, CatSEE”

Kasprzaka 44/52, PL-01 224 Warsaw, Poland

Tel.: +48 22 343 3215

Fax: +48 22 343 3448

jcarloscolmenares@ichf.edu.pl

<http://photo-catalysis.org/>

July 21, 2017

TO WHOM IT MAY CONCERN

Please, find below my contribution to the publications included in the PhD dissertation of Agnieszka Magdziarz entitled: “SonoPhotoDeposition: coupling of sonication and photodeposition in the synthesis of titanium dioxide-based photocatalytic materials”:

1. Method of depositing metal nanoparticles on the surface of semiconductor materials and surface obtained by this process, Juan Carlos Colmenares and Agnieszka Magdziarz, Polish Patent PL222050 (submitted Nov 2012, Accepted Nov 2015).

I designed and projected the method. I did part of the literature searching. I wrote part of the patent and prepared some of the figures.

2. A new photocatalytic tool in VOCs abatement: Effective synergetic combination of sonication and light for the synthesis of monometallic palladium-containing TiO₂, J.C. Colmenares, A. Magdziarz, D. Łomot, O. Chernyayeva, D. Lisovytskiy, *Applied Catalysis B: Environmental*, **147**, 624-632, 2014.

I designed the research and the paper structure. I analyzed experimental data and wrote most of the manuscript. I did a part of the research literature and analyzed it. I carried out the photocatalytic tests.

3. Iron-Containing Titania Photocatalyst Prepared by the Sonophotodeposition Method for the Oxidation of Benzyl Alcohol, A. Magdziarz, J.C. Colmenares, O. Chernyayeva, K. Kurzydłowski, J. Grzonka, *ChemCatChem*, **8**, 536-539, 2016.

I took part in discussion of the results and corrections of the manuscript. I helped in the preparation of the replies to the reviewers' comments.

4. Sonication and light irradiation as green energy sources simultaneously implemented in the synthesis of Pd-Fe- and Pt-Fe-doped TiO₂-based photocatalysts, A. Magdziarz, J.C. Colmenares, O. Chernyayeva, D. Łomot, K. Sobczak, *Journal of Molecular Catalysis A: Chemical*, **425**, 1-9, 2016.

<http://ichf.edu.pl>

<http://rcin.org.pl>

I took part in discussion of the results and corrections of the manuscript. I helped in the preparation of the replies to the reviewers' comments.

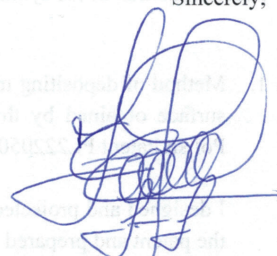
5. Insight into the synthesis procedure of $\text{Fe}^{3+}/\text{TiO}_2$ -based photocatalyst applied in the selective photo-oxidation of benzyl alcohol under sun-imitating lamp, A. Magdziarz, J.C. Colmenares, O. Chernyayeva, D. Lisovytskiy, J. Grzonka, K. Kurzydłowski, K. Freindl, J. Korecki, *Ultrasonics Sonochemistry*, **38**, 189-196, 2017.

I took part in discussion of the results and corrections of the manuscript. I helped in the preparation of the replies to the reviewers' comments.

6. In Situ Coupling of Ultrasound to Electro- and Photo-Deposition Methods for Materials Synthesis, A. Magdziarz, J.C. Colmenares, *Molecules*, **22**, 216, 2017.

I proposed the topic of this review and took part in corrections of the manuscript. I helped in the preparation of the replies to the reviewers' comments.

Sincerely,



Juan Carlos Colmenares Q.

**Institute of Physical Chemistry PAS
Kasprzaka 44/52
01-224 Warsaw, Poland**



Institute of Physical Chemistry Polish Academy of Sciences

Department Catalysis on Metals

Kasprzaka 44/52, PL-01 224 Warsaw, Poland

Tel. +(48 22) 343 20 93
Fax +(48 22) 343 33 33
+(48 22) 632 52 76
E-mail: dlomot@ichf.edu.pl

July 21, 2017

Please, find below my contribution to the publications included in the PhD dissertation of Agnieszka Magdziarz entitled: "SonoPhotoDeposition: coupling of sonication and photodeposition in the synthesis of titanium dioxide-based photocatalytic materials":

1. A new photocatalytic tool in VOCs abatement: Effective synergetic combination of sonication and light for the synthesis of monometallic palladium-containing TiO_2 , J.C. Colmenares, A. Magdziarz, D. Łomot, O. Chernyayeva, D. Lisovytskiy, *Applied Catalysis B: Environmental*, **147**, 624-632, 2014.

I performed HRTEM measurements and helped in the interpretation of the data, assisted in the photocatalytic measurements and contributed to the presentation of the results in Figure 2 and Figure 4.

2. Sonication and light irradiation as green energy sources simultaneously implemented in the synthesis of Pd-Fe- and Pt-Fe-doped TiO_2 -based photocatalysts, A. Magdziarz, J.C. Colmenares, O. Chernyayeva, D. Łomot, K. Sobczak, *Journal of Molecular Catalysis A: Chemical*, **425**, 1-9, 2016.

I took part in HRTEM measurements, helped in the interpretation of the data and contributed to the presentation of the results in Figure 4.

Sincerely,

D. Łomot



Institute of Physical Chemistry Polish Academy of Sciences

Department: Laboratorium Analizy
Powierzchni

Kasprzaka 44/52, PL-01 224 Warsaw, Poland

Tel. +(48 22) 343 32 60

+(48 22) 343 20 00

Fax +(48 22) 343 33 33

+(48 22) 632 52 76

E-mail: ichf@ichf.edu.pl

July 27, 2017

To whom it may concern,

Please, find below my contribution to the publications included in the PhD dissertation of Agnieszka Magdziarz entitled: "SonoPhotoDeposition: coupling of sonication and photodeposition in the synthesis of titanium dioxide-based photocatalytic materials":

1. A new photocatalytic tool in VOCs abatement: Effective synergetic combination of sonication and light for the synthesis of monometallic palladium-containing TiO₂, J.C. Colmenares, A. Magdziarz, D. Łomot, O. Chernyayeva, D. Lisovytskiy, *Applied Catalysis B: Environmental*, **147**, 624-632, 2014.
I performed XPS measurements and helped in the interpretation of the data.
2. Iron-Containing Titania Photocatalyst Prepared by the Sonophotodeposition Method for the Oxidation of Benzyl Alcohol, A. Magdziarz, J.C. Colmenares, O. Chernyayeva, K. Kurzydłowski, J. Grzonka, *ChemCatChem*, **8**, 536-539, 2016.
I performed XPS measurements and helped in the interpretation of the data.
3. Sonication and light irradiation as green energy sources simultaneously implemented in the synthesis of Pd-Fe- and Pt-Fe-doped TiO₂-based photocatalysts, A. Magdziarz, J.C. Colmenares, O. Chernyayeva, D. Łomot, K. Sobczak, *Journal of Molecular Catalysis A: Chemical*, **425**, 1-9, 2016.
I performed XPS measurements and helped in the interpretation of the data.
4. Insight into the synthesis procedure of Fe³⁺/TiO₂-based photocatalyst applied in the selective photo-oxidation of benzyl alcohol under sun-imitating lamp, A. Magdziarz, J.C. Colmenares, O. Chernyayeva, D. Lisovytskiy, J. Grzonka, K. Kurzydłowski, K. Freindl, J. Korecki, *Ultrasonics Sonochemistry*, **38**, 189-196, 2017.
I performed XPS measurements and helped in the interpretation of the data.

Sincerely,

O. Chernyayeva



Instytut Katalizy i Fizykochemii Powierzchni
im. Jerzego Habera
Polskiej Akademii Nauk



Kraków, 21.07.2017 r.

Oświadczenie

Niniejszym oświadczam, że mój wkład do publikacji:

Insight into the synthesis procedure of Fe³⁺/TiO₂-based photocatalyst applied in the selective photo-oxidation of benzyl alcohol under sun-imitating lamp, A. Magdziarz, J.C. Colmenares, O. Chernyayeva, D. Lisovytskyi, J. Grzonka, K. Kurzydłowski, K. Freindl, J. Korecki, *Ultrasonics Sonochemistry*, **38**, 189-196, 2017, włączonej do rozprawy doktorskiej Pani Agnieszki Madziarz, zatytułowanej "SonoPhotoDeposition: coupling of sonication and photodeposition in the synthesis of titanium dioxide-based photocatalytic materials" polegał na udziale w pomiarach mössbauerowskich i ich interpretacji podsumowanych na rys. 3 i w tabeli S1.

Kinga Freindl

ul. Niezapominajek 8, 30-239 Kraków, Polska
tel. +48 12 639 51 01, +48 12 425 19 23
fax +48 12 425 19 23

Nr konta: Bank PEKAO S.A. Kraków
PL 19 1240 4722 1111 0000 4851 4662
NIP: 6750001805, REGON: P-000326351



AKADEMIA GÓRNICZO-HUTNICZA im. STANISŁAWA STASZICA
WYDZIAŁ FIZYKI I INFORMATYKI STOSOWANEJ

Prof. dr hab. Józef Korecki

Katedra Fizyki Ciała Stałego

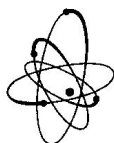
Kraków, 21.07.2017

Oświadczenie

Niniejszym oświadczam, że mój wkład do publikacji:

“Insight into the synthesis procedure of $\text{Fe}^{3+}/\text{TiO}_2$ -based photocatalyst applied in the selective photo-oxidation of benzyl alcohol under sun-imitating lamp”, A. Magdziarz, J.C. Colmenares, O. Chernyayeva, D. Lisovytskyi, J. Grzonka, K. Kurzydowski, K. Freindl, J. Korecki, *Ultrasonics Sonochemistry*, **38**, 189-196, 2017,

włączonej do rozprawy doktorskiej Pani Agnieszki Madziarz, z tytułu której “SonoPhotoDeposition: coupling of sonication and photodeposition in the synthesis of titanium dioxide-based photocatalytic materials” polegał na udziale w pomiarach mössbauerowskich i ich interpretacji, podsumowanych na rys. 3 i w tabeli S1.



AKADEMIA GÓRNICZO-HUTNICZA
WYDZIAŁ FIZYKI I INFORMATYKI STOSOWANEJ
al. A. Mickiewicza 30, 30-059 Kraków, tel. +48 12 617 2911, fax +48 12 6341247
e-mail: korecki@agh.edu.pl, www: korek.ucl.agh.edu.pl/



Institute of Physical Chemistry Polish Academy of Sciences

Department V

Kasprzaka 44/52, PL-01 224 Warsaw, Poland

Tel. +(48 22) 343 32 60

+(48 22) 343 20 00

Fax +(48 22) 343 33 33

+(48 22) 632 52 76

E-mail: ichf@ichf.edu.pl

July 27, 2017

To whom it may concern,

Please, find below my contribution to the publications included in the PhD dissertation of Agnieszka Magdziarz entitled: "SonoPhotoDeposition: coupling of sonication and photodeposition in the synthesis of titanium dioxide-based photocatalytic materials":

1. A new photocatalytic tool in VOCs abatement: Effective synergetic combination of sonication and light for the synthesis of monometallic palladium-containing TiO_2 ,

J.C. Colmenares, A. Magdziarz, D. Łomot, O. Chernyayeva, D. Lisovytskiy, *Applied Catalysis B: Environmental*, **147**, 624-632, 2014.

I performed XRD measurements and helped in the interpretation of the data.

2. Insight into the synthesis procedure of $\text{Fe}^{3+}/\text{TiO}_2$ -based photocatalyst applied in the selective photo-oxidation of benzyl alcohol under sun-imitating lamp, A. Magdziarz, J.C. Colmenares, O. Chernyayeva, D. Lisovytskiy, J. Grzonka, K. Kurzydłowski, K. Freindl, J. Korecki, *Ultrasonics Sonochemistry*, **38**, 189-196, 2017.

I performed XRD and XRF measurements and helped in the interpretation of the data.

Sincerely,

D. Lisovytskiy

Warszawa, dn 03.03.2017 r.

To whom it may concern,

Please, find below my contribution to the publication included in the PhD dissertation of Agnieszka Magdziarz entitled: "SonoPhotoDeposition: coupling of sonication and photodeposition in the synthesis of titanium dioxide-based photocatalytic materials":

Sonication and light irradiation as green energy sources simultaneously implemented in the synthesis of Pd-Fe- and Pt-Fe-doped TiO₂-based photocatalysts, A. Magdziarz, J.C. Colmenares, O. Chernyayeva, D. Łomot, K. Sobczak, *Journal of Molecular Catalysis A: Chemical*, **425**, 1-9, 2016.

I performed HRTEM measurements.

Sincerely,



K. Sobczak



To whom it may concern,

Please, find below my contribution to the publications included in the PhD dissertation of Agnieszka Magdziarz entitled: "SonoPhotoDeposition: coupling of sonication and photodeposition in the synthesis of titanium dioxide-based photocatalytic materials":

1. Iron-Containing Titania Photocatalyst Prepared by the Sonophotodeposition Method for the Oxidation of Benzyl Alcohol, A. Magdziarz, J.C. Colmenares, O. Chernyayeva, K. Kurzydłowski, J. Grzonka, *ChemCatChem*, **8**, 536-539, 2016.

I performed TEM measurements, helped in the interpretation of the data and contributed to the presentation of the results in Figure 2.

2. Insight into the synthesis procedure of Fe³⁺/TiO₂-based photocatalyst applied in the selective photo-oxidation of benzyl alcohol under sun-imitating lamp, A. Magdziarz, J.C. Colmenares, O. Chernyayeva, D. Lisovytskiy, J. Grzonka, K. Kurzydłowski, K. Freindl, J. Korecki, *Ultrasonics Sonochemistry*, **38**, 189-196, 2017.

I performed TEM measurements, helped in the interpretation of the data and contributed to the presentation of the results in Figure 4 and Figures S2 and S3.

Sincerely,

A handwritten signature in blue ink, appearing to read 'Grzonka Justyna', is written over the printed name.

J. Grzonka



To whom it may concern,

Please, find below my contribution to the publications included in the PhD dissertation of Agnieszka Magdziarz entitled: "SonoPhotoDeposition: coupling of sonication and photodeposition in the synthesis of titanium dioxide-based photocatalytic materials":

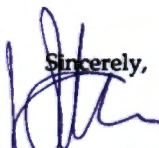
1. Iron-Containing Titania Photocatalyst Prepared by the Sonophotodeposition Method for the Oxidation of Benzyl Alcohol, A. Magdziarz, J.C. Colmenares, O. Chernyayeva, K. Kurzydłowski, J. Grzonka, *ChemCatChem*, 8, 536-539, 2016.

I took part in the interpretation and discussion of TEM data.

2. Insight into the synthesis procedure of Fe³⁺/TiO₂-based photocatalyst applied in the selective photo-oxidation of benzyl alcohol under sun-imitating lamp, A. Magdziarz, J.C. Colmenares, O. Chernyayeva, D. Lisovytskiy, J. Grzonka, K. Kurzydłowski, K. Freindl, J. Korecki, *Ultrasonics Sonochemistry*, 38, 189-196, 2017.

I took part in the interpretation and discussion of TEM data.

B 490/17

Sincerely,

K. Kurzydłowski



Biblioteka Instytutu Chemii Fizycznej PAN

F-B.498/17



90000000200939



INSTITUTE OF PHYSICAL CHEMISTRY
POLISH ACADEMY OF SCIENCES
KASPRZAKA 44/52
01-224 WARSAW, POLAND



CATALYSIS FOR SUSTAINABLE
ENERGY PRODUCTION
AND ENVIRONMENTAL
PROTECTION

<http://rcin.org.pl>